MoDOT

Research, Development and Technology

University of Missouri-Rolla
University of Missouri-Columbia

RDT 01-002A

Destructive and Non-Destructive Testing of Bridge J857 Phelps County, Missouri

Volume I
Strengthening and Testing to Failure of Bridge Decks

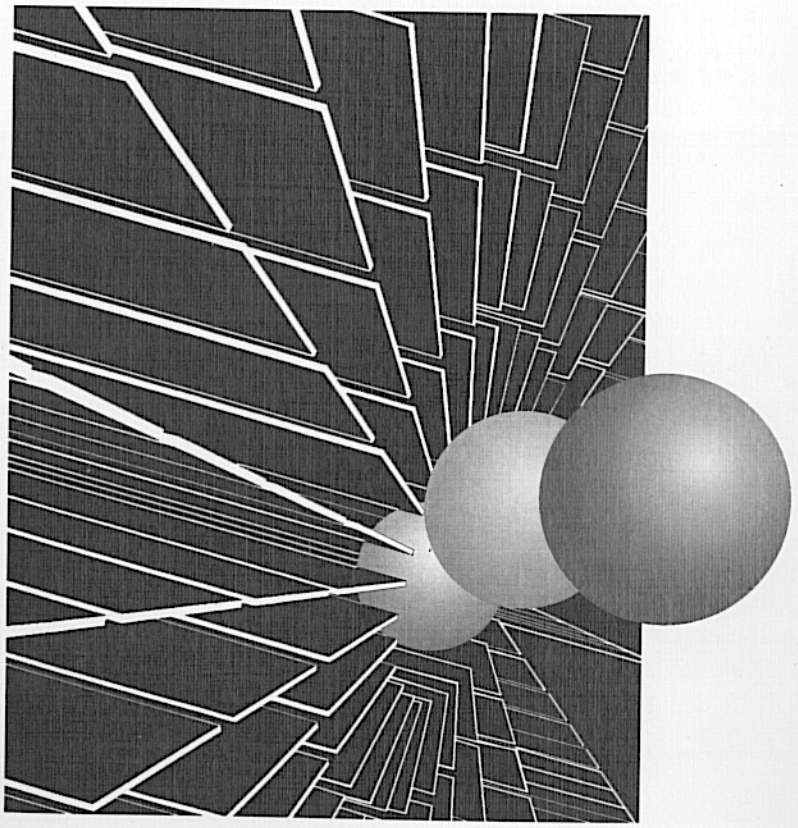

RI 98-013

April, 2001

CENTER FOR INFRASTRUCTURE ENGINEERING STUDIES

DESTRUCTIVE AND NON-DESTRUCTIVE TESTING OF BRIDGE J857 PHELPS COUNTY, MISSOURI

VOLUME I
STRENGTHENING AND TESTING TO FAILURE OF BRIDGE DECKS

by

Tarek Alkhrdaji
Antonio Nanni
Genda Chen
University of Missouri-Rolla

Michael Barker
University of Missouri-Columbia

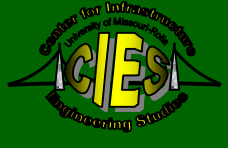

CIES 99-08A

DISCLAIMER

The mission of CIES is to provide leadership in research and education for solving society's problems affecting the nation's infrastructure systems. CIES is the primary conduit for communication among those on the UMR campus interested in infrastructure studies and provides coordination for collaborative efforts. CIES activities include interdisciplinary research and development with projects tailored to address needs of federal agencies, state agencies, and private industry as well as technology transfer and continuing/distance education to the engineering community and industry.

Center for Infrastructure Engineering Studies (CIES)
University of Missouri-Rolla
223 Engineering Research Lab
1870 Miner Circle
Rolla, MO 65409-0710
Tel: (573) 341-6223; fax -6215
E-mail: cies@umr.edu
www.umr.edu/~cies

DESTRUCTIVE AND NON-DESTRUCTIVE TESTING OF BRIDGE J857 PHELPS COUNTY, MISSOURI
VOLUME I
STRENGTHENING AND TESTING TO FAILURE OF BRIDGE DECKS

EXECUTIVE SUMMARY

Concrete bridges are conventionally reinforced with steel bars and/or prestressed with steel tendons. When subjected to aggressive environments, corrosion of the reinforcing and prestressing steel occurs and eventually leads to premature structural deterioration and loss of serviceability. In addition, the increasing service loads as well as seismic upgrade requirements result in a need to strengthen many of these bridges. The use of externally bonded steel plates for flexural and shear strengthening of concrete members is well established. However, corrosion related problems have limited the use of this technique for outdoor application. Fiber reinforced polymer (FRP) composites are corrosion resistant and exhibit several properties that make them suitable for repair/strengthening of reinforced concrete (RC) structures. However, the database for performance of FRP strengthened RC members is based on small-scale specimens that do not account for the variation of boundary conditions of a real structure. Full-scale field tests can demonstrate the actual behavior of a structure and can lead to a better understanding of the performance of the system and therefore strengthening design requirements.

This part of the research program aimed at demonstrating the feasibility and effectiveness of strengthening bridge RC decks with two systems of externally bonded FRP reinforcement to increase their flexural strengths as well as verify design methodology and capacity improvement. Two of the three simply supported decks were strengthened and tested to failure. One span was strengthened using near-surface mounted (NSM) CFRP rods while the second span was strengthened using externally bonded CFRP strips. The objective of the strengthening scheme was to increase the flexural capacity by approximately 30%. Each of the three spans was tested to failure by applying quasi-static load cycles. Test results indicate that the actual capacity of the bridge decks were higher than anticipated due to higher actual material strengths. In addition, the decks had end fixities that were estimated by comparison of experimental and theoretical results. The experimental moment capacities compared well with theoretical values based on the actual material properties obtained from laboratory testing and the determined end fixity. Strengthened decks exhibited ductile behavior prior to FRP failure. The short-term behavior of FRP strengthening system applications has been experimentally evaluated. Research into long-term performance should be conducted even though FRP used in highway bridges is expected to perform for a long time.

The final report consists of three volumes. Volume I depicts the strengthening and testing to failure of the three bridge decks. Volume II focuses on the laboratory and field dynamic tests. Volume III focuses on the strengthening and testing to failure of the bridge piers.

ACKNOWLEDGMENTS

Coordination and implementation of this research program were achieved by Tarek Alkhrdaji in partial fulfillment of the requirement for the degree of Doctor of Philosophy in Civil Engineering at the University of Missouri at Rolla (UMR). Technical support during field testing was provided by Jeff Bradshaw, BsEE, P.E. (UMR), and C. H. Cassil of the University of Missouri-Columbia (UMC).

The research program was made possible with the financial support received from the Missouri Department of Transportation, Mid-America Transportation Center, University of Missouri-Rolla/University Transportation Center on Advanced Materials and NDT Technologies. Master Builders Technologies, Cleveland, OH, and Structural Preservation Systems, Baltimore, MD, provided and installed the FRP systems, respectively. Chester Bross Construction Company, Hannibal, MO, was the general contractor.

TABLE OF CONTENTS

LIST OF ILLUSTRATIONS

LIST OF TABLES

NOTATION

A	=	Load factor used for bridge rating calculations
A_f	=	Area of FRP (in.^{2})
$A_{f,n}$	=	Area of NSM FRP rods (in.^{2})
$A_{f,sh}$	=	Area of surface bonded FRP sheets (in.^{2})
A_f	=	Area of FRP (in.^{2})
A_{rod}	=	Area of one NSM FRP rod (in.^{2})
A_s	=	Area of tensile steel reinforcement (in.^{2})
a	=	Depth of equivalent stress block for compression concrete (in.)
b	=	Width of the section (in.)
c	=	Depth to the neutral axis (in.)
d	=	Depth to the tension steel reinforcement centroid (in.)
d_n	=	Depth to the NSM reinforcement centroid (in.)
E	=	Effective deck strip width (ft)
E_c	=	Approximate elastic modulus of concrete in compression (psi)
E_f	=	Elastic modulus of the FRP fiber material (psi)
E_s	=	Elastic modulus of reinforcing steel (psi)
F	=	End fixity level
f'_c	=	Compressive strength of concrete (psi)
f_f	=	Stress level developed in the FRP (psi)
$f_{f,n}$	=	Stress level developed in the NSM FRP (psi)
$f_{f,sh}$	=	Stress level developed in the FRP sheets (psi)
f_{fu}	=	Ultimate strength of the FRP material (psi)
f_s	=	Stress level in the tension steel (psi)
f_y	=	Yield strength of mild steel (psi)
h	=	Total height of the section and depth to the FRP flexural reinforcement (in.)
I_{cr}	=	Moment of inertia of the cracked concrete section (in.^{4})
I_g	=	Moment of inertia of the gross concrete section (in.^{4})
k	=	Ratio of the depth to the elastic neutral axis to the effective depth, d
K^c_m	=	Coefficient to determine mid-span moment due to a concentrated load
K^c_e	=	Coefficient to determine end moment due to a concentrated load
K^D_m	=	Coefficient to determine mid-span moment due to a distributed load
K^D_e	=	Coefficient to determine end moment due to a distributed load
L	=	Deck span (ft)
$M^c(x)$	=	Moment at x due to a concentrated load and a given fixity, F
M^{*c}	=	Mid-span moment due to a concentrated load considering simple supports
$M^D(x)$	=	Moment at x due to a distributed load and a given fixity, F
M^{*D}	=	Mid-span moment due to a distributed load considering simple supports
M_{DL}	=	Moment due to self weight (ft-k/ft)
$M_{(LL+I)}$	=	Moment due to live load plus impact (ft-k/ft)
M_e	=	End moment (at the support)
M^c_e	=	End moment due to a concentrated load considering simple supports
M^D_e	=	Mid-span moment due to distributed load considering simple supports
M_i	=	Moment due to loads in place at the time of FRP installation (ft-k/ft)
$M_{(L+I)}$	=	Nominal moment capacity of a section (ft-k/ft)

M_m = Mid-span moment
M^c_m = Mid-span moment due to a concentrated load considering simple supports
M^D_m = Mid-span moment due to distributed load considering simple supports
M_n = Nominal moment capacity of a section
ϕM_n = Design moment capacity of a section
$M_{n,str}$ = Upgraded (desired) moment capacity
M_u = Ultimate moment due to factored loads
n = Number of fiber plies
$n_{f,n}$ = Ratio of NSM FRP stiffness to steel stiffness
$n_{f,sh}$ = Ratio of surface bonded FRP stiffness to steel stiffness
P = Point load, or
P_L = Point live load
Q = Uniform Load
r_g = Radius of gyration of the gross concrete section = $\sqrt{I_g / A_g}$ (in.)
S = Span length (ft)
S_{nsm} = Spacing of NSM rods (in)
T = Tension force (lb) or Period of vibration (sec)
t_f = Thickness of *one* ply of fiber sheet (in.)
v_c = Nominal concrete shear strength (psi)
w = Uniformly distributed load
w_f = Total width of the FRP laminate (in.)
W_s = Width of strip (in.)
α_1 = Multiplier on concrete strength to determine the equivalent concrete strength of an equivalent rectangular stress block
β_1 = Multiplier on c to determine the depth of an equivalent rectangular stress block
Δ = Deflection of flexural member
ε_b = Strain level in the concrete substrate developed by a given bending moment. Tension is positive. (in./in.)
ε_{bi} = Initial strain level in the concrete at the extreme tension fibers (in./in.)
ε_c = Compressive strain in concrete at any load level (in./in.)
ε_{cc} = Maximum compressive strain level in the concrete (in./in.)
ε'_c = Strain level in the concrete corresponding to the peak concrete stress, f'_c (in./in.)
ε_{cu} = Maximum usable compressive strain in the concrete = 0.003 (in./in.)
ε_f = Strain level in the FRP developed by a given bending moment (in./in.)
ε_{fu} = Ultimate strain (elongation) of the FRP material (in./in.)
ε_n = Strain level in the NSM FRP reinforcement (in./in.)
ε_{ni} = Initial strain level in the concrete at the level of NSM rods (in./in.)
ε_{sh} = Strain level in the surface bonded FRP sheets (in./in.)
ε_s = Strain level in the tension steel (in./in.)
ε_y = Strain level in the tension steel at its yield point = f_y/E_s (in./in.)
ϕ = Strength reduction factor
Φ = Curvature of a flexural member

1. INTRODUCTION

1.1. GENERAL

Concrete bridges are conventionally reinforced with steel bars and/or prestressed with steel tendons. When subjected to aggressive environments (e.g., treatment with deicing salts or exposure to marine environment), combinations of moisture, temperature and chlorides, corrosion of the reinforcing and prestressing steel occurs and eventually leads to premature structural deterioration and loss of serviceability. In addition, the continuous increase in service loads due to growing axle weights and traffic volumes and the current building codes demand on seismic performance result in a need to strengthen many of these bridges. In the United States alone, over 40 percent of the 590,000 structures in the National Bridge Inventory database need repair, strengthening, or replacement (Small, 1998). Due to budget constraints, the cost to replace these structures is beyond the financial means of most Departments of Transportation (DOT).

The use of externally bonded steel plates for flexural and shear strengthening of concrete members is well established for interior applications and for non-corrosive environments (L'Hermite and Bresson 1967, Swamy et al. 1987). However, corrosion related problems have limited the use of this technique for outdoor application.

Advanced composites made of fibers embedded in a polymeric resin, also known as fiber reinforced polymer (FRP) materials, are corrosion resistant and exhibit several properties suitable for their use as structural reinforcement (ACI Committee 440 1996, Meier 1987). Repair and strengthening of structures with FRP composites involves the use of externally bonded sheets, prefabricated laminates, and near surface mounted bars.

The most important characteristic of FRP in repair and strengthening applications is the speed and ease of installation. The higher material cost of FRP is typically offset by reduced labor, machinery, and shut-down costs, making FRP strengthening systems very competitive with traditional strengthening techniques such as steel plate bonding and section enlargement. FRP reinforcement could provide significant savings in costly corrosion problems and provide a more efficiently built infrastructure into the next century. However, the extensive use of bonded FRP composites in bridges and structures requires the development of official design guidelines and construction specifications. The lack of these guidelines has so far limited the number of applications for the strengthening of U.S. bridges and structures. In response to this, the Federal Highway Administration (FHWA) is currently sponsoring research programs to develop specifications for repair/strengthening of existing bridges using FRP composites and to ensure the quality and performance of FRP strengthening.

Strengthening by externally bonded FRP has been studied and implemented worldwide (Nanni, 1997). However, the database for performance of FRP strengthened RC members is based on laboratory tests, which are usually conducted on small-scale specimens that do not account for the variation of boundary conditions of a real structure. Full-scale field tests, on the other hand, can demonstrate the actual behavior of a structure and can lead to a better understanding of the performance of the system as a whole and therefore the strengthening design requirements.

1.2. PROJECT PHILOSOPHY

This project was intended to bridge the gap between theoretical and small-scale experiments typically performed in a controlled environment to the full-scale, real-life, behavior of structural bridge components strengthened with FRP. The project involved the elaboration of a research program to demonstrate the effectiveness of FRP for strengthening of highway bridges. The study was to result in recommendations for FRP strengthening of highway bridges for consideration and use by state highway agencies overseeing strengthening projects. It was intended to provide supporting full-scale test data to develop design criteria based on a scientifically valid foundation.

1.3. COOPERATIVE FEATURES OF THE RESEARCH PROGRAM

The research team assembled for this project provided an ideal combination of talents. The joint effort of two universities, industry, and a state DOT provided the premise for a successful outcome. Participation of the Missouri Department of Transportation (MoDOT) in the research effort ensured that the project was carried out with a thrust on practicality. Within the University of Missouri-Rolla (UMR), expertise was provided through two research centers that directly relate to the use of composites in construction. The first center is the Center for Infrastructure Engineering Studies (CIES), and the second center is the University Transportation Center (UTC) focusing on advanced composite materials for infrastructure upgrade and non-destructive testing technologies. The University of Missouri-Columbia (UMC) provided the expertise and technical assistance based on previous experience in field-testing of bridges (Kemna, A. C., 1999 and Kemna, D. J., 1999)

Among the industry participants was Structural Preservation Systems, Baltimore, MD, which is recognized nationwide as one of the industry's leading contractors in the field of structural repair and protection; and Master Builders Technologies, Cleveland, OH, which distributes FRP strengthening systems.

In addition to planning, activity coordination, and task implementation, the work of the UMR team was coordinated with MoDOT officials. This included holding periodic meetings and requesting technical assistance when needed.

1.4. ANTICIPATED BENEFITS

With the expertise of the research team in FRP applications, field-testing capabilities, contribution of the industrial partners, and field demonstrations, the result of this project should help in verifying and demonstrating the effectiveness of FRP strengthening systems for the flexural upgrade of bridge components. Repair/strengthening of concrete bridges using FRP composites could save public funds and provide more efficient rehabilitation of structures. Standard specifications for design, construction, and quality control tests for FRP repair/strengthening are necessary to allow for its use in concrete highway structures. Although very interested in the benefits of FRP application, most state DOTs, design consultants and bridge engineers are unprepared or unwilling to use material systems not “sanctioned” by FHWA or AASHTO. With this project, capacity improvement will be verified in the field and the test results will be made available to public agencies.

1.5. BACKGROUND ON FIBER REINFORCED POLYMERS

FRP materials have superior properties with respect to strength, weight, durability, creep, and fatigue. They exhibit several properties that make them suitable for use with concrete

structures (Iyer and Sen 1991, Neale and Labossiere 1992, White 1992, Nanni 1993, Nanni and Dolan 1993, Taerwe 1995, ACI Committee 440 1996, El-Badry 1996, Japan Society of Civil Engineers (JSCE) 1997(a&b), Benmokrane and Rahman 1998, Saadatmanesh and Ehsani 1998, and Dolan, Rizkallah, and Nanni 1999). The current commercially available FRP reinforcements are made of continuous fibers of aramid (AFRP), carbon (CFRP), or glass (GFRP) impregnated in a resin matrix. FRP composites can be produced by different manufacturing methods in many shapes and forms. The most popular FRPs for concrete reinforcement are bars, prestressing tendons, pre-cured laminates/shells and fiber sheets. Commonly used rods have various types of deformation systems, including externally wound fibers, sand coatings, and separately formed deformations. These types are commonly used for internal concrete reinforcement. FRP pre-cured laminates/shells and sheets are commonly used for external concrete reinforcement. FRP plane laminates have been used to replace bonded steel plates (Sharif and Baluch 1996, Castro et al 1996) and FRP shells have been used as jackets for columns (Xiao and Ma 1997). Bonded FRP essentially works as additional reinforcement to provide tensile strength. FRP may be used on beams, girders, and slabs to provide additional flexural strength; on the sides of beams and girders to provide additional shear strength; or wrapped around columns to provide confinement and additional ductility (a primary concern in seismic upgrades). Quality control is crucial to the successful application of FRP systems. Most FRP strengthening systems are simple to install. However, improper installation (e.g., not properly mixing epoxy components or saturating the fibers, misaligning the fibers, etc.) could be avoided with careful attention.

In Europe, research on the use of FRP in concrete structures started in the 1950's (Rubinsky and Rubinsky 1954, Wines et al. 1966). In the field of strengthening with FRP composites, pioneering work took place in the 1980's, in Switzerland and resulted in successful practical applications (Meier 1987, Meier and Kaiser 1991). It was in Switzerland where the first on-site repair by externally bonded FRP took place in 1991. Since the first FRP reinforced highway bridge in 1986, programs have been implemented to increase the research and use of FRP reinforcement in Europe. The European BRITE/EURAM Project, "Fiber Composite Elements and Techniques as Non-Metallic Reinforcement," conducted extensive testing and analysis of the FRP materials from 1991 to 1996 (Taerwe, 1997). A pan-European collaborative research program (EUROCRETE) was established. The program started in December 1993 and ended in 1997. It aimed to develop FRP reinforcement for concrete and included industrial partners from the United Kingdom, the Netherlands, Switzerland, France, and Norway.

Along with Europe, Japan developed some of the first FRP applications for construction in the early 1980's. A sudden increase in the use of FRP composites occurred after the 1995 Hyogoken Nanbu Earthquake in Japan. As of 1997, the Japanese led FRP reinforcement usage with more than one thousand demonstration/commercial projects and FRP design provisions in their standard specifications of the Japan Society of Civil Engineers (JSCE, 1997).

Until only a few years ago, application of FRP materials to concrete structures was only a subject of research in the United States and Canada. Today, several companies are involved in the manufacturing, design, and installation of these systems in construction projects (Goldstien 1996, Gangarao et al. 1997). FRP materials have quickly risen from state-of-the-art to mainstream technology. Composite strengthening systems have become very competitive with traditional strengthening techniques. The United States had the leadership in the initial development of GFRP reinforcing bars. Marshall-Vega, Marshall, Arkansas, first developed GFRP rebars for the purpose of reinforcing polymer concrete due to its thermal incompatibility with steel bars. In the late 1970s, International Grating, Inc. entered the North American FRP

reinforcement market. These two companies led the research and development of the FRP reinforcing bars for an expanding market into the 1980's.

1.6. OVERVIEW OF THE RESEARCH PROGRAM

This research program aimed at conducting experimental destructive and non-destructive tests on bridge J857, located in Phelps County, Missouri, in order to validate new strengthening technologies (i.e., externally bonded FRP sheets and near-surface mounted FRP rods). The bridge was constructed in 1932 and consisted of three solid reinforced concrete (RC) decks. The original drawings of the bridge are given in Appendix A. The research program aimed at demonstrating the feasibility and effectiveness of bridge deck and bridge pier strengthening using different types of externally bonded FRP reinforcement to increase their flexural strength.

Bridge J857 was ideal for this demonstration since it represented typical conditions of several bridges in Missouri and the surrounding Mid-America states constructed during the first half of the 20th century.

1.6.1. Task I – Strengthening and Non-Destructive Testing

Two of the three spans of the bridge were strengthened using externally bonded carbon FRP (CFRP) reinforcement. One span was selected to be strengthened with surface bonded CFRP strips and the second span using near-surface mounted (NSM) CFRP rods. The third deck was used as a reference point for comparison purposes. Strengthening design was such that both strengthened decks have similar flexural strengths. The objective of the strengthening scheme was to increase the current flexural capacity of the bridge by approximately 30%. Two of the four columns, which were originally designed to carry only gravity loads, were upgraded by improving their flexural capacities using FRP composites and were tested to failure. The piers were upgraded to a concrete structure under seismic performance category (SPC) B. Two columns of the bridge were strengthened with NSM CFRP rods to achieve different modes of failure (e.g., concrete crushing and CFRP bar rupture). The columns were jacketed with carbon FRP (CFRP) to provide lateral support to the mounted rods and to meet certain seismic code requirements. A third column was jacketed with Glass FRP (GFRP) to investigate its influence on the ductility and flexural capacity of the column. A certified contractor implemented the bridge strengthening under UMR supervision. Pull-off tests, a quality control measure of FRP sheets, was conducted.

1.6.2. Task II – Destructive Testing of Bridge Decks

1.6.2.1. Static Load Testing

Each of the three spans was tested to failure by the application of quasi-static load cycles. The magnitude of the maximum load used in each successive load cycle was incremented until failure of the slab was achieved. Destructive tests provided conclusive evidence as to the strength of the bridge deck. The results of this test were used to:

a) Verify theoretical models
b) Determine the mode of failure of the structure with and without strengthening
c) Determine the effect of skewed support on behavior and failure mode
d) Determine the effect of FRP materials on the elastic response of the strengthened structure

Deformations, steel strain, and strain in CFRP bars and CFRP sheets were measured at different locations. The maximum load of each cycle was incremented gradually until failure is achieved. After each load cycle, a dynamic load was applied and the dynamic signature was recorded.

1.6.2.2. Dynamic Load Testing

Dynamic test was conducted on the deck strengthened with CFRP sheets. Dynamic loads were induced using a mechanical shaker mounted on top of the deck. The shaker was placed at mid-span along the deck centerline to appreciably energize the fundamental vibration of the bridge slab. Dynamic tests were carried out after each load cycle. Since the stiffness and frequency of the slab varies with the degree of damage, a range of frequencies was applied at each stage to achieve resonance of the slab.

Four accelerometers were deployed at the center point and quarter points along the longitudinal and transverse centerlines of the deck. The results of dynamic tests were used to:

a) Correlate the dynamic signature (i.e., natural frequency and damping ratio) with the degree of damage induced by quasi-static loading
b) Perform a feasibility study of using the dynamic signature technique as a viable method to rapidly assess the health condition of RC structures.

1.6.3. Task 3 – Destructive Pier Testing

Testing of the bridge piers supporting the bridge deck could provide valuable information regarding flexural strengthening. The piers were upgraded to a concrete structure under seismic performance category (SPC) B.

Three of the four columns were strengthened using different materials and strengthening schemes. The behavior of strengthened columns, influence of different strengthening schemes and failure modes were compared and conclusions were drawn. Flexural strengthening was achieved by mounting near-surface mounted CFRP rods on two opposite faces (north and south) of the columns. Two columns were also wrapped with carbon and glass sheets. The columns were tested to failure by applying cyclical lateral loads to the pier cap beams.

1.6.4. Task 4 – Analysis of Results and Development of Analytical Models

The test results of the various tasks are used to investigate the behavior of the strengthened bridge components and verify the predicted capacities and modes of failure. Recommendations for strengthening design and seismic upgrade are made. The concept of using dynamic tests to assess structural integrity is investigated and conclusions are drawn.

1.7. ORGANIZATION OF THE FINAL REPORT

The final report consists of three volumes. The current Volume (Volume I) focuses on the strengthening and static load testing to failure of the three decks of the bridge. Volume I also includes an introduction to FRP materials and their use and application for structural upgrade, general description of the test bridge and bridge rating method, description of the strengthening systems and their application procedure. Theoretical model for flexural strength calculations of the strengthened decks are introduced. Test setup description and the experimental results are presented, comparisons of theoretical and experimental results are made, and conclusions are

drawn. Conclusions are also made regarding the effect of FRP strengthening on the stiffness of the bridge decks as well as the effect of bridge accessories and boundary conditions.

Volume II focuses on a feasibility study on damage detection by the dynamic testing. The experimental work in the field is backed by laboratory testing for conceptual verification for the assessment method. Test results are presented and compared with theoretical predictions. Conclusions regarding the use of dynamic testing for structural assessment are presented. This Volume also includes a summary of the elastic field-testing system as well as the elastic test results of the middle deck of the bridge. Conclusions are made on the effect of bridge accessories and boundary conditions on the continuity of deck slabs.

Volume III focuses on the strengthening and testing to failure of the bridge columns. The strengthening systems and applications procedure are described. Theoretical models for flexural strength calculations are introduced. The test setup and test procedure are described. Experimental data are interpretation, comparison of the experimental and theoretical capacities are made, and conclusions are drawn.

2. BRIDGE DESCRIPTION, INSPECTION, AND RATING

2.1. GENERAL

Bridges may suffer deterioration due to overload and exposure to harsh environment, which usually calls for reassessment of the structural components to determine their safe load carrying capacity. Inspection of bridges is performed periodically by state DOTs in accordance with the *Manual for Maintenance Inspection of Bridges* published by the American Association of State Highway and Transportation Officials (AASHTO, 1983). This process includes the review of construction drawings, visual inspection, and capacity evaluation using established state and federal guidelines. Any detected deterioration or flaws (e.g., concrete spalling, reinforcement corrosion, excessive cracking) is reflected in the calculation of the safe load carrying capacity of the bridge. The determined capacity of the bridge must then meet specific load rating criteria to ensure adequate and safe service life. The rating procedure is available in the *Bridge Inspection Rating Manual* (MoDOT, 1996). Load rating is the first step in determining the need for strengthening.

2.2. DESCRIPTION OF BRIDGE J857

Bridge J857 consisted of three simply supported decks made of 18.5 in. (460 mm) thick, solid reinforced concrete slabs, as shown in Figures 2.1 through 2.4. Each deck had an original roadway width of 25 feet (7.6 m) and spanned 26 ft (7.9 m). The original plans of the bridge show that the deck slabs had #8 (25 mm) bottom deformed steel bars spaced at 5 in. (127 mm) on centers in the longitudinal direction and #4 (13 mm) deformed steel bars spaced at 18 in. (457 mm) on centers in the transverse direction. Figure 2.5 illustrates a cross section of the bridge deck. Two abutments and two bents supported the bridge decks. Each bent consisted of two columns connected at the top by a RC cap beam. The abutments and bents are at a 15-degree skew. The columns had a 2 by 2 ft (0.6 x 0.6 m) square cross-section and were reinforced with four #6 (19 mm) deformed steel bars, located at the corners of the cross section. The transverse reinforcement was made of #2 (6 mm) steel ties spaced at 18 in. (457 mm) on centers. The original drawings of the bridge indicated that the clear height (end of haunch to top of footing) of the columns varied from 3.5 to 5.0 ft. Each column was supported by a 4 ft by 4 ft by 2.5 ft (1.2 m X 1.2 m X 0.75 m) square spread footing. The reinforced concrete parapet walls were approximately 2.5 ft (0.75 m) high and run the entire length of the bridge. The original drawings of the bridge are shown in Appendix A.

2.3. BRIDGE INSPECTION

Bridge dimensions were verified through field inspection. The spacing of the steel reinforcement was verified using a bar locator. Steel reinforcement size and the thickness of the concrete cover were verified by exposing some of the rebars. The bridge deck had an asphalt overlay that varied from 0.25 to 0.5 in. (6 to 12 mm). The asphalt overlay was removed at different spots and the deck was inspected. No deterioration was observed on the deck and the deck concrete was fully intact. According to bridge plans, the height of the columns varied from 3.5 to 5.0 ft. Upon field inspection, it was found that the actual heights of the columns varied from 6 to 11 ft (1.8-3.4 m). In addition, while bridge plans indicate that the cap beams were 2 ft wide and 2.5 ft deep; it was found that all the cap beams had a 2.5 ft by 2.5 ft square section. In

general, the condition of the bridge was good and no major damage (e.g., corrosion of reinforcement, or concrete spalling) was observed.

The original plans of the bridge J857 did not provide any specifications for the materials used in bridge construction other than a concrete mix proportions (1:2:3½) and reinforcement schedule. Since construction of the new road was not completed at the time the research program was started, the bridge had to be strengthened while in service. To avoid damaging the bridge, the material properties used in the preliminary analysis were based on the materials strength values recommended by MoDOT (MoDOT, 1996), which relate the material properties to the age of the structure. Older bridges are assumed to have lower strength of concrete and steel reinforcement than newer bridges. When the strength of the concrete is not known, concrete strength f'_c is be taken as 2363 psi (16.3 MPa). For bridges built in the 1930's, a default value of 33,000 psi (227 MPa) is used for the yield of steel reinforcement. For simplicity, a concrete strength of 2500 psi (17.2 MPa) was used in preliminary calculations.

2.4. BRIDGE DECK FLEXURAL CAPACITY

The preliminary investigation of bridge capacity was based on a unit strip, simple beam analysis. The geometry of a unit strip of a bridge deck slab and material properties are shown in Table 2.1.

Table 2.1. Slab Unit Strip Properties.

b (in.) [mm]	h (in.) [mm]	d (in.) [mm]	A_s ($in.^2$) [mm^2]	E_c (ksi) [GPa]	f'_c (psi) [MPa]	E_s (ksi) [GPa]	f_y (psi) [MPa]
12 [305]	18.5 [470]	16.5 [419]	1.88 [3980]	2850 [19.5]	2500 [17.2]	29,000 [200]	33,000 [227]

Figure 2.1. Bridge J857

Figure 2.2. Bridge piers.

Figure 2.3. Detail of deck slab support at the bents.

Figure 2.4. Details of the deck slab support at the abutments.

The nominal flexural capacity, M_n, of a unit strip can be calculated using the following expressions:

$$M_n = A_s f_y \left(d - \frac{a}{2} \right) \tag{2.1}$$

$$a = \frac{A_s f_y}{0.85 f'_c b} \tag{2.2}$$

The nominal moment capacity of a unit strip was calculated as 79.2 ft-k/ft (352 kN-m/m). The ultimate moment M_u should not exceed the design moment capacity ϕM_n:

$$M_u \leq \phi M_n \tag{2.3}$$

In which the strength reduction factor ϕ is equal to 0.9. Hence, the design moment capacity is 71.3 ft-k/ft (317 kN-m/m). The maximum moment at mid-span due to the weight of the bridge, M_{DL}, was calculated to be 22.6 ft-k/ft (101 kN-m/m). This included the weight of the bridge parapet walls and asphalt overlay. A simple span of 25.5 ft (7.8 m) was used in the calculations.

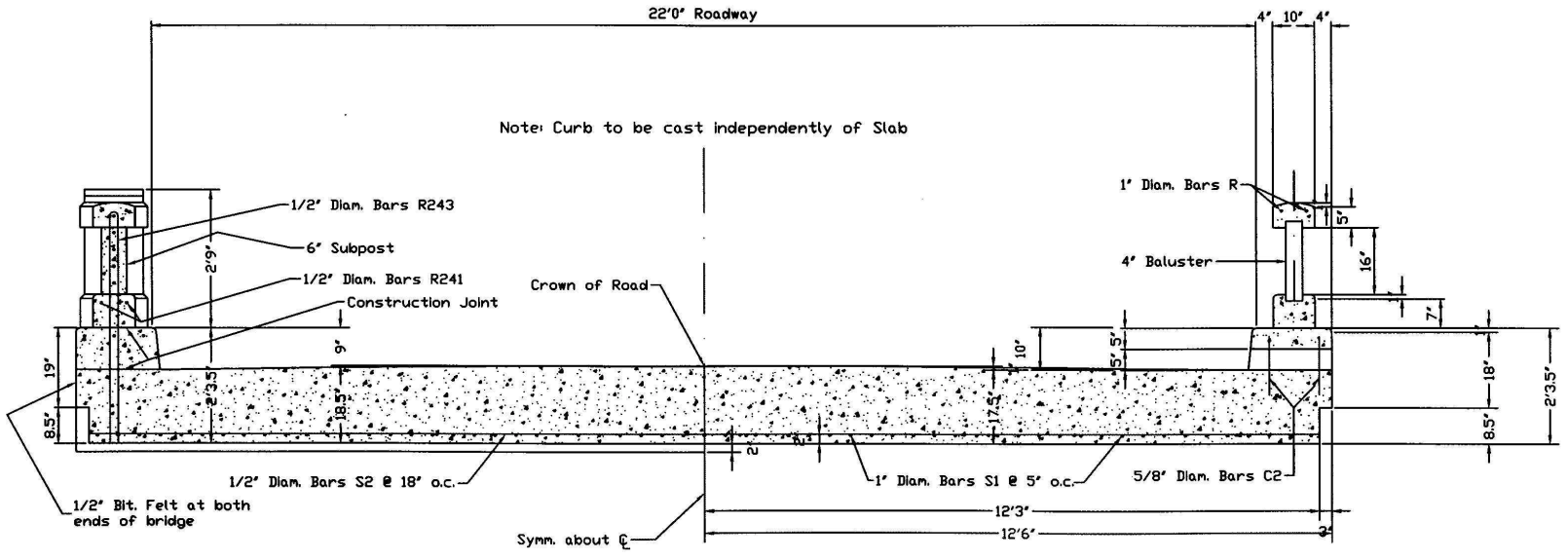

SECTION AT ABUTMENT SECTION THRU SPAN

Note: 1 ft = 0.305 m, 1 in = 25.4 mm

Figure 2.5. A cross section showing typical details of the bridge deck.

2.5. BRIDGE DECK SHEAR CAPACITY

According to AASHTO (1996), bridge slabs designed for bending moment in accordance with the specifications are considered satisfactory in shear. Since strengthening with FRP bonded to the soffit of the deck cannot improve the deck shear strength, a check must be made to ensure that the new loads and test loads would not cause shear failure. The shear strength of concrete V_c is calculated using the American Concrete Institute ACI (1995) approach, as follows:

$$V_c = 2.0\sqrt{f'_c}bd \qquad (2.4)$$

Considering a concrete strength of 2500 psi (17.2 MPa), a unit width of 12 in. (0.305 m), and a depth of reinforcement of 16.5 in. (0.411 m), the shear strength is 19.8 kips/ft (289 kN/m). The one–way action shear capacity of the deck is determined by multiplying this value by the bridge width of 25 ft (7.6 m). The one–way action shear capacity of the deck is therefore 495 kips (2202 kN).

A check for the two-way action was also made to ensure that the deck would not fail in punching shear due to concentrated load of truck wheels or hydraulic jacks. For this case, the critical section is perpendicular to the plane of the slab and is located at a distance d/2 from the perimeter of the concentrated load. Using a load footprint of 12 in. X 12 in. (300 mm X 300 mm), the shear capacity was calculated to be 188 kips (837 kN). The actual shear capacity of the deck based on one-way and two-way action is higher that the calculated values because the concrete strength was expected to be higher than 2500 psi (17.2 MPa). As will be shown later, the maximum load to be applied by the jacks (approximately 440 kips) and the load applied by each jack or an HS-20 modified truck wheel is less than the shear strength calculated from the one-way and two-way shear action, respectively. Therefore, the bridge decks had adequate shear capacity.

2.6. BRIDGE RATING

The results of bridge deck rating are influenced by proper identification of material properties and incorporation of its actual boundary conditions. When the material properties are not known, the rating is typically achieved using recommended material properties based on the age of the bridge, which in most cases results in a conservative rating. Since the rating of a bridge is ultimately linked to its decommission, careful consideration should be given to the factors that can unnecessarily cut short the service load/life of the bridge.

In Missouri, bridges built, rehabilitated, or reevaluated are rated using the Load Factor Rating Method. Bridges are rated at two load levels, the maximum load level, called the Operating Rating, and a lower load level, called the Inventory Rating (MoDOT, 1996). The Operating Rating is the maximum permissible live load that should be allowed on the bridge. Exceeding this level could damage the bridge. Allowing unlimited number of vehicles to use the bridge at operating level may shorten the life of the bridge. The Inventory Rating corresponds to the customary design level of stresses, but reflects the existing bridge and material conditions with regard to deterioration and loss of section. It results in a live load that the bridge can carry safely on a daily basis without damaging the bridge.

In Missouri, the Operating Rating is based on the appropriate ultimate strength using AASHTO specifications. The vehicle used for the live load calculations is the HS20 truck or the equivalent MS18 truck if a metric load rating is desired.

In Missouri, load posting is established using the H20 and 3S2 vehicles at 86% of the Operating Rating. Additionally, the Operating Rating is calculated for the MO5, HS20 and the 4S3P vehicles. Typical axle loads and spacing for the various rating vehicles are shown in Figures 2.6 through 2.10.

2.6.1. Live Load Distribution Factors.

Two live load distribution factors are considered in bridge rating: AASHTO two-lane live load distribution factor and MoDOT one-lane live load distribution factor.

2.6.1.1. Two-Lane Live Load Distribution Factor.

This factor is determined in accordance with AASHTO Standard Specifications for Highway Bridges (AASHTO, 1996). The effective deck strip width for a wheel load is determined as follows:

$$E = 4 + 0.06(S) \leq 7.0\text{ft} \tag{2.5}$$

In which S is the span length in feet. For the bridge under investigation this formula yields 5.53 ft (1.7 m). The two-lane live load distribution factor is the inverse of the effective strip width and is determined as follows:

$$LLDF_{2LANE} = {}^{1}\!/_{E} = {}^{1}\!/_{5.53} = 0.1808 \tag{2.6}$$

2.6.1.2. One-Lane Live Load Distribution Factor.

The live load distribution factor for one-lane loading on slab-type structures is calculated by assuming that the two wheel loads are distributed over the roadway width, which should not exceed 24 ft (7.3 m). This is expressed as follows:

$$LLDF_{1LANE} = \frac{2\text{ Wheel Lines}}{\text{Roadway Width}} \tag{2.7}$$

Substituting the 22 ft (6.7 m) roadway width results in the one-lane distribution factor.

$$LLDF_{1LANE} = \frac{2}{22} = 0.0909 \tag{2.8}$$

2.6.2. Load Factor Bridge Rating

The load factor rating is achieved using the following expression:

$$\text{Rating}_{LF} = \frac{\phi M_n - 1.3M_{DL}}{AM_{(LL+I)}} \times (\text{Truck Weight}) \tag{2.9}$$

Where A is a load factor taken as 2.17 for Inventory Rating and 1.3 for Operating and Posting Rating. The design moment capacity ϕM_n of the deck was previously determined as 71.3 ft-k/ft (317 kN-m/m) and the moment due to the self-weight of the deck as 22.6 ft-k/ft (89 kN-m/m).

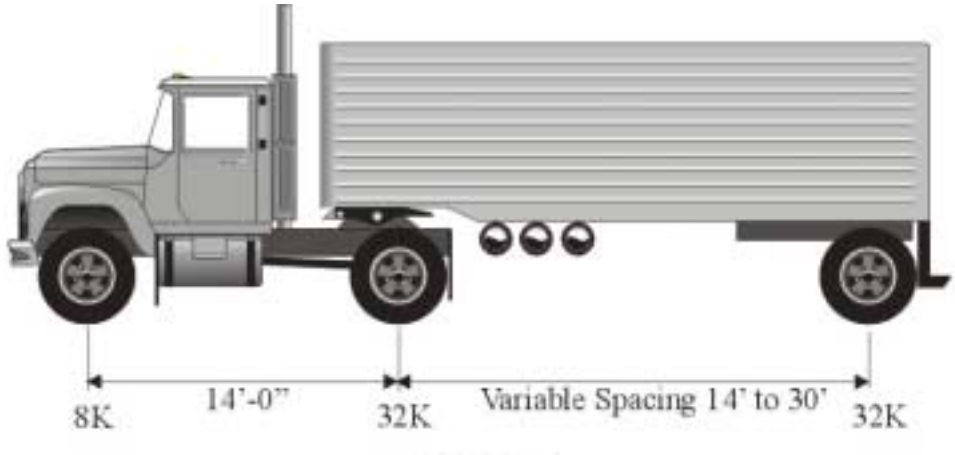

Figure 2.6. Truck HS20

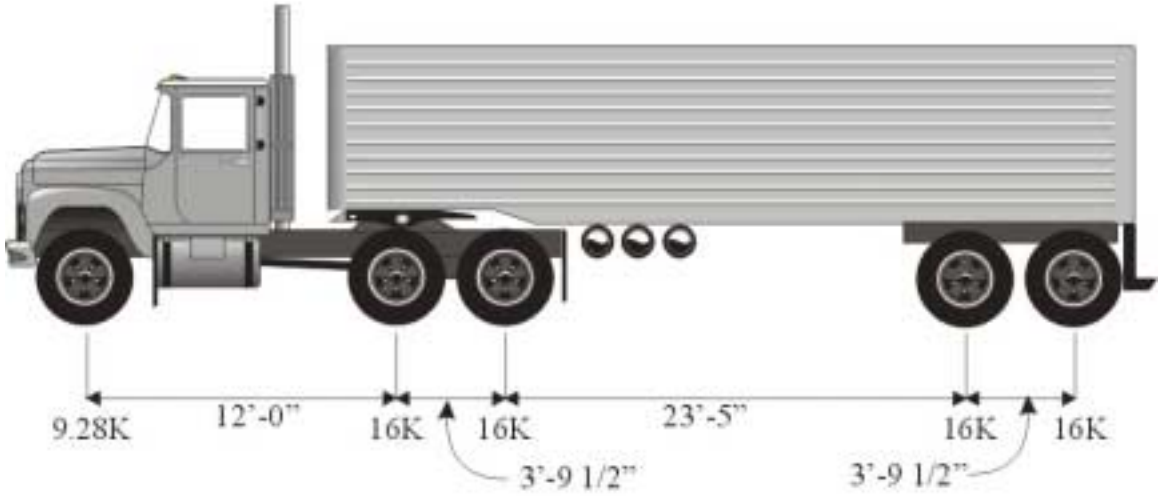

Figure 2.7. Truck 3S2

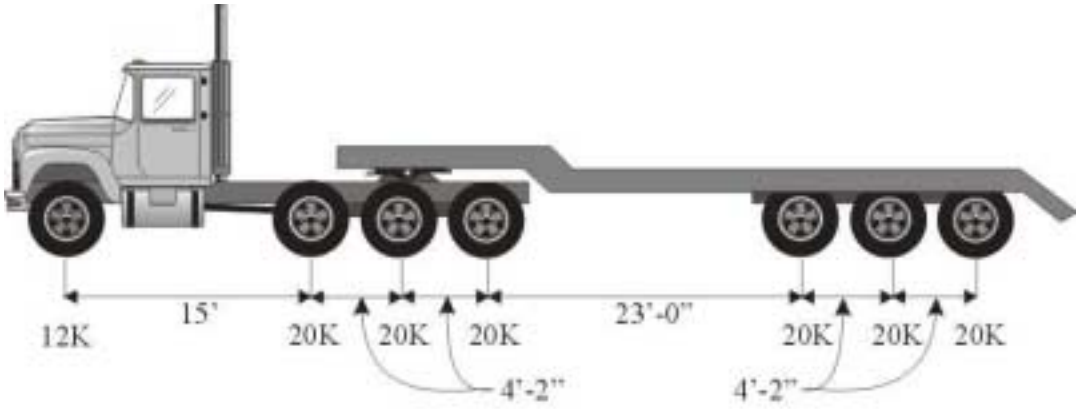

Figure 2.8. Truck 4S3P

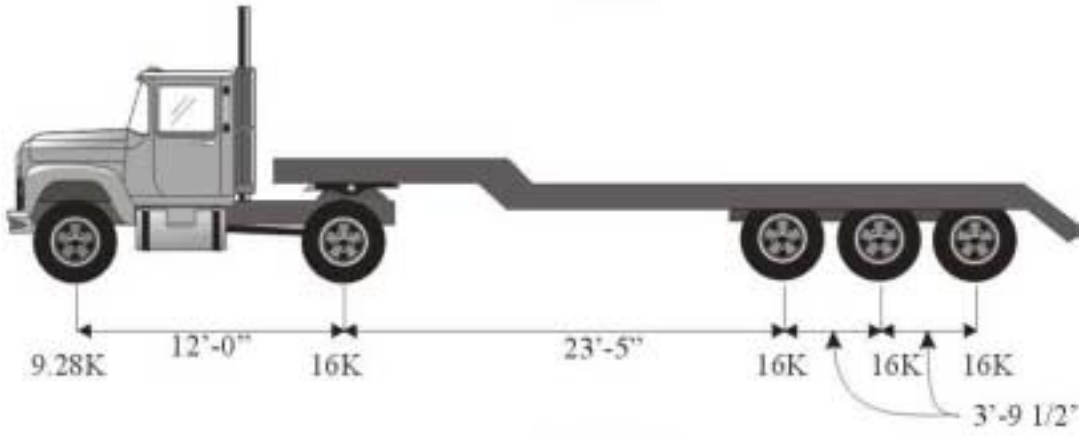

Figure 2.9. Truck MO5

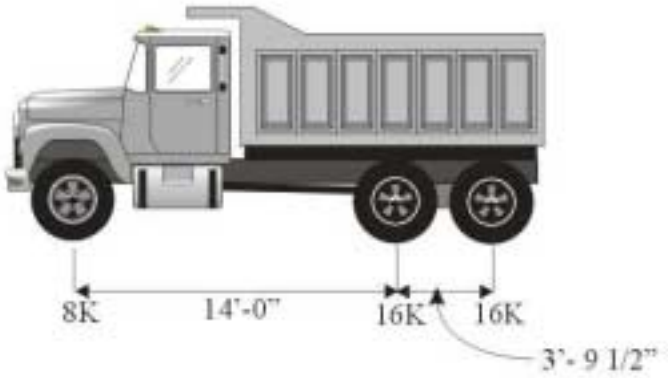

Figure 2.10. Truck H20

The moment capacity available for live load plus 30% impact is the difference of the dead load moment and the total moment capacity, taking into account the incorporation of the loading factor as follows:

Table 2.2. Available Capacity for Live Load plus Impact/Foot Width.

Truck	Rating Level	Formula	$M_{(LL+I)}$ (ft-k)
HS20	Inventory	$\frac{\phi M_n - 1.3M_{DL}}{2.17}$	19.32
MO5	Operating	$\frac{\phi M_n - 1.3M_{DL}}{1.3}$	32.25
HS20	Operating	$\frac{\phi M_n - 1.3M_{DL}}{1.3}$	32.25
4S3P	Operating	$\frac{\phi M_n - 1.3M_{DL}}{1.3}$	32.25
3S2	Posting	$0.86\times\frac{\phi M_n - 1.3M_{DL}}{1.3}$	27.74
H20	Posting	$0.86\times\frac{\phi M_n - 1.3M_{DL}}{1.3}$	27.74

The maximum live load moment induced by the wheel loading of the standard vehicles is calculated using the influence line for moment at center span. To calculate the two-lane and one-lane induced live load moments for a unit strip, the determined live load moments are multiplied by $LLDF_{2LANE}$ and $LLDF_{1LANE}$, respectively. The maximum unit strip live load moments for the standard trucks are therefore:

Table 2.3. Two Lane and One-Lane Live Load Calculations/Foot Width.

Truck Type	$M_{(LL+I)}$ (ft-k)	
	Two-Lane	One-Lane
HS20	25.3	12.7
MO5	28.7	14.4
HS20	25.3	12.7
4S3P	35.6	17.9
3S2	20.5	10.3
H20	20.7	10.4

Load factors are determined by dividing the available live load capacities given in Table 2.2 by the required live load capacities given in Table 2.3. The results of load factor ratings are tabulated in Table 2.4.

An Inventory Rating factor greater than 1.0 indicates that the live load capacity is greater than the applied live load and vice-a-versa. The two-lane inventory rating for the HS20 truck indicated that the bridge was deficient in terms of ultimate capacity. No posting was needed for bridge J857.

Table 2.4. Load Factor Bridge Rating

Truck Type	Truck Weight (Tons)	Rating Type	Load Factors		Safe Load Capacity (Tons)	
			Two-Lane	One-Lane	Two-Lane	One-Lane
HS20	36.00	Inventory	0.764	1.521	24.7	49.3
MO5	36.64	Operating	1.124	2.240	41.2	82.1
HS20	36.00		1.275	2.539	45.9	91.4
4S3P	60.00		0.906	1.802	54.4	108.1
3S2	36.64	Operating	1.353	2.693	49.6	98.7
H20	20.00	Operating	1.340	2.667	26.8	53.3

Note: 1 Ton = 2 kips = 0.906 kN

3. STRENGTHENING DESIGN AND APPLICATION

3.1. GENERAL

Bridge rating results indicated that bridge J857 did not need strengthening to meet posting requirements. According to MoDOT specifications, all new bridges on the national highway systems and in commercial zones should be designed for HS20 Modified loading. An HS20 Modified loading is defined as HS20 loading modified by a factor of 1.25. These requirements were used to establish an appropriate strengthening level that reflects a strengthening significance and takes into account the feasibility of testing to failure.

3.2. PRELIMINARY INVESTIGATION

The design of reinforced concrete members, as set by AASHTO, is made either with reference to service loads and allowable stresses, which is known as *Service Load Design*, or with reference to load factors and limit state strength, which is known as *Strength Design* (AASHTO, 1996). The latter was used for preliminary investigation.

According to the strength design method, the factored moment is as follows:

$$M_u = 1.3(M_{DL} + 1.67M_{(L+I)}) \tag{3.1}$$

The flexural capacity calculation was based on the unit strip method adopted by AASHTO for design and analysis of solid concrete slab bridges (AASHTO, 1996). Considering simple supports and an impact factor of 1.3, the maximum live load moment induced by an HS20 wheel loading is 140 ft-k/ft (623 kN-m/m). The maximum live load moment induced by an HS20 modified wheel loading is determined by multiplying this value by 1.25, which yields 175 ft-k/ft (779 kN-m/m). These moments are acting on a deck strip with an effective width of E, defined by AASHTO as follows:

$$E = 4 + 0.06(S) \tag{3.2}$$

In which S is the span of the slab taken as 25.5 ft (7.8 m). The value of E should not exceed 7.0 ft (2.1 m). Hence, the effective strip width is E = 5.53 ft (1.7 m). The maximum live moment per linear foot is determined by diving the maximum moment by 5.53 ft (1.7 m), which yield 25.3 ft-k/ft (112.5 kN-m/m) and 31.6 ft-k/k (140.6 kN-m/m) for HS20 and HS20 Modified loading, respectively. The corresponding factored moments are 84.3 ft-k/ft (374 kN-m/m) and 98.0 ft-k/ft (436 kN-m/m), respectively.

The factored moments should not exceed the design moment capacity, which is expressed as follows:

$$\phi M_n \geq M_u \tag{3.3}$$

In which, the strength reduction factor ϕ is equal to 0.9. In order for the bridge to carry an HS20 or HS20 modified truck, its nominal moment capacity should not be less than 93.7 ft-k/ft (417 kN-m/m) or 108.9 ft-k/ft (484 kN-m/m), respectively. Comparing these values with the

deck capacity of 79.2 ft-k/ft (352 kN-m/m), the required levels of strengthening are established as 18% and 37%. A capacity increase of 18% may not provide a clear differentiation between the flexural behaviors of the strengthened and unstrengthened decks. A 37% strengthening, on the other hand, required a more complex test setup to achieve failure loads. Accordingly, it was decided to strengthen the decks by approximately 30% to improve their flexural capacity. This level of strengthening was considered to be sufficient to meet HS20 Modified truck loading requirement based on the belief that the assumed material properties were overly conservative.

3.3. STRENGTHENING SYSTEMS

Two of the three decks of the bridge were to be strengthened to the same level of nominal capacity using two different FRP systems: near surface mounted (NSM) FRP rods and MBrace™ Composite Strengthening System. Conceptually, FRP strengthening systems are similar to bonding steel plates to concrete system. However, due to their light weight, the installation of an FRP strengthening system is easier than bonding steel plates and does not require the use of heavy equipment and is usually achieved with minimal installation time.

3.3.1. Near-Surface Mounted FRP Rods.

This strengthening system consists of FRP rods embedded in surface grooves and bonded in place using an epoxy adhesive. The rods considered for this application were $^{7}/_{16}$ in. (11 mm) diameter, CFRP rods, with surface roughened by sandblasting to improve their bond properties. The physical properties of the CFRP rods are given in Table 3.1. The binder was LPL concessive paste, a two-component, 100% solids, epoxy adhesive, manufactured by Master Builders Technologies, Cleveland, OH. The high viscosity of this binder facilitated the over-head application of the rods. A cross section illustrating details of the final product is shown in Figure 3.1.

Table 3.1. Mechanical Properties of Carbon FRP Rods.

Diameter in (mm)	Design Strength ksi (MPa)	Design Strain in/in or mm/mm	Tensile Modulus ksi (GPa)
$^{7}/_{16}$ (11)	144 (992)	0.0105	17,200 (119)

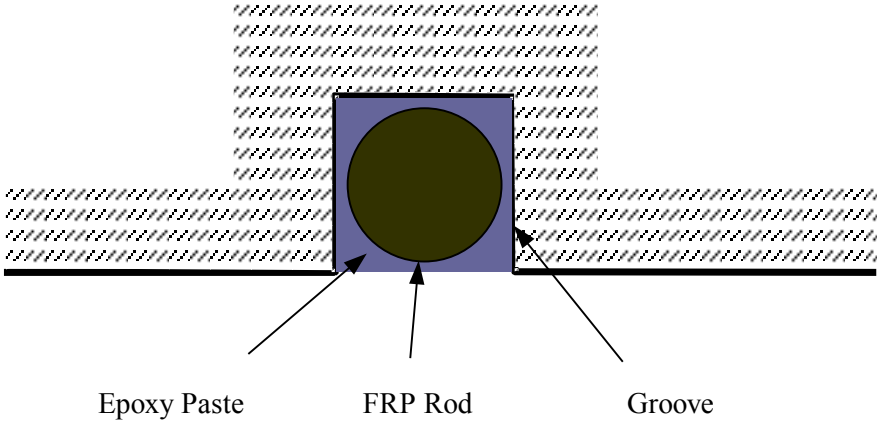

Figure 3.1. Cross section showing NSM details.

3.3.2. MBrace Composite Strengthening System.

This composite system is manufactured by Master Builders Technologies, Inc., Cleveland, OH. The system consisted of four basic components, CF-130 unidirectional carbon fiber sheets and three, two-component, resins that when combined, form an FRP laminate. The fibers are bonded using the three epoxy-based resins known as primer, putty filler, and saturant resin. The mechanical properties of the carbon fiber sheets are given in Table 3.2. The components of MBrace strengthening system are illustrated in Figure 3.2. The primer is applied to improve the bond of the composite system to the base concrete by penetrating the pores of the concrete. The putty is a thick, paste-like epoxy used to fill bug holes, surface defects, and level uneven spots.

Table 3.2. Mechanical Properties of MBrace CF 130 Carbon Fiber Reinforcement.

Thickness in (mm)	Design Strength ksi (MPa)	Design Strain in/in or mm/mm	Tensile Modulus ksi (GPa)
0.0065 (0.165)	550 (3800)	0.017	33,000 (228)

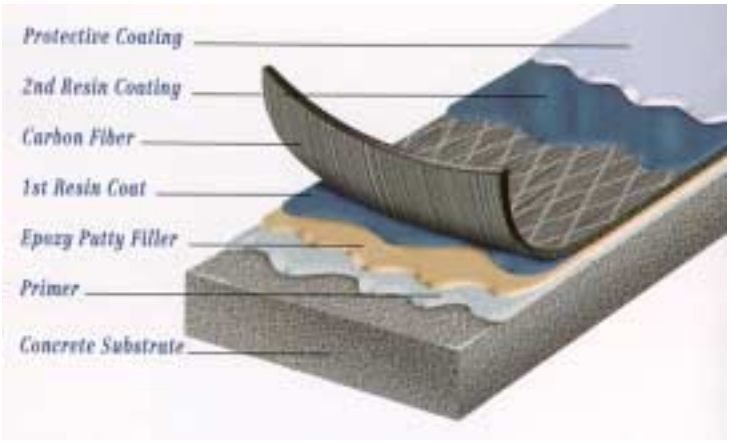

Figure 3.2. Components of the MBrace FRP composite strengthening system.

Quality bond between the composite system and concrete is crucial for the effectiveness of the system. If the FRP follows the contour of the irregular concrete surface, the curvature of the laminate may initiate pull-off forces, creating a localized delamination and jeopardizing the strength of the system. Bridging over formwork marks may result in stress concentration and cause the fibers to rupture at load levels lower than anticipated in the design.

3.4. STRENGTHENING DESIGN

The design of strengthening with surface bonded FRP composites is described in detail in Chapter 6. To avoid repetition, detailed calculations will not be given here, but a summary of the design approach is provided.

The design of FRP strengthening may involve many unknowns. The stresses in each of the materials at failure will depend on the strain distribution and the governing failure mode. Because of the number of variables involved, there is no closed form solution to determine the

flexural capacity failure mode directly. Strengthening design is based on iterative procedure in which the amount of added FRP is varied and the section capacity is calculated. This process is continued until the desired nominal moment capacity is achieved. Iteration to determine FRP amount is made simple by setting up a spreadsheet or by using any software for numerical calculations.

The first step in strengthening design is to estimate the required amount of FRP reinforcement. This could be estimated from the additional tensile force, T, needed to upgrade the moment capacity.

$$T = \frac{M_{n,str} - M_n}{0.90 \cdot d} \tag{3.4}$$

In which $M_{n,str}$ is the desired nominal moment capacity calculated as follows:

$$M_{n,str} = \frac{M_u}{\phi} \tag{3.5}$$

The initial cross-sectional area of FRP, A_f, is then determined as follows:

$$A_f = \frac{T}{R \cdot f_{fu}} \tag{3.6}$$

Where R is a reduction factor that accounts for the novelty of the strengthening system. There is no predetermined value for R. Its value is used at the discretion of the designing engineer and may vary for the different FRP strengthening systems. Since an objective of this research program was to verify FRP strengthening design methodology, this factor was taken as 1.0.

The iterative strengthening design approach was carried out using this initial amount of FRP reinforcement. FRP amount was varied until the desired capacity was achieved. Based on this approach, the design called for 0.042 in^2/ft (89 mm^2/m) of CFRP sheets and 0.12 in^2/ft (254 mm^2/m) of CFRP NSM rods. Summaries of the strengthening design are given in Appendix B. Based on this, the equivalent width of CFRP sheet per unit strip, w_f, is determined as follows:

$$w_f = \frac{A_f}{n \cdot t_f} \tag{3.7}$$

In which n is the number of CFRP plies and t_f is the thickness of each ply. The spacing of the NSM rods, S_{nsm}, is determined as follows:

$$S_{nsm} = \frac{A_{rod}}{A_{f,n}} . W_s \tag{3.8}$$

In which A_{rod} is the cross-sectional area of one NSM rod and $A_{f,n}$ is the required amount of NSM FRP. The results of the strengthening design are given in Table 3.3.

Table 3.3. Summary of Decks Strengthening Design Calculations.

	ε_{cc}	β_1	α_1	c	ε_f	f_f	ε_s	f_s	M_n
NSM	0.00214	0.818	0.915	3.53	0.00837	143.9	0.00787	33.0	102
Sheets	0.003	0.833	0.900	3.51	0.01240	409.3	0.01162	33.0	102

According to these calculations, the design called for eight, 20-in (500 mm) wide, single-ply CFRP strips on the deck soffit, which produced a capacity of 102 ft-k/ft (453 kN-m/m) and failure governed by concrete crushing. Similarly, the required number of near-surface mounted reinforcement was determined to be 20 rods spaced at 15 in. (375 mm), which produce a capacity of 102.5 ft-k/ft (456 kN-m/m) and a mode of failure governed by the rupture of FRP rods. Summary of the flexural capacity requirements for the bridge decks and strengthened capacity is given in Table 3.4. The required amounts of FRP required for deck strengthening are given in Table 3.5. The strengthening schemes of the bridge decks are shown in Figure 3.3.

3.5. INSTALLATION OF THE NSM CFRP RODS

The required number of near-surface mounted rods to strengthen the west deck of the bridge (deck 1) was determined to be 20, $^{7}/_{16}$ in. (11 mm) diameter, CFRP rods spaced at 15 in. (375 mm). The FRP rods were staggered such that at least 50% of the area of FRP reinforcement extended to the support, as shown in Figure 3.4. The rods were embedded in 20 ft (6.6 m) long, ¾ in. (19 mm) deep, and $^{9}/_{16}$ in. (14 mm) wide grooves cut onto the soffit of the bridge deck parallel to its longitudinal axis. Groove dimensions were chosen based on the previous experience of the research team.

The NSM rods were installed in grooves made by making two parallel saw cuts on the concrete surface using hand-held grinders with a diamond tip masonry cutting wheels. The two cuts were spaced at a distance equal to the desired groove width. The concrete in between the two cuts was then chipped off, thus creating the groove.

Table 3.4. Current and Upgraded Flexural Capacity in ft-k/ft of a Typical Bridge Deck.

Dead Moment ft-k/ft (kN-m/m)	Induced Live Moment Plus Impact ft-k/ft (kN-m/m)		Required Nominal Capacity ft-k/ft (kN-m/m)		Current Nominal Capacity ft-k/ft (kN-m/m)	Upgraded Capacity ft-k/ft (kN-m/m)
	HS20	HS20 Mod.	HS20	HS20 Mod.		
22.6 (100)	25.3 (113)	31.6 (141)	93.7 (417)	108.9 (484)	79.2 (352)	102 (458)
Required Strengthening			18%	37%	N/A	30 %

Table 3.5. Required Materials for the Strengthening of Bridge Deck.

Strengthening Material	Design Requirement	Quantity	Linear ft (m)
7/16" ϕ – CFRP rods	20'-0" long CFRP rods @ 15" o.c.	20 rods	400 (122)
20" wide - CF-130 sheets	22'-6" long, single ply @ 37.5" o.c.	8 sheets	180 (55)

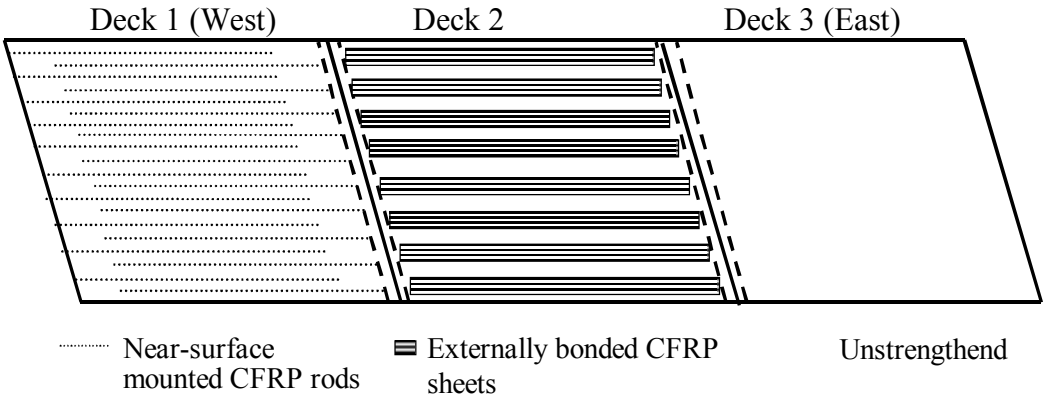

Figure 3.3. Bridge deck strengthening schemes.

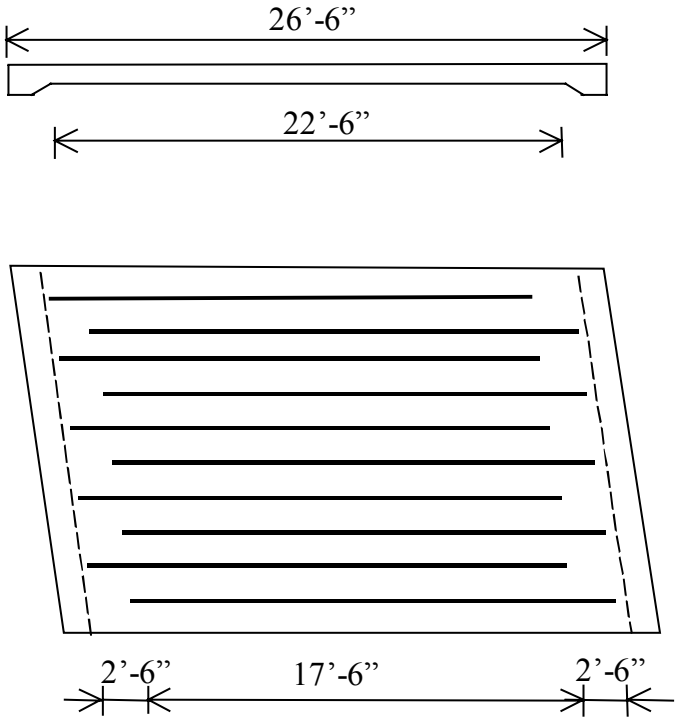

Figure 3.4. Deck strengthened with NSM CFRP rods.

Grooves were cleaned using sandblasting to remove all loose particles and dust. To apply the NSM rod, each groove was initially filled half way with a high viscosity epoxy adhesive compatible with the FRP systems. An FRP rod was then placed into the groove and lightly pressed in place. This action forced the adhesive to flow around the rod and cover the sides of the groove. The FRP rods were held in place using wooden wedges at an appropriate spacing. The grooves were then filled with the same adhesive and the surface was leveled. Photos showing the installation of the NSM rods are shown in Figures 3.5 through 3.8.

Figure 3.5. Installing the CFRP rods after filling the grooves halfway with epoxy paste.

Figure 3.6. Filling the groove with epoxy paste after installing the CFRP rods.

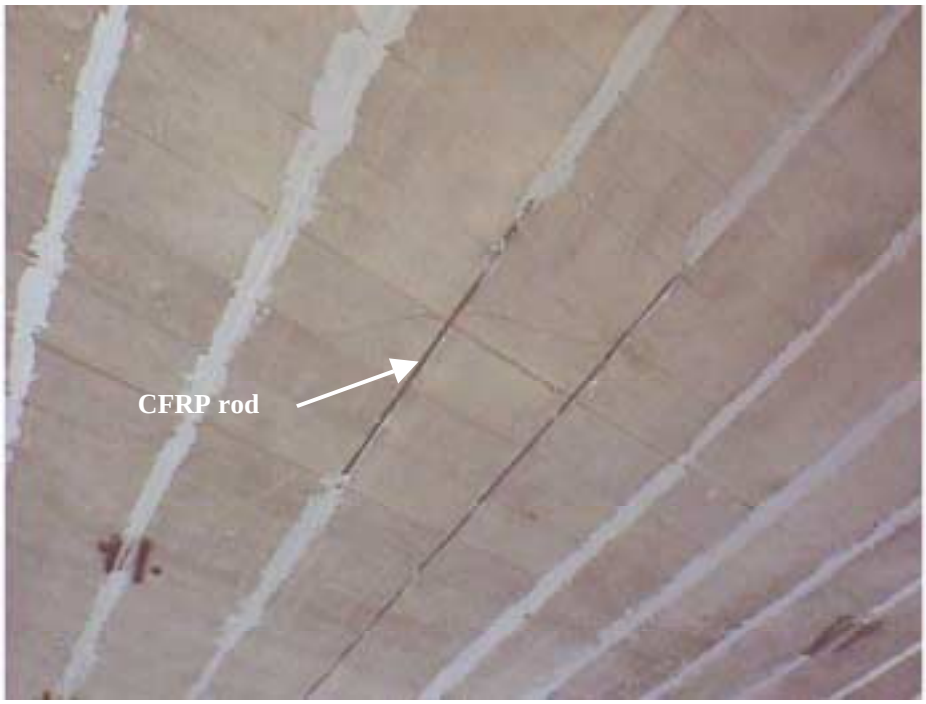

Figure 3.7. FRP rods before applying the second layer of paste.

Figure 3.8. Deck 1 after strengthening with NSM rods.

3.6. INSTALLATION OF CFRP SHEETS

The middle deck of the bridge (deck 2) was strengthened with eight, 20-in (500-mm) wide, single-ply, CFRP sheets. The sheets were spaced at 37.5 in. (950 mm) on centers with a clear distance of 17.5 in. (444 mm) in-between and ran the entire length of the slab, as shown in Figure 3.9. The FRP sheets were applied in accordance with the specifications of the composite system manufacturer (MBT, 1998). A certified specialty contractor applied the FRP strengthening system.

Prior to applying the FRP, existing form lines on the deck soffit from the original construction were ground smooth with hand grinders and the entire slab was lightly sandblasted to remove any loose material and laitance; and to provide an open pore structure. The primer was applied to the concrete area to receive FRP using a nap roller and was allowed to cure for approximately two hours. The putty was applied using a trowel. Immediately after the putty was applied, the first coat of saturant was applied over the entire area to receive the FRP using a roller. A strip of CFRP was then measured, cut, and applied on top of the saturant similar to wallpaper. One end of the FRP sheet was first placed on the slab and pressed into the saturant and the sheet was gradually attached by pressing it into the saturant. The sheet was pressed again using a "bubble roller" to eliminates the entrapped air between the fibers and resin and ensures the full impregnation of the FRP sheet with resin. The second and final layer of impregnating resin was then applied and the system was pressed with a bubble roller once again. After allowing the system to cure, the bonded laminates were inspected for voids and spots of delamination (none was detected). An additional, 5 ft (1.5 m) long, sheet of CFRP was attached to the side of the cap beam for pull-off bond strength tests, as shown in Figure 3.10.

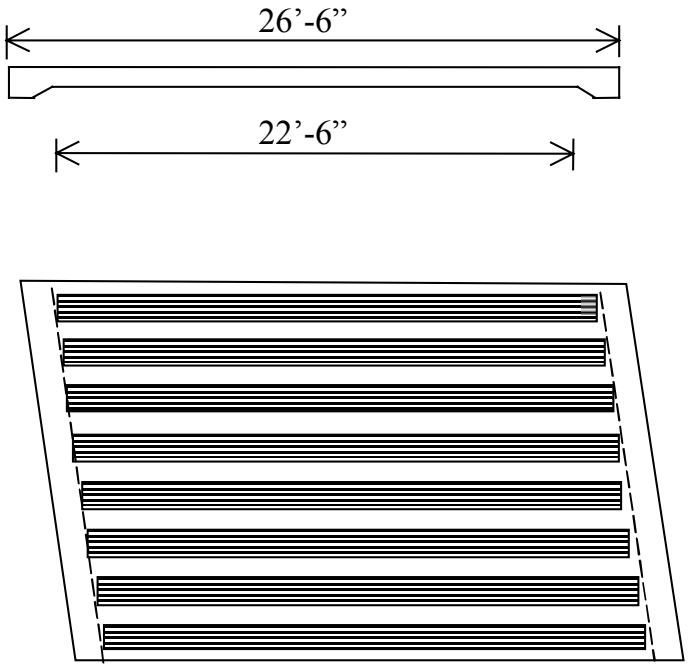

Figure 3.9. Deck strengthening with FRP sheets.

Figure 3.10. Deck 2 after strengthening with CFRP sheets.

3.7. BOND OF CFRP SHEETS

In total, six pull-off tests were conducted on the CFRP sheets. Four tests were conducted before testing deck 2 to failure. The tests were conducted on the additional CFRP sheet that was bonded to the side of a cap beam. Locations of the four tests are shown in Figure 3.11. Two additional tests were conducted after testing deck 2. The two tests were done on one of the sheets bonded to the bridge deck at locations closer to the end of a sheet, where no damage due to testing was detected, as shown in Figure 3.12.

Tests were conducted in accordance with the recommended test methods for direct tension pull-off tests of surface bonded sheets (Benmokrane et al., 1999).

The load was applied using the apparatus shown in Figure 3.13. The loading apparatus has an adhesion fixture with a 2-in^2 (1290 mm^2) flat surface on one end and can be screwed to the loading apparatus on the other end. A 3000-psi (20.7-MPa), 5-minute, bonding agent was used to bond the adhesion fixtures to the FRP sheet. The maximum pull-off load is obtained from a force indicator. The surface of the FRP sheet was cleaned using medium grid sandpaper, after which the surface was wiped with a dry and clean cloth. An adhesion fixture was bonded to the surface of the FRP and allowed to cure for 30 minutes. A core drill, with 2-in. diameter on the inside, was used to cut through the FRP and the substrate concrete to a depth of about 0.25 in. into the concrete. Figure 3.14 shows a close up of a prepared adhesion fixture. The loading apparatus was then attached to the adhesion fixture, force indicator set to zero, and load was applied until the fixture was pulled off. The pull-off strength was computed by dividing the maximum indicated load by the surface area of the adhesion fixture.

According to the recommendations, the preferred mode of failure is a tension failure within the surface concrete at a stress level in excess of 200 psi (1.38 MPa). The pull-off strength of the six tests varied from 200 to 1050 psi (1.38 to 7.23 MPa) with an average of 632 psi (4.35 MPa). Test #2 was the only test in which failure occurred in the concrete. The pull-off strength from this test was 386 psi (2.66 MPa). The failure in all other tests occurred at the adhesion fixture/ FRP interface (bond failure).

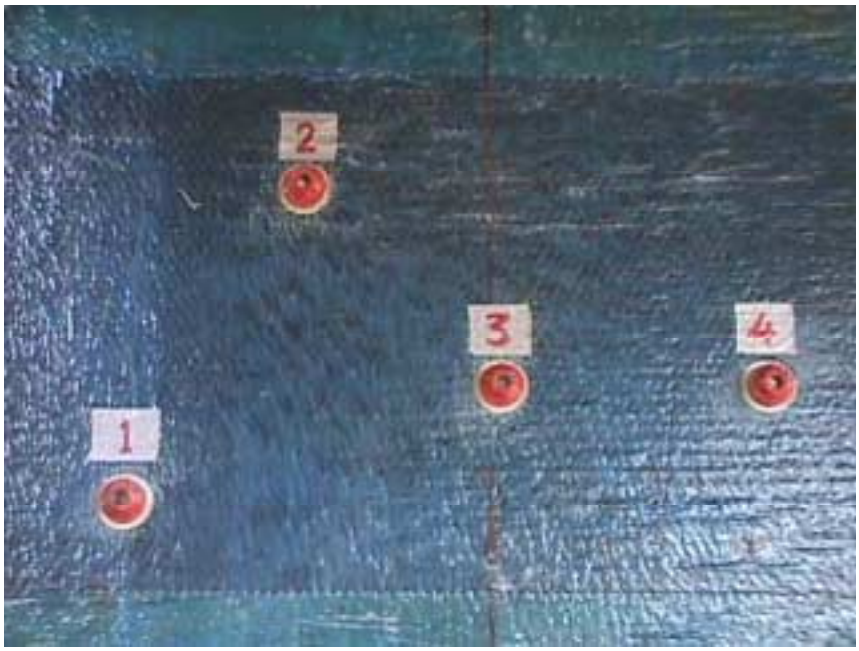

Figure 3.11. Locations of the pull-off tests conducted on the cap beam

Figure 3.12. Locations of the pull-off tests conducted on bridge deck.

Figure 3.13. Adhesion fixture bonded to the FRP sheet.

Figure 3.14. Loading apparatus attached to the fixture.

4. TEST SET UP AND INSTRUMENTATION

4.1. GENERAL

Preliminary analysis of the simply supported bridge decks indicated that the total life load capacity was 402 kips (1788 kN). This capacity was based on assumed concrete strength of 2500 psi (17.2 MPa) and steel yield strength of 33,000 psi (227 MPa). To account for higher material strengths, uncertainties related to support conditions (e.g., existence of some fixity), and the additional load requirement due to strengthening, the loading system was designed to produce a total external load of 800 kips (3558 kN). This level of loading was applied by means of hydraulic jacks.

Different loading/reaction configurations were investigated including the driving of small piles under the decks to provide the loading reaction. Due to the low clearance under the bridge, which was as low as 7.5 ft (2.3 m), most of these configurations were ruled out because it was not possible to operate heavy machinery under the bridge. A decision was finally made to construct a steel reaction frame consisting of steel girders and spreader beams to create a closed loop test setup. A closed-loop configuration ensured that only the decks were loaded and that the cap beams and the piers were not carrying any load other than their self-weight and the weight of the decks and the loading system.

4.2. LOADING CONFIGURATION

Figure 4.1 illustrates a plan of the test setup for the middle deck (deck 2). This configuration was also used to test decks 1 and 3 with simple modification to produce the end reaction at the abutment. The loading system comprised of an electric pump, four hydraulic jacks, and control valves. Hoses connected the jacks in parallel so that equal pressure was achieved in the jacks.

The four hydraulic jacks rested on the bridge deck on a skew line at mid-span, parallel to the skewed bents of the bridge. The jacks were spaced four feet (1.2 m) apart. The two jacks on the outside were approximately seven feet (2.1 m) from the edge of the deck slab, as seen in Figure 4.2. Locations of the hydraulic jacks on the decks are shown in Figure 4.3. Each jack had a 200 kips (890 kN) capacity and 18 in. (457 mm) stroke. Prior to placing the jacks, four two-inch (50-mm) diameter cores were drilled at their intended locations. The jacks were then placed and commercially available, high strength steel rods were dropped through the jacks and the holes. Dywidag-Systems International, Bolingbrook, IL, manufactures the rods used in this application. The Dywidag rods were made of grade 150-ksi (1033-MPa) steel and had a diameter of $1^3/_8$ in. (35 mm). Dywidag rods are patented threaded rods that come with accessories, such as high strength plates and nuts, which made them very suitable for this test. The rods were used to transfer the load from the jacks to the reaction system, as shown in Figure 4.2. The jacks pulled against two steel spreader beams located under the deck. Each spreader beam was made of two standard W14 x 90 steel shapes (see Figure 4.2). Steel strips were used to join the two W14 x 90 shapes together through welding to form one spreader beam. A clearance of two inches (50-mm) was provided between the two shapes to allow for a Dywidag rod to go through the spreader beam. Details of the spreader beam are shown in Figure 4.4.

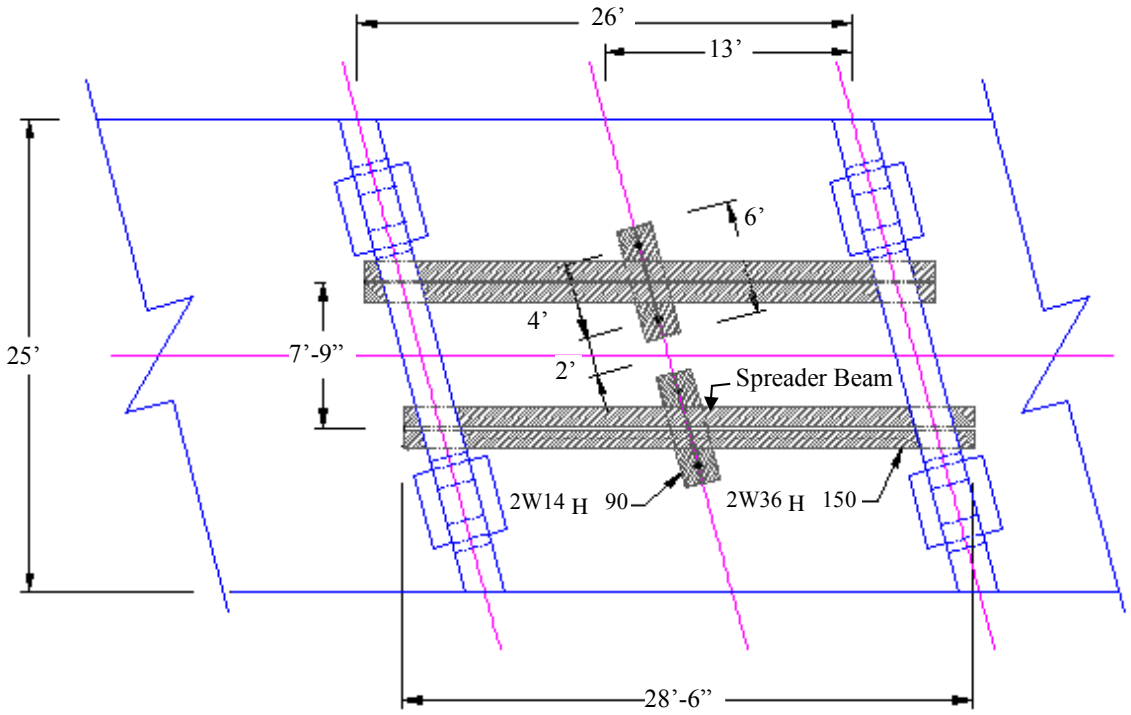

Note: 1ft = 0.305 m, 1 in. = 25.4 mm

Figure 4.1. Test setup plan for the middle deck showing points of load application.

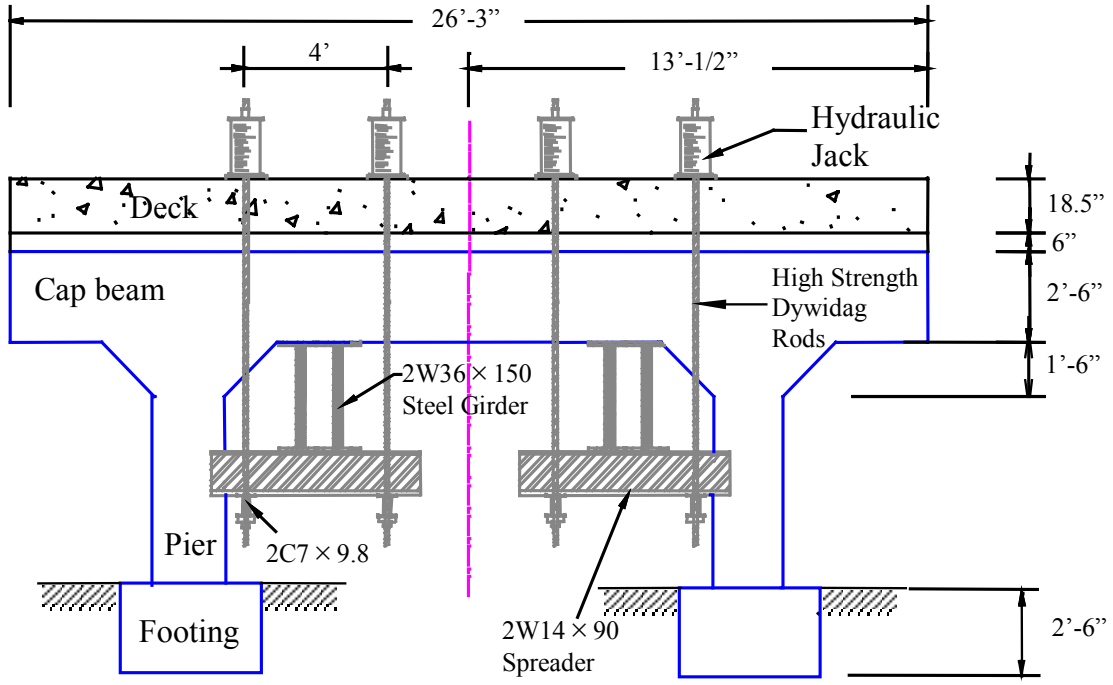

Note: 1ft = 0.305 m, 1 in. = 25.4 mm

Figure 4.2. Section at the middle deck showing details of the loading apparatus.

(a) Jack locations on deck 2

(b) Jack locations on deck 3

Figure 4.3. Location of the hydraulic jacks on the bridge deck.

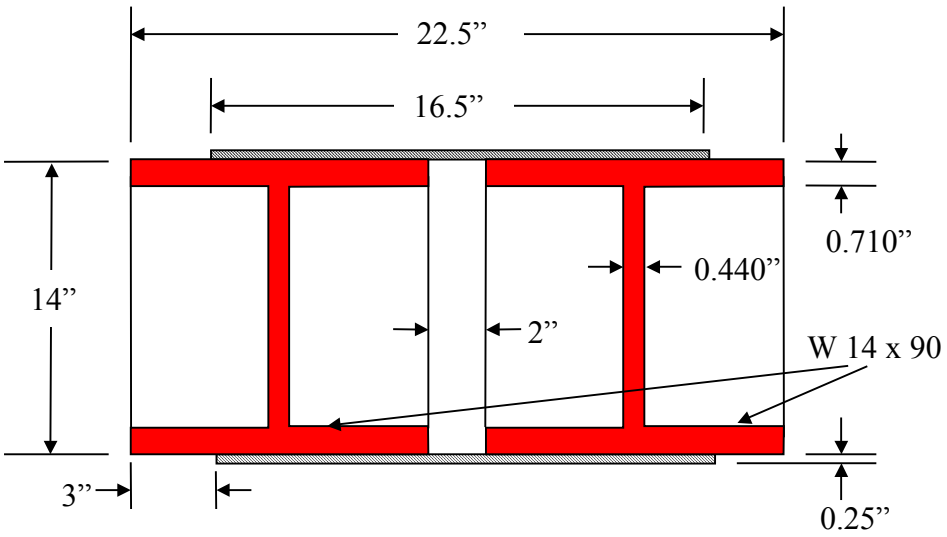

(a) Cross-section of a spreader beam

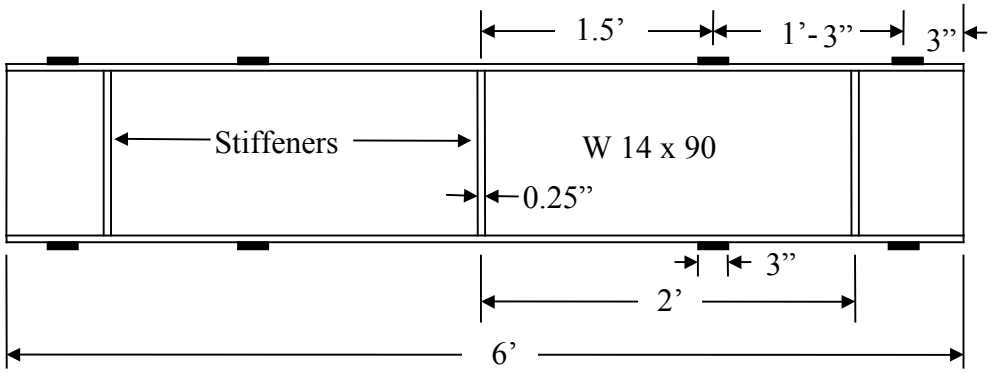

(b) Side view of a spreader beam

Figure 4.4. Details of a spreader beam.

To avoid damage of the spreader beam, a distribution beam made of two back-to-back C7 x 9.8 standard steel channels were used to distribute the load across the width of a spreader beam, as shown in Figure 4.5. Each spreader beam transferred the load to a steel girder made of two W36 x 150 standard steel shapes. Welded steel strips were used to join the two shapes together to form the girder. Two inches (50-mm) of clearance was provided between the two steel shapes to allow for a Dywidag rod to go through the girder when needed. Each girder reacted against the cap beams (see Figures 4.1 and 4.2). Details of a girder are shown in Figure 4.6. A local contractor assembled the test setup components mentioned above, as shown in Figure 4.7. Figure 4.8 shows the unloading of the test setup components at the bridge site.

The loading system described above reacted against the cap beams. To provide the reaction at the abutments, two rectangular cuts were made on each abutment to accommodate the ends of the girders. The upper edge of each cut was aligned with the bottom of the cap beams to

ensure levelness of the girders. Once the saw cuts were made, an attempt was made to remove the concrete using a jackhammer, as shown in Figure 4.9.

To facilitate this operation, the soil behind the abutment walls was excavated with a backhoe, as shown in Figure 4.10. This provided the advantage of extra workspace for the construction workers to jackhammer the concrete on both sides of the abutment. Figure 4.11 shows this process.

Each of the girders weighed about 8,200 lb (36.4 kN), and with the low clearance of the bridge, it was not possible to use a forklift to move them around (see Figure 4.12). The girders were dragged under the bridge by chaining them to a backhoe. A chain was then dropped through the holes made on the deck, hooked to the girder, and used to lift it using the backhoe. To avoid overloading the deck prior to the initiation of the destructive testing, the backhoe lifted the girders from a location next to the bridge. Once the girders were lifted, wooden blocks were stacked under their ends to seat them. The rest of the loading system was then assembled. Figure 4.13 shows the assembled setup for an end span showing the end of a girder resting in the cuts made in the abutment. Similarly, Figure 4.14 shows the assembled tests setup for the middle deck.

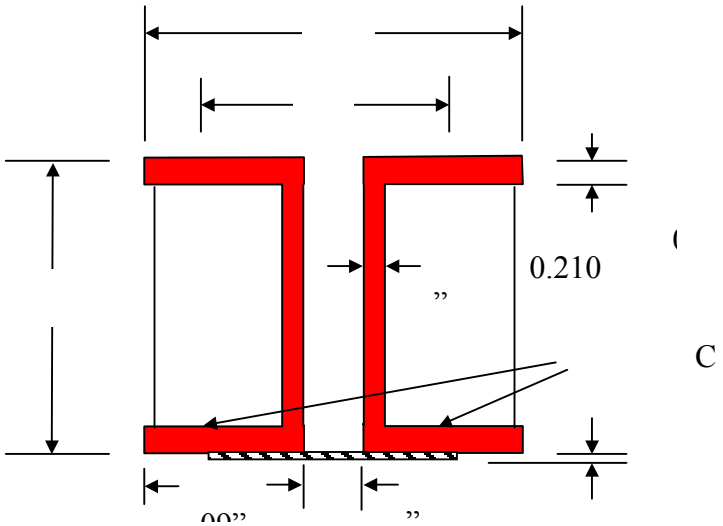

(a) Cross-section of a distribution beam

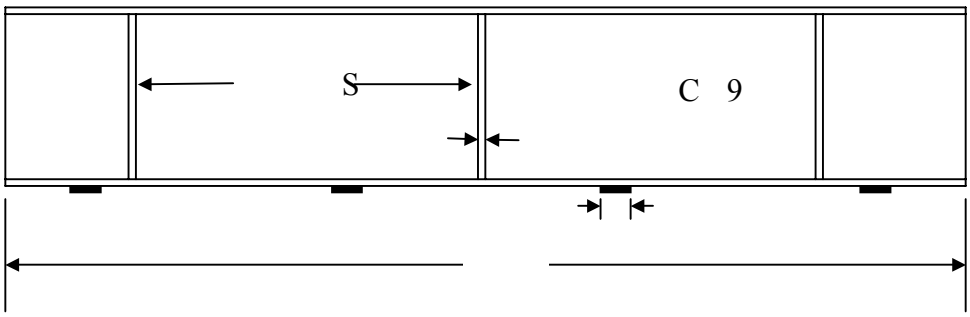

(b) Side view of a distribution beam

Figure 4.5. Details of a distribution beam.

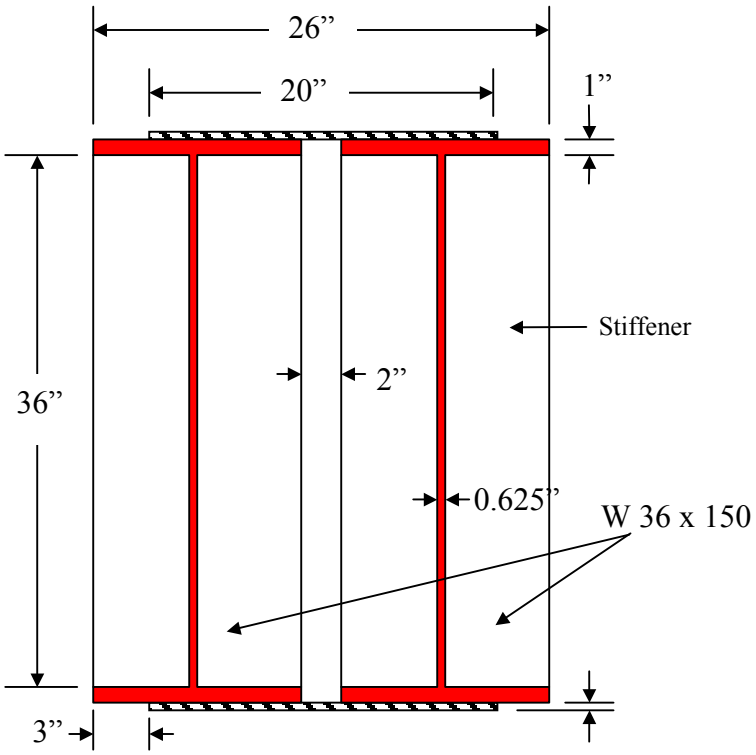

(a) Cross section of a girder

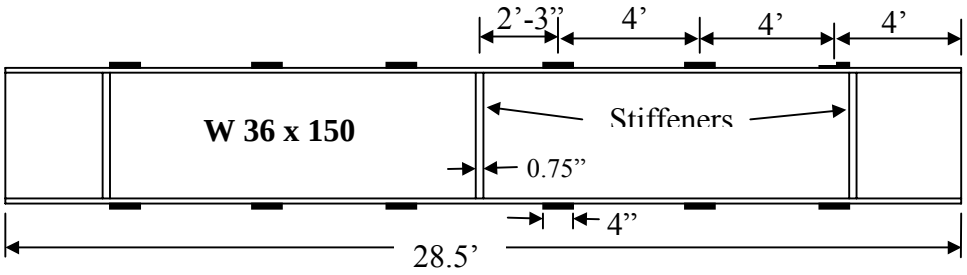

(b) Side vie of a girder

Figure 4.6. Details of a steel girder.

Figure 4.7. Manufacturing the steel girders.

Figure 4.8. Unloading the test setup components at the bridge site.

Figure 4.9. Cutting the bridge abutment.

Figure 4.10. Excavating behind the bridge abutment.

Figure 4.11. Bridge abutment after excavation and cutting.

Figure 4.12. Installation of the steel girders.

Figure 4.13. Assembled test setup for an end deck.

Figure 4.14. Assembled test setup for the middle deck (deck 2).

4.3. DECK PREPARATION FOR TESTING

The original plans of the bridge indicated that shear keys existed between the deck and the cap beam at the two bents of the bridge. However, field inspection of the bridge showed that shear keys were not implemented during construction.

To minimize the influence of deck end fixity on the behavior of the decks, the joints between deck slabs were saw cut to remove filler material. In addition, the parapet walls were saw cut at five feet (1.5 m) intervals to minimize their contribution to the stiffness of the decks. The saw cuts created gaps that were approximately ¼ in. (6 mm) wide. However, upon testing of deck 1, it was found that these narrow cuts were not sufficient to eliminate the contribution of the parapet walls. Therefore, prior to testing decks 2 and 3, the cuts were enlarged using a jackhammer. Photographs showing the cutting of the decks joints and the parapet walls are given in Figures 4.15 and 4.16.

4.4. INSTRUMENTATION

An objective of the research program was to evaluate the flexural behavior of the decks. Instrumentation was required to permit reliable correlation between the analytically predicted and the measured responses of the bridge. Instrumentation for bridge decks testing included strain gages to measure reinforcement strains, Linear Variable Differential Transformers (LVDTs) to measure deflections and a load cell to measure the applied load.

4.4.1. Strain Measurement.

Strain measurements were achieved using foil strain gages manufactured by Vishay Measurement Group, Inc., Raleigh, North Carolina. The strain gages were attached to the steel and FRP reinforcement. Figure 4.17 shows the layout of the strain gages on the three decks. The numbers of strain gages for steel reinforcement used on decks 1, 2, and 3 were 6, 15, and 19, respectively. The numbers of strain gages for FRP reinforcement used on respective decks were 13, 15, and 0. To attach the strain gages to the steel reinforcement, the concrete cover was chipped away at the predetermined locations and the steel reinforcement was exposed. The surface of the steel bars was smooth polished using a high-speed rotary tool. The strain gages were bonded such that they measured the longitudinal strain of the reinforcement. After the application of the strain gages, they were coated using a product supplied by the manufacture to provide them with environmental and mechanical protection. The coating consisted of a layer of butyl rubber sealant and layer of neoprene rubber sheet. For the deck to receive CFRP sheets the voids at the exposed steel bars were filled with epoxy paste and the surface of the concrete was leveled. Strain gages were also installed on the CFRP sheets after they were bonded to the deck soffit and allowed to cure. Strain gages were attached to the CFRP rods prior to their installation of the bridge deck.

4.4.2. Deflection Measurements.

Ten LVDTs were used to measure the deflection of each deck. The LVDTs were arranged along two lines parallel to the axis of the bridge, five LVDTs on each line. LVDT lines were at mid-width and quarter-width of each deck. Placement details and spacing of the LVDTs are shown in Figure 4.18. To avoid any possible instrument damage and testing delays caused by possible flooding of the creek, the LVDTs were mounted on two steel beams that spanned the bridge deck, as shown in Figure 4.19. Each beam was made of a 23 ft-4 in. (7.1 m) long, C8 x 11.5, standard steel channel.

Figure 4.15. Cutting bridge deck joints.

Figure 4.16. Cutting bridge parapet walls.

4.4.3. Load Measurement.

The load measurement was achieved using a 200-kips (90-Ton) capacity load cell. The load cell had a donut shape with a hollow core. It was placed between the hydraulic jack and the plate and nut on the Dywidag rod.

4.4.4. Data Acquisition.

Data was acquired using the data acquisition recreational vehicle developed at the University of Missouri-Columbia. The vehicle houses two computers with five connection boxes. Each box can accommodate 19 strain gages and 5 LVDT connections. Since only 19 strain gage were used for deck 1 and 3, only one box was needed to acquire the data. Deck 2, however, had a total of 30 strain gages and more than one box needed to be used. Lists of the strain gages used on each deck and the associated channel number on the box are listed in Figure 4.22.

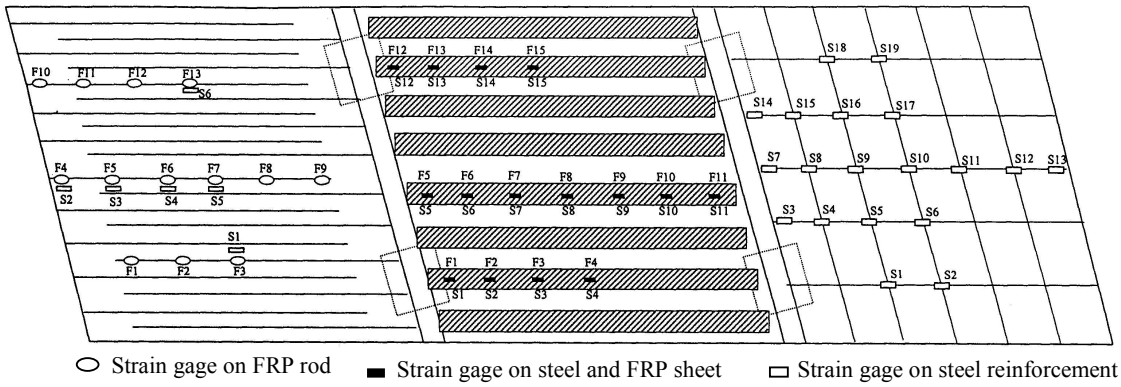

Figure 4.17. Location of strain gages on steel and FRP reinforcement.

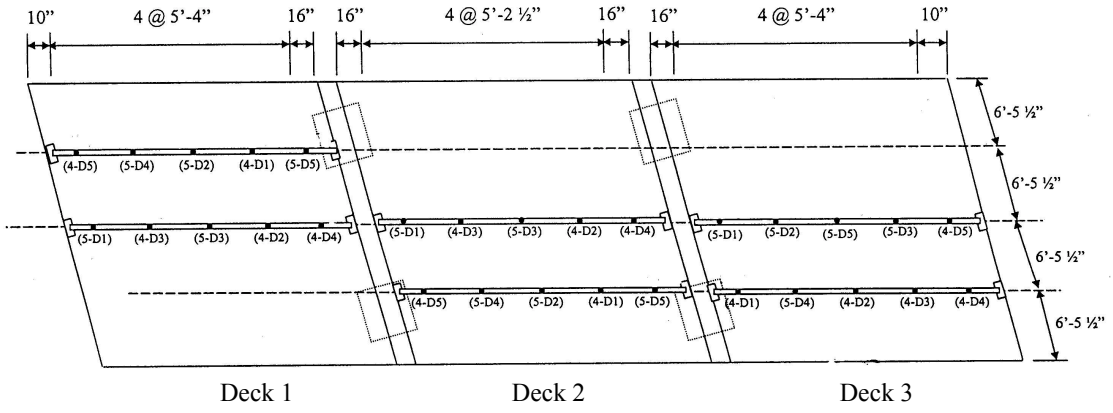

Figure 4.18. Location of the LVDTs on the bridge decks.

Figure 4.19. Support of the holder beam.

Figure 4.20. LVDTs attachment.

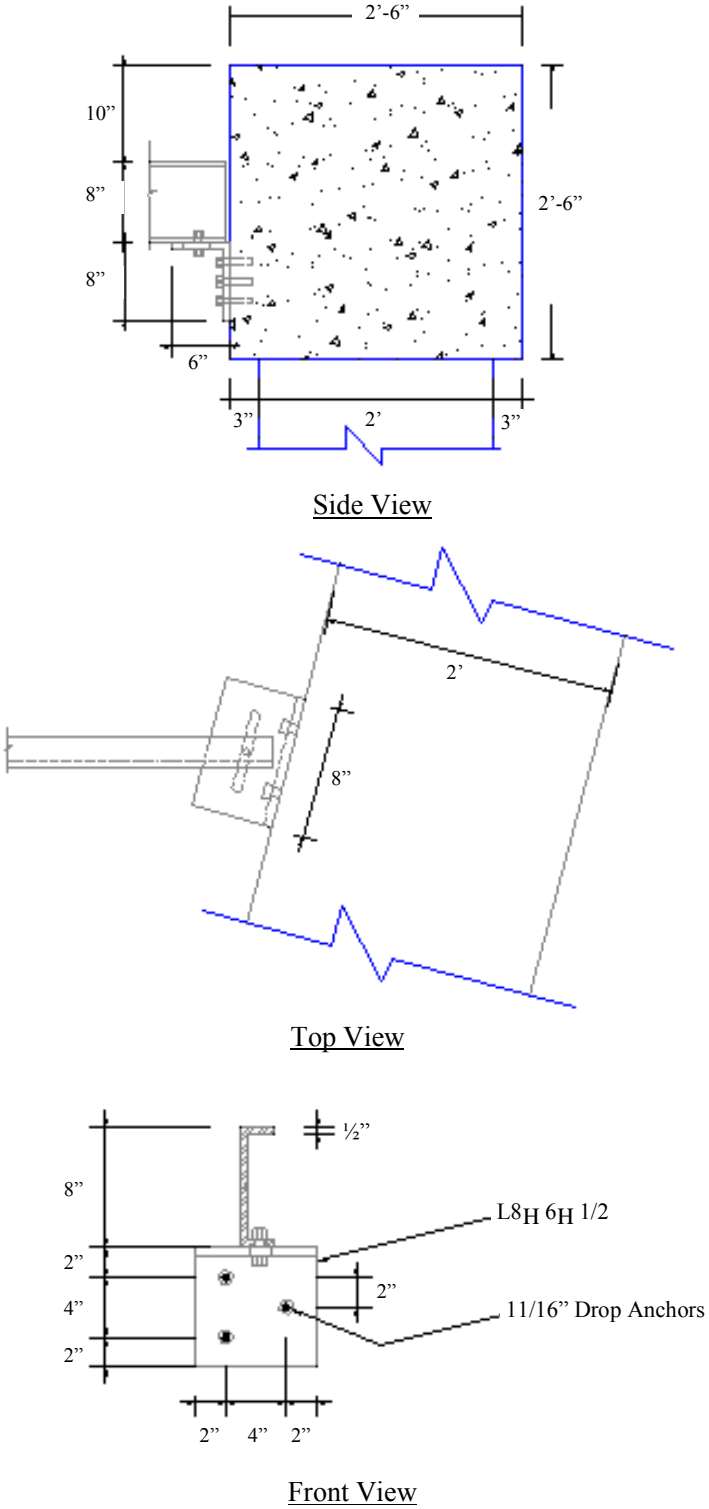

Figure 4.21. Details of the support for the holder beam for the LVDTs.

4.5. LOAD TEST PROTOCOL

The three decks of the bridge were tested to failure by applying quasi-static load cycles. Prior to testing, the LVDTs were adjusted, as shown in Figure 4.23. Unfortunately, it was found that some of the strain gages had failed due to exposure to the harsh environment for over six months. The transverse beams were leveled manually by tightening the nuts of the Dywidag rods above the hydraulic jacks, as shown in Figure 4.24. Data acquisition was then initiated and the steel girders were raised until they were in contact with the cap beams. The weights of the transverse beams and girders are therefore included as a part of the applied load.

The load was increased gradually until the desired load level was achieved. The load was maintained for a period of time until the readings of the strain gages and the LVDTs stabilized. The deck was then unloaded until the applied load reached zero and a second loading cycle was started. The magnitude of the maximum load applied in the successive load cycles was incremented until failure of the deck was achieved.

4.6. MATERIALS TESTS

After the completion of the deck destructive testing, concrete cylinders and coupons of steel reinforcement were obtained for material properties verification. In addition, pull-off tests were conducted to verify the bond between the CFRP sheets and the concrete surface.

4.6.1. Concrete

Twelve 4 in. x 8 in. (100 mm x 200 mm) cylindrical concrete cores were obtained from different locations of the bridge decks for laboratory evaluation of the concrete strength. Three of these concrete cylinders were tested under uniaxial compression to determine the compressive strength of the concrete, as shown in Figure 4.25. Test results indicated that the average concrete compressive strength was 8147 psi (56.2 MPa). Table 4.1 summarizes the results of concrete cylinder tests.

Deck 1 – Box 5

Channel	SG	Channel	SG
S1	S1	S11	F5
S2	S2	S12	F6
S3	S3	S13	F7
S4	S4	S14	F8
S5	S5	S15	F9
S6	S6	S16	F10
S7	F1	S17	F11
S8	F2	S18	F12
S9	F3	S19	F13
S10	F4		

Deck 2 Box 5

Channel	SG	Channel	SG
S1	F1	S11	S2
S2	F2	S12	S3
S3	F3	S13	S4
S4	F4	S14	S5
S5	F5	S15	S6
S6	F6	S16	S7
S7	F7	S17	S8
S8	F8	S18	S9
S9	F9		
S10	S1		

Deck 2 Box

Channel	SG	Channel	SG
S1	F10	S11	S14
S2	F11	S12	S15
S3	F12		
S4	F13		
S5	F14		
S6	F15		
S7	S10		
S8	S11		
S9	S12		
S10	S13		

Deck 3 – Box 5

Channel	SG	Channel	SG
S1	S1	S11	S11
S2	S2	S12	S12
S3	S3	S13	S13
S4	S4	S14	S14
S5	S5	S15	S15
S6	S6	S16	S16
S7	S7	S17	S17
S8	S8	S18	S18
S9	S9	S19	S19
S10	S10		

Figure 4.22. Data acquisition channels for strain gages.

Figure 4.23. Checking the strain gages prior to testing.

Figure 4.24. Tightening the nuts on the jacks in order to raise the steel girders.

Table 4.1. Results of Concrete Cylinder Tests.

Sample No.	Height in. (mm)	Diameter in. (mm)	Compressive Strength psi (MPa)
1	8.35 (212)	3.72 (94)	8,199 (56.5)
2	8.4 (213)	3.73 (94)	7,528 (51.9)
3	8.4 (213)	3.72 (94)	8,714 (60.1)
		Average	8,147 (56.2)

4.6.2. Reinforcing Steel.

Three coupons were obtained from the deck after the completion of the testing to failure of the decks. These were 24-inch (610 mm) long, deformed rebars. The three coupons were tested under uniaxial tension to determine their yielding and ultimate strengths. Test results indicated that the average yield strength was 43,333 psi (298 MPa) and the average ultimate strength was 70,844 psi (488 MPa). Table 4.2 summarizes the results of steel coupon tests.

Table 4.2. Results of Steel Coupon Tests.

Sample No.	Length in. (mm)	Yielding psi (MPa)	Ultimate Strength psi (MPa)
1	24 (610)	44,620 (308)	70,633 (487)
2	24 (610)	43,165 (298)	71,772 (495)
3	22 (610)	42,215 (291)	70,127 (484)
	Average	43,333 (299)	70,844 (488)

4.6.3. Summary of Material Strength Tests

The average concrete compressive strength of 8,147 psi and the average steel yield strength of 43,333 psi are significantly higher than the initial values for preliminary analyses and strengthening design. The compressive strength of concrete is more than 3 times higher than the assumed value of 2,500 psi while the yield strength is about 31 percent higher that the assumed value of 33,000 psi. Implication of strength variation on the behavior of the three decks is discussed further when examining experimental results. Summary of these findings is given in Table 4.3.

Table 4.3. Comparison of Assumed and Actual Material Properties.

	Concrete Strength psi (MPa)	Steel Yield Strength psi (MPa)
Assumed	2500 (17.2)	33,000 (227)
Actual	8147 (56)	43,333 (298)
% Difference	226	31

(a) Uniaxial compression test setup

(b) Tested specimen

Figure 4.25. Uniaxial compression test of concrete cores.

5. EXPERIMENTAL RESULTS

5.1. INTRODUCTION

The following sections will discuss the experimental results obtained from static testing to failure of the bridge decks. These include the measured loads, deflections, and reinforcement strains. Decks 1 and 2 were strengthened with NSM CFRP rods, and bonded CFRP sheets, respectively, to improve their flexural capacity by approximately 30%. Deck 3 was used as a benchmark. Each of the three decks was tested to failure using static load cycles. The maximum load applied in each cycle was incremented until failure was achieved.

5.2. DECK 1 – NSM CFRP RODS

A plot of the applied load vs. deflection of deck 1 is shown in Figure 5.1. From this figure, it can be seen that the deck was loaded in three cycles. For each cycle, the slope of the loading portion of the curve is an indicator of the stiffness of the deck at the beginning of the cycle. Observing the loading portions of the curve, it can be seen that up to the last loading cycle the deck had minimal change in stiffness, which indicates that the steel reinforcement did not yield. Residual deflection is related to the reduced stiffness of the deck due to cracking. Initiation of yielding can be detected from the change of slope of the deflection envelope. This occurred at approximately 450 kips (2003 kN). At this same load level, it was observed that the cuts on the parapet walls had closed, engaging them into the load resistance mechanism of the deck. As the load was increased beyond 450 kips, cracking of the hardened epoxy adhesive was heard.

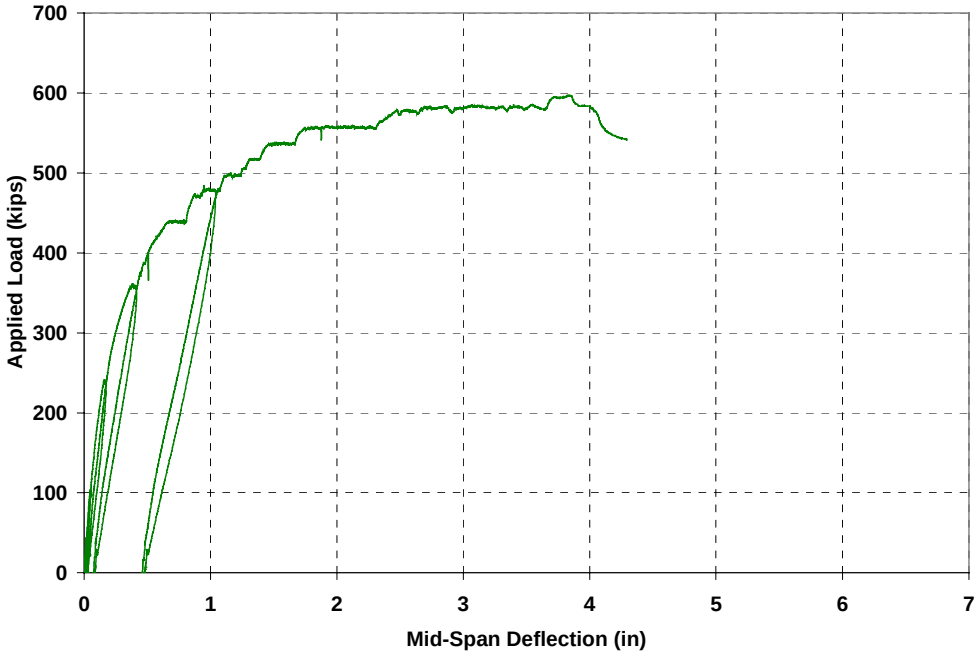

Note: 1 kip = 4.45 kN; 1 in = 25.4 mm

Figure 5.1. Experimental load-deflection relation for deck 1.

Although CFRP rods are not ductile, it can be seen from Figure 5.1 that some pseudo-ductile behavior was observed. This could be related to the internal slippage of the mounted rods at higher load levels as well as the gradual rupture of the rods at ultimate capacity. Failure occurred when some of the CFRP rods ruptured at mid-span at locations of the widest cracks. The failure load of this deck was 596 kips (2652 kN). Figures 5.2 and 5.3 show the failure of deck 1.

The measured deflections along the bridge axis at different load levels are shown in Figure 5.4. It can be seen from this figure that at lower load levels, the deflection was approximately proportional to the applied load. At higher load levels, the deflection started to increase much faster than the load due to stiffness degradation caused by the development of additional cracks. For example, when the load increased from 400 to 500 kips (1780 to 2225 kN) the deflection was more than double.

Figure 5.5 shows the measured deflections along a line at a quarter-point on the transverse axis of deck 1. Similar deflection behavior is observed on this line. The only difference is that the maximum measured deflection at mid-span was larger at the ultimate load. This could be related to the simple support/plate effect, in which the unsupported edges at mid-span are expected to deflect more than at the center of the deck due to minimal edge restraint. One of the LVDTs did not work close to maximum load because the deflection exceeded the range of the LVDT.

Figure 5.6 shows the measured strain of the steel reinforcement. Only four of the strain gages measured strain. The rest of the strain gages did not work due to exposure to harsh environment for a period of time. In this figure, it can be seen that the cracking of the deck initiated at approximately 235 kips (1045 kN). Between 235 and 430 kips (1045 and 1914 kN), the measured strain was proportional to the applied load. At that same load level, the cuts on the parapet walls closed causing an increase in the stiffness of the deck. Once the concrete of the parapet started to crush at about 557 kips (2479 kN), the steel reinforcement started to pick up strain again. The approximate steel strain at yielding was approximately 0.0018 in./in. (mm/mm). Similar behavior was observed on the measured strain of FRP, as shown in Figure 5.7. A number of the strain gages on the mounted FRP rods did not work.

In general, the measured strain in the reinforcement was dependant on the distance of the strain gage from the nearest crack. The closer the strain gage was to a crack, the higher the measured strain.

Figure 5.2. Cracks on the soffit of deck 1 after testing to failure.

Figure 5.3. Rupture of the mounted CFRP rods at different locations.

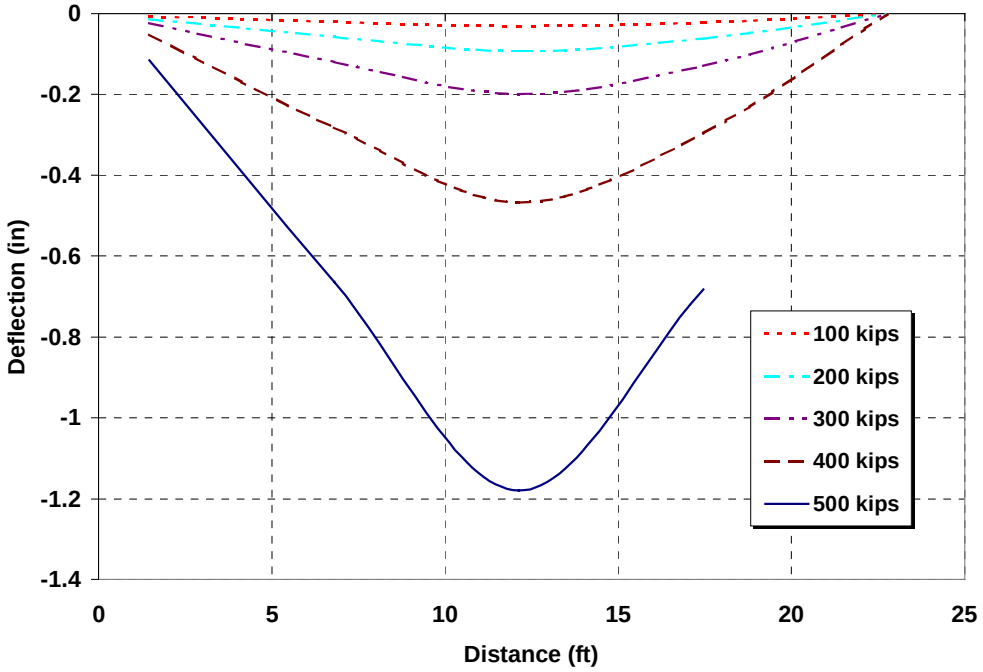

Note: 1 in = 25.4 mm; 1 ft = 0.305 m

Figure 5.4. Measured deflection along the longitudinal axis of deck 1.

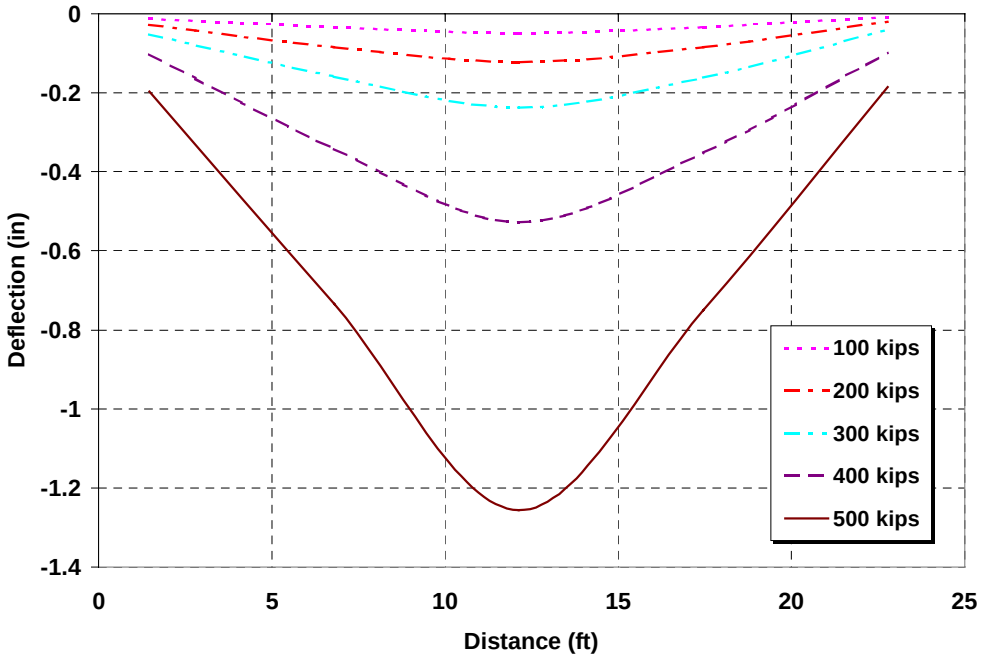

Note: 1 in = 25.4 mm; 1 ft = 0.305 m

Figure 5.5. Measured deflection along quarter-point on the transverse axis of deck 1.

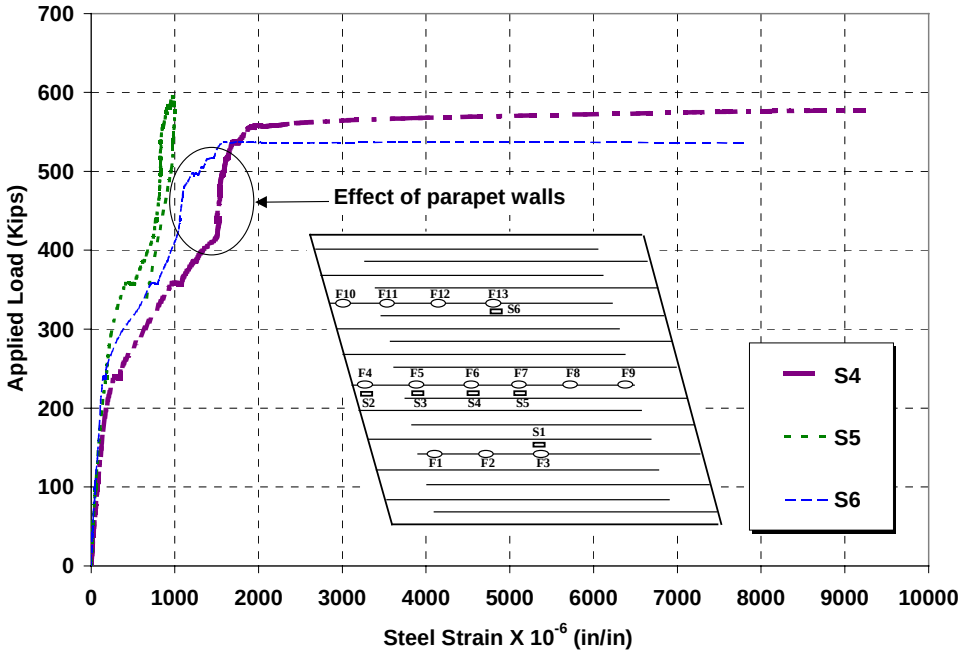

Note: 1 kip = 4.45 kN; 1 in/in = 1 mm/mm

Figure 5.6. Measured strain of the steel reinforcement of deck 1.

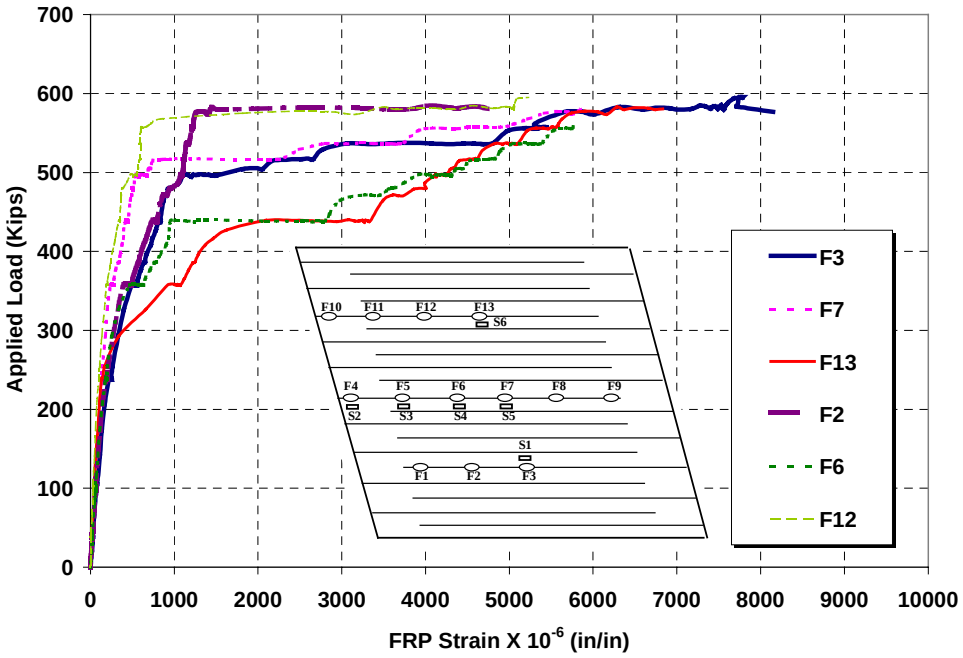

Note: 1 kip = 4.45 kN; 1 in/in = 1 mm/mm

Figure 5.7. Measured strain of the mounted CFRP rods for deck 1.

5.3. DECK 2 - BONDED CFRP SHEETS

The second deck of the bridge was strengthened with CFRP sheets. A plot of the applied load vs. deflection is shown in Figure 5.8. From this figure, it appears that steel yielding started at about 473 kips (2105 kN), where deflection started to increase under constant loading. Some residual defection was observed when the load was removed. Compared to the slope of the diagram right after cracking, the slope of the loading curve for the final cycle indicates that the stiffness did not degrade significantly. As the load was increased, cracking sounds from the rupture of the FRP sheets was heard. Rupture of the CFRP sheets rupture occurred at various locations along the original formlines of the deck. In addition, small strips of FRP started to peel-off. This gradual failure mode of CFRP sheets resulted in a pseudo-ductile behavior prior to failure. The final failure mode was a combination of rupture and delamination of the sheets. The failure load for this deck was 542 kips (2412 kN). Figures 5.9 and 5.10 show the failure of deck 2.

The measured deflections along the bridge axis at different load levels are shown in Figure 5.11. Deflections of this deck were smaller than those measured on deck 1 at similar load levels, indicating higher stiffness for deck 2. Figure 5.12 shows the measured deflections along a line at quarter-point on the transverse direction of deck 2. Similar to deck 1, the maximum measured deflection at quarter-point was larger than that at the center of the deck. The LVDTs closer to the support did not provide any measurement due to a bad connection. Figure 5.13 shows the measured strain of steel reinforcement. Most of the strain gages either did not work or provided corrupted data. Only three of the strain gages provide data. This figure indicates that the yielding of steel reinforcement is achieved at approximately 0.0017με, which is similar to that obtained for deck 1. The measured strain of FRP is shown in Figure 5.14. Strain gage F8, which was located at mid-span, measured higher strain than other strain gages. Strain measured started to increase rapidly close to ultimate.

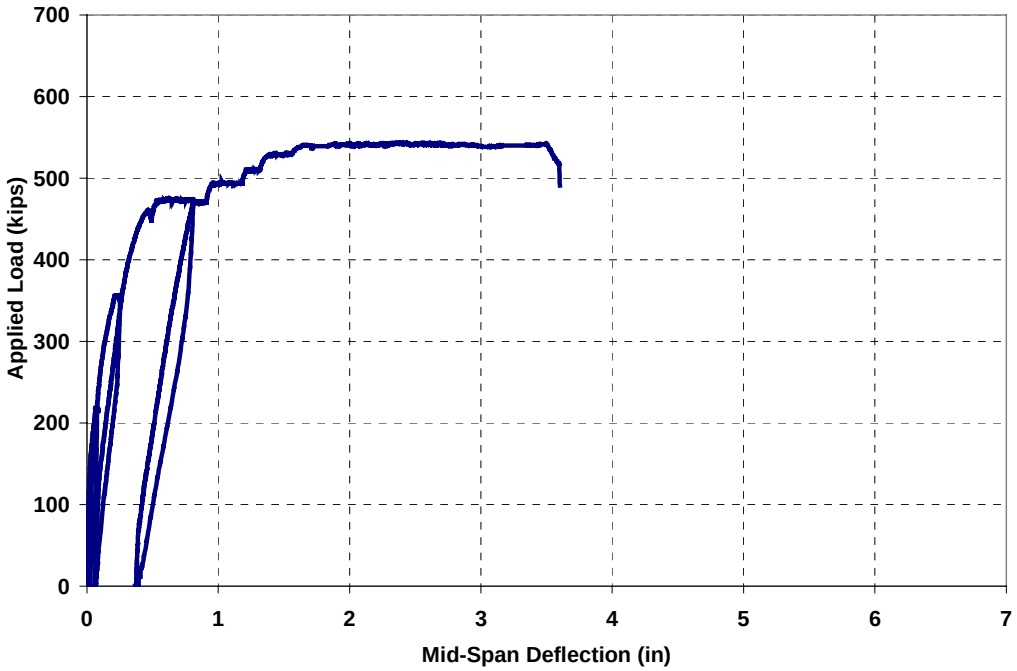

Note: 1 kip = 4.45 kN; 1 in = 25.4 mm

Figure 5.8. Experimental load-deflection relation for deck 2.

(a) Cracks on deck soffit

(b) Cracks on the side of the deck

Figure 5.9. Cracks on deck 2 after testing.

(a) Rupture of CFRP at formlines

(b) Peeling of CFRP sheets

(c) Close up showing peeling of CFRP sheets

Figure 5.10. Rupture of the Mounted CFRP at ultimate capacity.

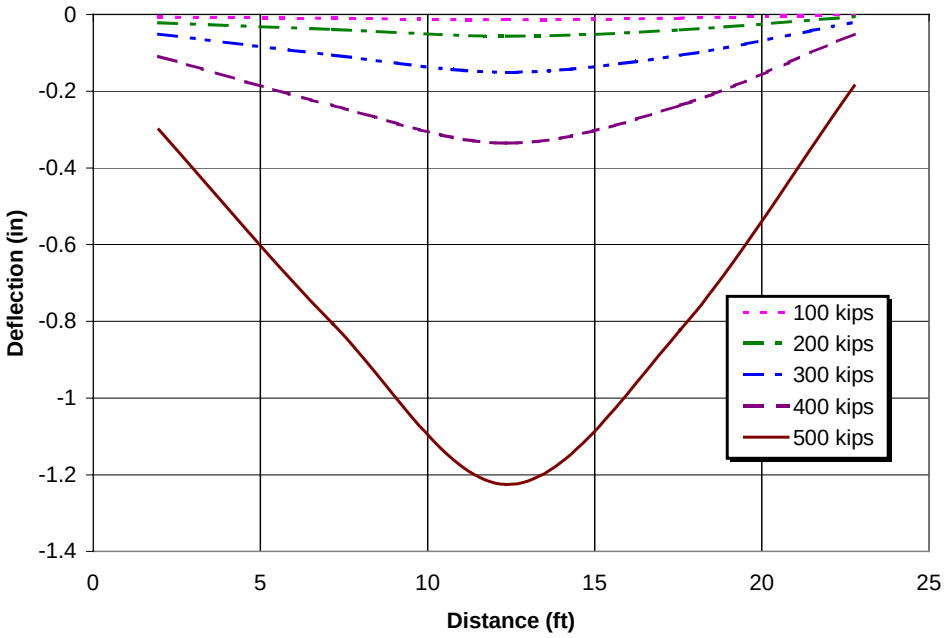

Note: 1 in = 25.4 mm; 1 ft = 0.305 m

Figure 5.11. Measured deflection along the longitudinal axis of deck 2.

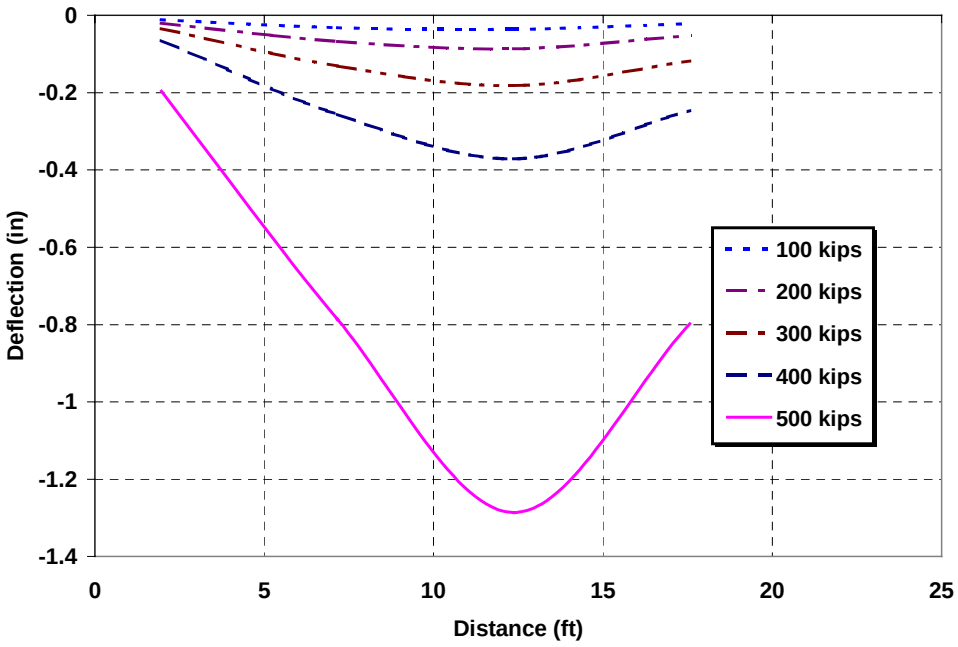

Note: 1 in = 25.4 mm; 1 ft = 0.305 m

Figure 5.12. Measured deflection along quarter-point on the transverse axis of deck 2.

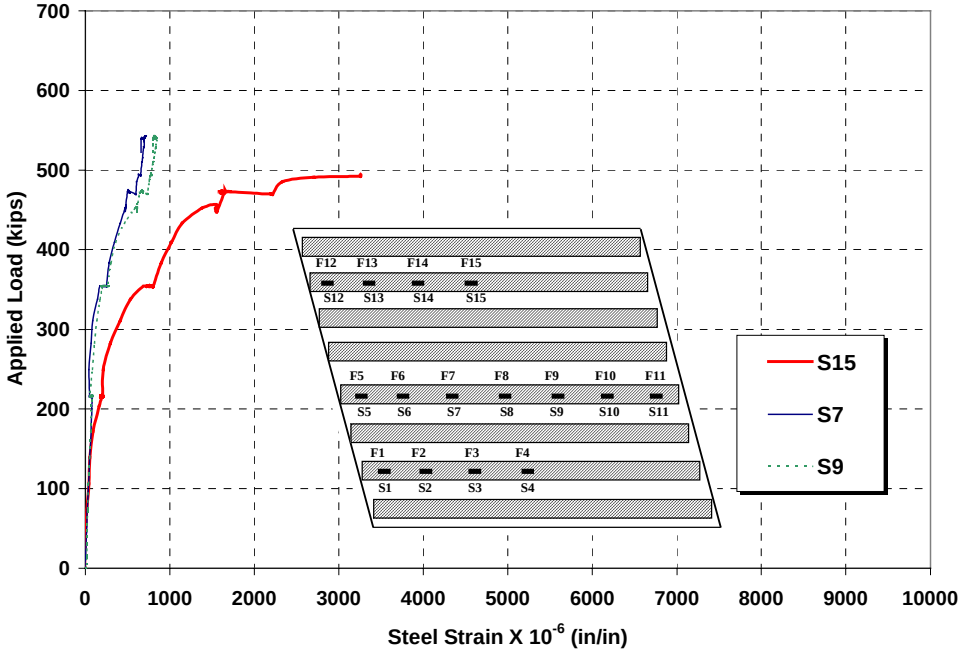

Note: 1 kip = 4.45 kN; 1 in/in = 1 mm/mm

Figure 5.13. Measured strain of the steel reinforcement of deck 2.

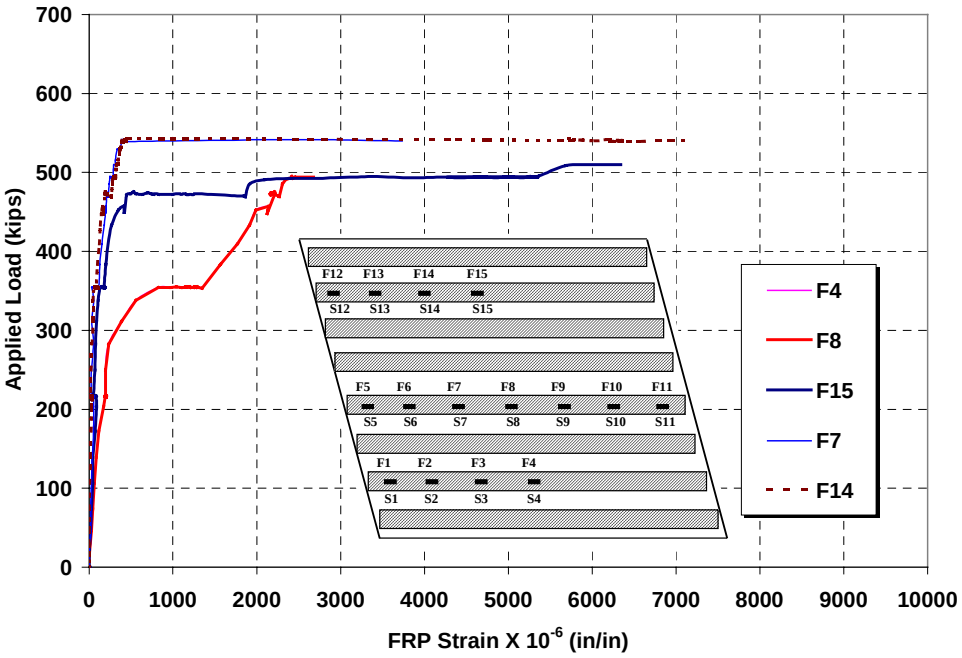

Note: 1 kip = 4.45 kN; 1 in/in = 1 mm/mm

Figure 5.14. Measured strain of the CFRP sheets for deck 2.

5.4. DECK 3 – NO STRENGTHENING

A plot of the applied load vs. deflection for this deck is shown in Figure 5.15. Before the last loading cycle, the decks had minimal change in stiffness, indicating that the steel reinforcement did not yield. Yielding of steel reinforcement occurred at approximately 417 kips (1856 kN), where the curve started to flatten due to loss of stiffness. The failure load of this deck was 463 kips (2060 kN). Figures 16 and 17 show the failure of deck 3.

The measured deflections along the bridge axis at different load levels are shown in Figure 5.18. At lower load levels, the measured deflections are similar to those of the deck with NSM rods. However, significantly larger deflections were measured at higher load levels. Figure 5.19 shows the measured deflections along a line at a quarter-point on the transverse axis of the deck. Unlike the strengthened decks, the measured deflection at the center of this deck was larger than that at the quarter-point. Figure 5.20 shows the measured strain on steel reinforcement. This Figure indicates that yielding of steel reinforcement occurred between 350 and 400 kips (1558 to 1780 kN). Yielding strain was approximately 0.0017 in./in. (mm/mm).

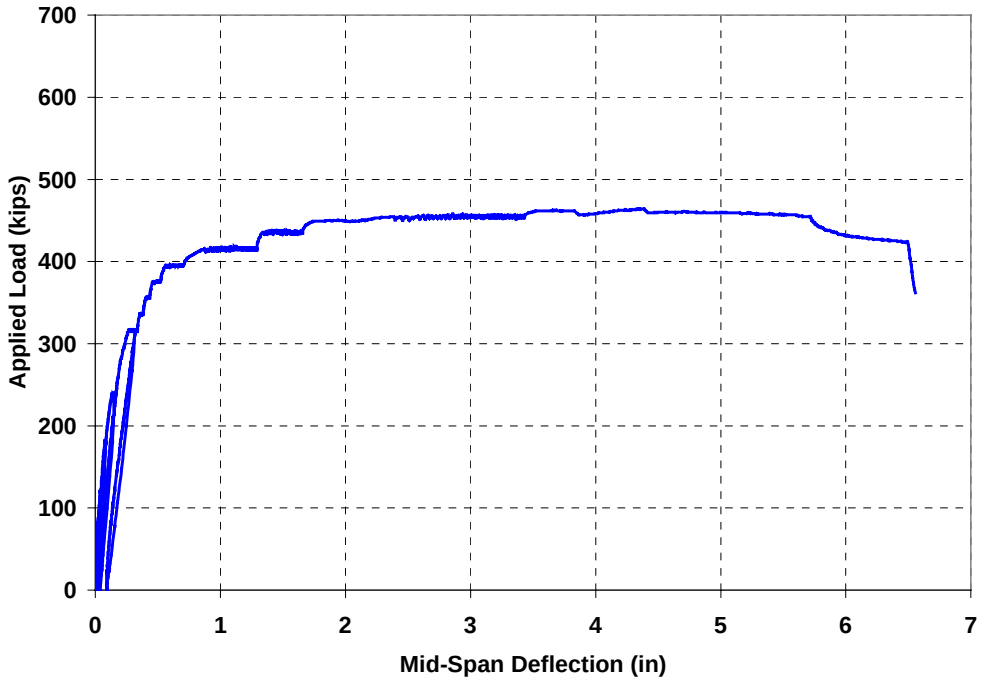

Note: 1 kip = 4.45 kN; 1 in = 25.4 mm

Figure 5.15. Experimental load-deflection relationship for deck 3.

(a) Cracks on the deck soffit testing

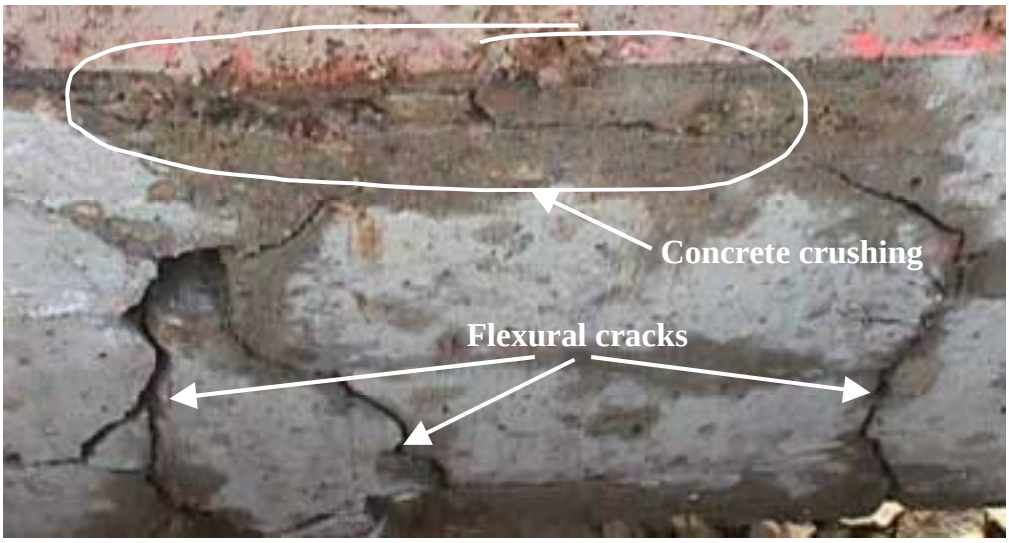

(b) Cross section through the deck showing concrete crushing

Figure 5.16. A section through deck 3 after testing at failure.

Figure 5.17. Deck 3 at failure.

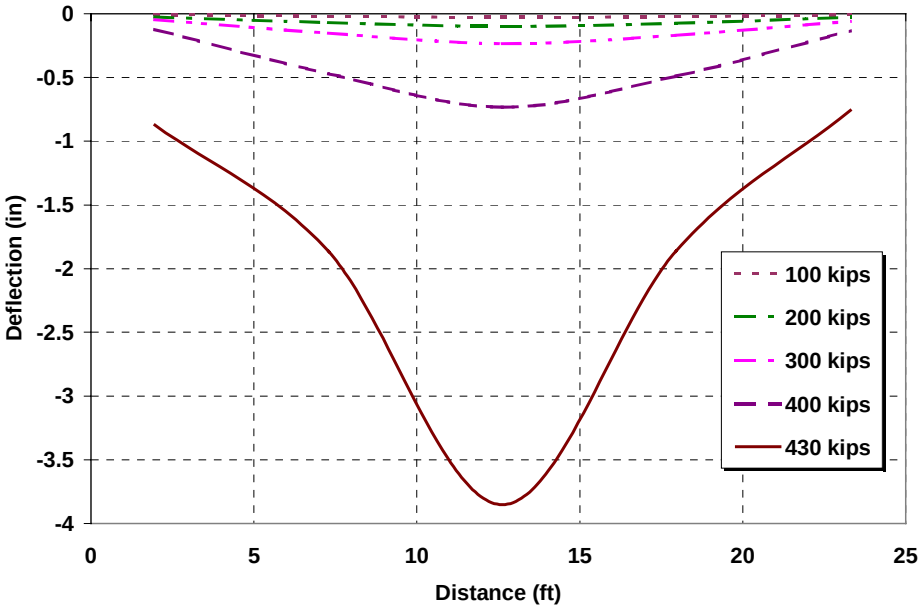

Note: 1 in = 25.4 mm; 1 ft = 0.305 m

Figure 5.18. Measured deflection along the longitudinal axis of deck 3.

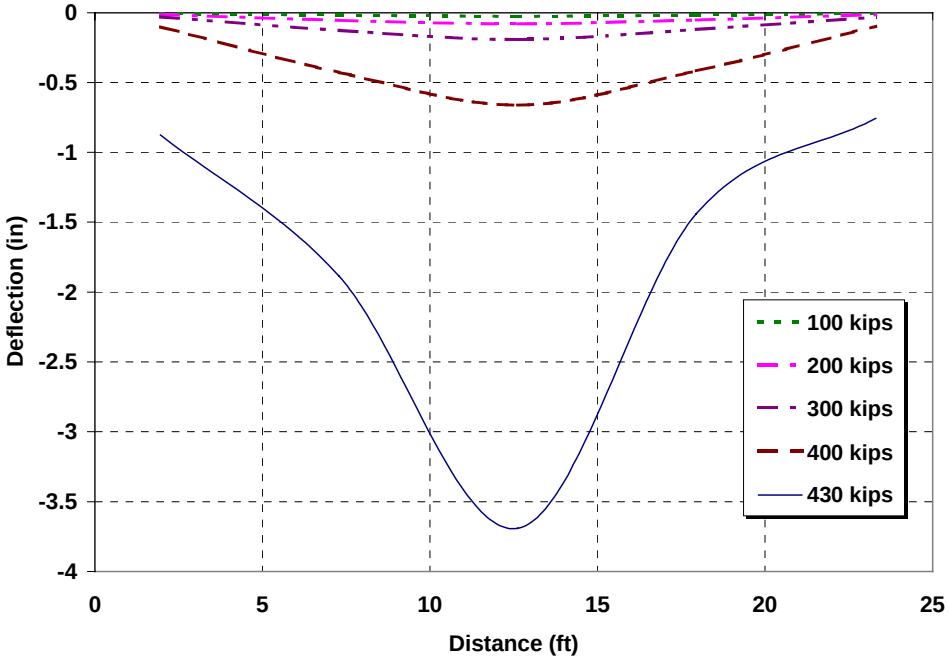

Note: 1 in = 25.4 mm; 1 ft = 0.305 m

Figure 5.19. Measured deflection along quarter-point on the transverse axis of deck 3.

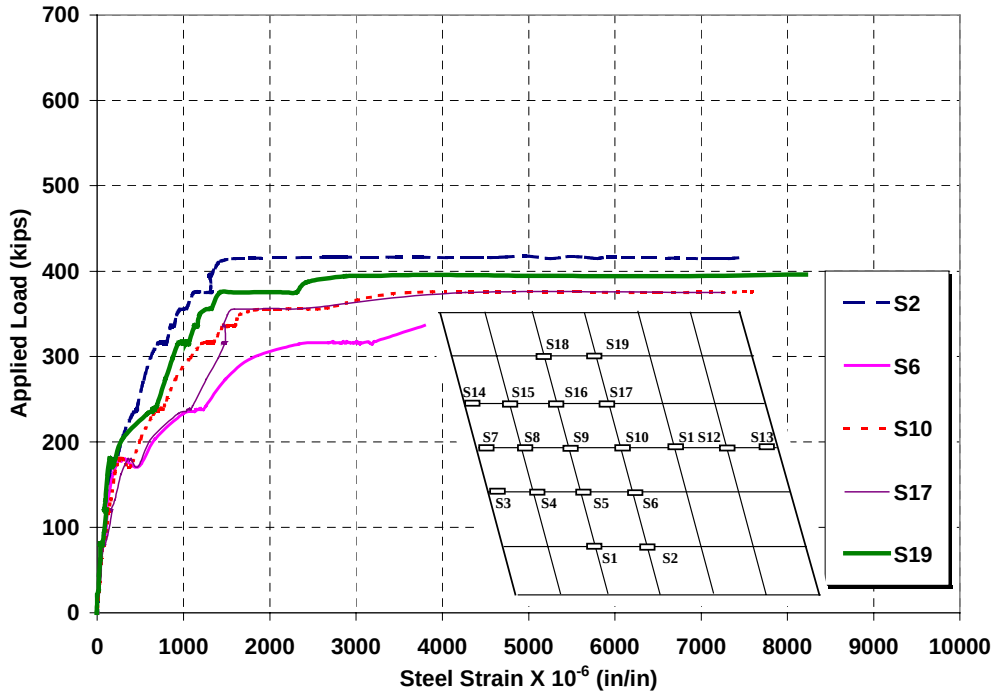

Note: 1 kip = 4.45 kN; 1 in/in = 1 mm/mm

Figure 5.20. Measured strain of the steel reinforcement of deck 3.

6. FLEXURAL ANALYSIS AND COMPARISON WITH EXPERIMENTAL RESULTS

6.1. GENERAL

This chapter introduces the analysis of the test results for the three bridge decks. Since one of the objectives of this study was to verify the contribution of the strengthening systems to the strength of the decks, ultimate strength and the complete flexural behavior were predicted and compared with experimental results. The former is intended to provide a simple tool for design/analysis of FRP strengthened decks. The latter is intended to provide an in-depth study of the structural condition and flexural performance of the bridge decks. The results of the destructive tests are presented in this section in the form of load-deflection and load-reinforcement strain curves. Comparisons between analytical and experimental results are made and conclusions are provided.

Once the destructive testing of the bridge decks was completed, concrete cores and steel coupons were obtained from the bridge deck. Testing of these specimens indicated that the actual material properties significantly exceed those used in design of the strengthening.

To verify the experimental results, the decks are analyzed using the strength analysis method (SAM) and the actual materials properties. The deck strengthened with FRP sheets is investigated first. The same approach is used to analyze the deck strengthened with NSM FRP rods with the proper modifications.

The boundary conditions are calibrated by comparing the experimental results of reinforcement strains and deflections to the predicted values.

6.2. BASIC ASSUMPTIONS

Experimental results of RC flexural members strengthened with surface bonded FRP composites show that flexural capacity can be predicted using the same assumptions made for members reinforced with steel bars (Nanni et al., 1998). Behavior prediction of a given member cross-section is performed based on of the following assumptions:

- At any loading level, strain in the concrete (ε_c), steel (ε_s), and FRP (ε_f) are proportional to their distance from the neutral axis, N/A (see Figure 6.1);
- The maximum strain attainable in compression concrete is 0.003 in./in. (mm/mm), provided that the specified ultimate strain of FRP reinforcement does not occur first;
- Concrete in tension is ignored;
- The stress-strain relationship of concrete is based on the parabolic equation proposed by Vecchio and Collins (1986), as shown in Figure 6.2;
- The stress strain relationship for steel reinforcement is assumed to be elastic-perfectly-plastic, as shown in Figure 6.3;
- The stress-strain relationship of FRP is linear with an ultimate strain, ε_{fu}, taken as the ultimate strength, f_{fu}, divided by the modulus of elasticity of FRP, E_f, as shown in Figure 6.3;
- The compressive stress distribution in the concrete is represented by Whitney's equivalent rectangular compressive stress block, provided that the appropriate stress block factors are used;

- Concrete and existing steel reinforcement have an initial strain at FRP installation due to the self-weight of the member.
- Perfect bond exists between the concrete and steel and FRP reinforcement.

The failure of FRP-strengthened flexural members could be governed by the rupture of FRP reinforcement (tension-controlled failure) or by the crushing of concrete (compression-controlled failure). The steel reinforcement may or may not yield prior to failure. Hence, the concept of under-reinforced and over-reinforced sections is applicable for FRP-strengthened flexural members.

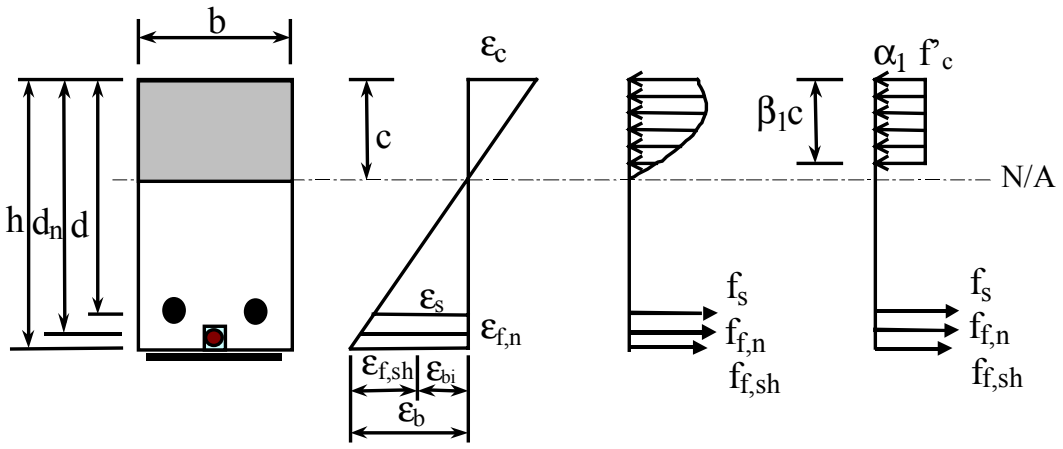

Subscript key:
f,n = near surface mounted bars
s = steel
f,sh = FRP sheets

Figure 6.1. Strain and stress conditions of a RC section strengthened with FRP reinforcement.

6.3. STRENGTH ANALYSIS METHOD

6.3.1. Deck Strip with Surface Bonded Carbon FRP Sheets

Figure 6.4 illustrates a unit strip of the deck strengthened with CFRP sheets. The strip has a width b of 12 in. (305 mm), a depth h of 18.5 in. (470 mm) and an effective depth to steel reinforcement d of 16.5 in. (419 mm). To increase the capacity by 30%, the strengthening design called for 0.042 in^2 (27 mm^2) of FRP per foot of deck. As indicated earlier, field inspection of the concrete surface under the asphalt overlay revealed the concrete was sound. Hence, the full depth of the member was considered effective.

Considering the geometry shown in Figure 6.1, the dead load moment was calculated as M_{DL} = 22.6 ft-kip/ft (101 kN-m/m). This includes the weight of the parapets of the bridge, which was uniformly distributed over the deck. The initial concrete strain at the bridge soffit, ε_{bi}, at the time of FRP installment, assuming a cracked section, is determined using the following equation:

$$\varepsilon_{bi} = \frac{M_{DL}(h - kd)}{I_{cr} E_c} \qquad (6.1)$$

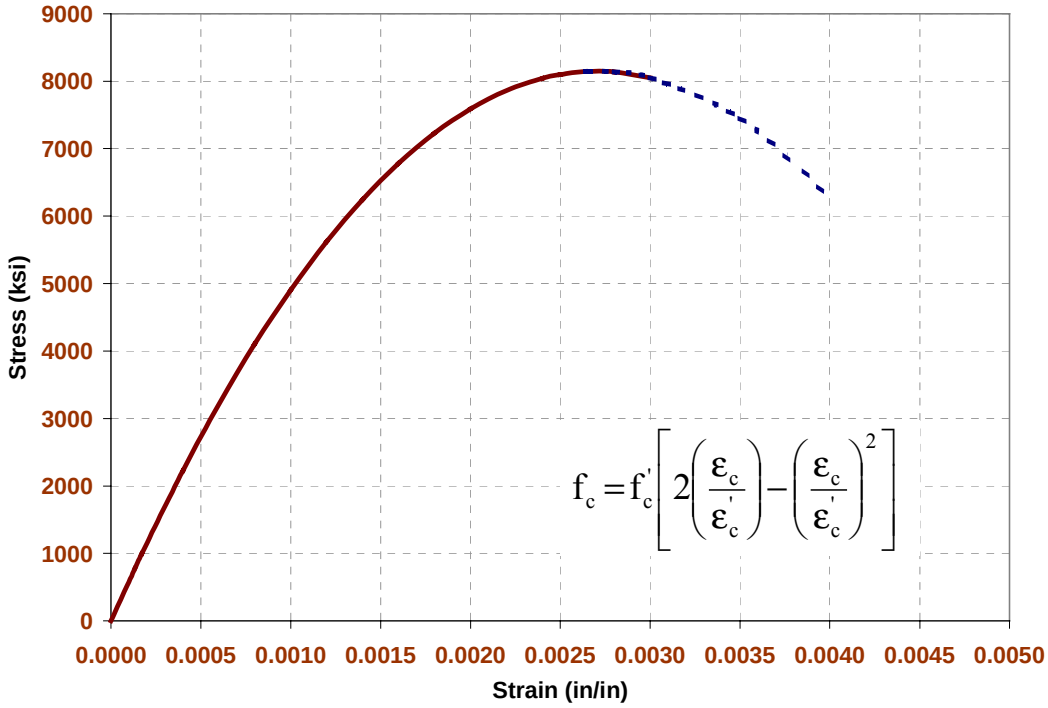

Note: 1 ksi = 6.895 MPa, 1 in./in. = 1 mm/mm

Figure 6.2. Parabolic stress-strain relationships of concrete.

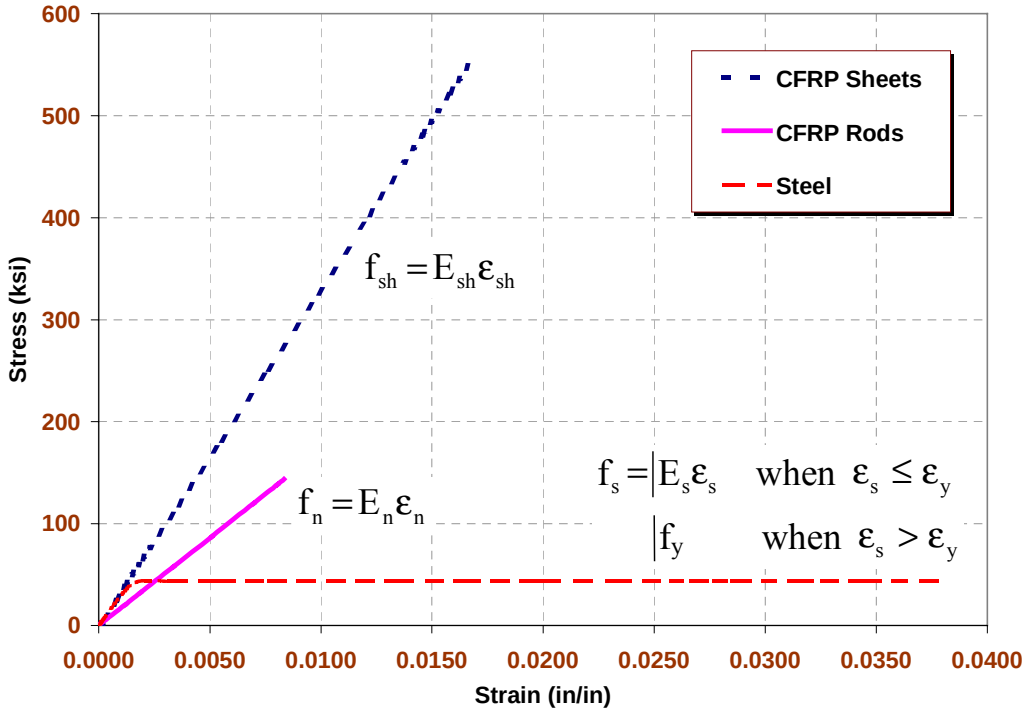

Note: 1 ksi = 6.895 MPa; 1 in/in = 1 mm/mm

Figure 6.3. Stress-strain relationships of reinforcing materials.

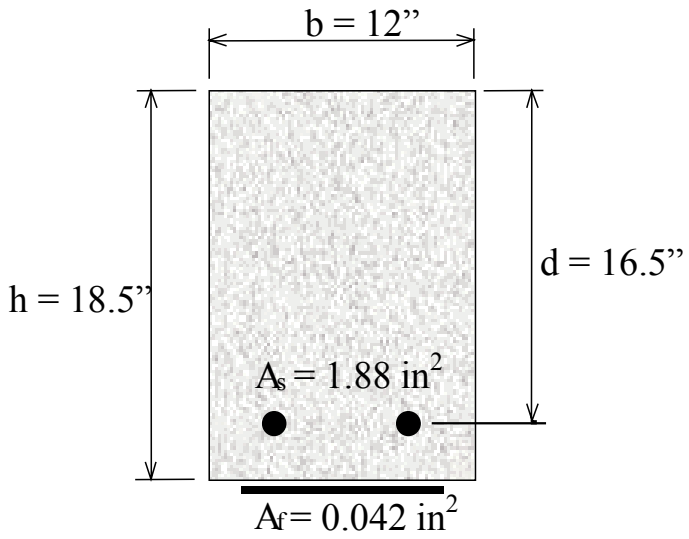

Figure 6.4. Cross-section of a deck strip showing bridge deck details.

In which kd is the depth of the neutral axis, I_{cr} is moment of inertia of the cracked section, and E_c is the modulus of concrete. The parameter k is the ratio of the depth of the neutral axis to the depth of steel reinforcement, which can be determined using the following equation:

$$k = \sqrt{2\rho n + (\rho n)^2} - \rho n \qquad (6.2)$$

Using equation (6.2), the multiplier on the beam depth to find the depth of the neutral axis of the cracked section is calculated as k = 0.279. This produces a cracked moment of inertia of I_{cr} = 1907 in^4. The tensile strain at the deck soffit at the time of FRP installation is calculated to be 417 με. Incorporating this initial tensile strain in analysis has a small influence on the predicted capacity.

The strength analysis method calculates the capacity of the section by utilizing force equilibrium and strain compatibility based on the constitutive laws of the materials. The stress and strain distributions at ultimate are shown in Figure 6.5. For computational ease, the non-linear stress-strain distribution of compression concrete is replaced by the Whitney's equivalent rectangular stress block (Whitney, 1942). The equivalent stress block results in a uniform stress of $\alpha_1 f'_c$ extending over a depth of $\beta_1 c$. The ACI 318-95 provides the values for α_1 and β_1 for the case where the concrete strain reaches 0.003. However, it is likely to encounter cases in which the strengthening may result in the rupture of FRP rather than the crushing of concrete. In this case, the maximum concrete strain is less than 0.003. The values of the stress block factors given by the ACI are, therefore, not valid and different values for α_1 and β_1 should be calculated based on the expected concrete compressive strain at failure.

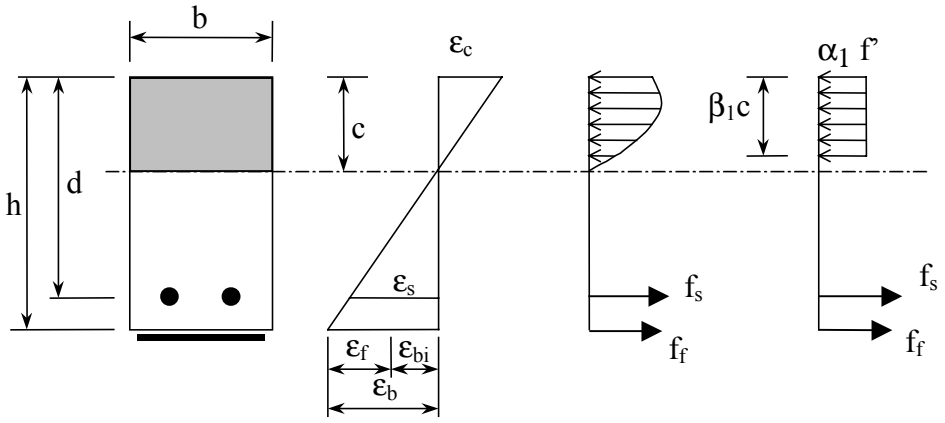

Figure 6.5. Strain and stress distribution in a RC section at ultimate.

The general equation for the nominal moment capacity of a reinforced concrete section strengthened with FRP reinforcement is as follows (ACI Committee 440, 2000):

$$M_n = A_s f_s\left(d - \frac{\beta_1 c}{2}\right) + 0.85 A_f f_f\left(h - \frac{\beta_1 c}{2}\right) \qquad (6.3)$$

The term f_s indicates that the steel may not yield at ultimate capacity. This case may be encountered when the addition of FRP reinforcement results in an over-reinforced section. A reduction factor of 0.85 is applied to the moment contribution of the FRP reinforcement accounts for the novelty of the system (ACI Committee 440, 2000). For this study, this reduction factor is taken as 1.0.

Because of the number of unknowns involved, the stresses in the steel and FRP reinforcement cannot be determined directly. The solution is achieved by iteration procedure in which the depth to the neutral axis, c, is estimated and the stresses in the materials are calculated. An initial assumption of c = 0.15d is reasonable in most cases. The depth of neutral axis is then calculated based on equilibrium and compared with the assumed values. Iteration is terminated when the two values of c converge.

Iteration Procedure. After the second iteration cycles, the value of c = 1.95 in. (49.5 mm) was used. The failure mode can be predicted as follows:

If $\varepsilon_{fu} + \varepsilon_{bi} > \varepsilon_{cu}\left(\frac{h-c}{c}\right)$, then $\varepsilon_c = \varepsilon_{cu} \rightarrow$ failure is controlled by concrete crushing.

If $\varepsilon_{fu} + \varepsilon_{bi} < \varepsilon_{cu}\left(\frac{h-c}{c}\right)$, then $\varepsilon_f = \varepsilon_{fu} \rightarrow$ failure is controlled by FRP rupture.

For the current case:

$$0.0167 + 0.000417 = 0.01711 < 0.003\left(\frac{18.5 - 1.95}{1.95}\right) = 0.0255 \text{ in./in.} \qquad (6.4)$$

Therefore, the failure mode is FRP rupture. From compatibility we get:

$$\varepsilon_f = \varepsilon_{fu} = 0.0167 \text{ in./in.} \tag{6.5}$$

$$\varepsilon_c = (\varepsilon_{fu} + \varepsilon_{bi})\left(\frac{c}{h-c}\right) = (0.01711)\left(\frac{1.95}{18.5-1.95}\right) = 0.0020 \text{ in./in.} \tag{6.6}$$

$$\varepsilon_s = (\varepsilon_{fu} + \varepsilon_{bi})\left(\frac{d-c}{h-c}\right) = (0.01711)\left(\frac{16.5-1.95}{18.5-1.95}\right) = 0.0153 \text{ in./in.} \tag{6.7}$$

which produces stress levels in the FRP and reinforcing steel of:

$$f_f = f_{fu} = 550 \text{ ksi} \tag{6.8}$$

$$\varepsilon_s \geq \varepsilon_{sy} \Rightarrow f_s = f_y = 43.33 \text{ ksi} \tag{6.9}$$

The parameters that define the equivalent stress block can be derived from any of the concrete stress-strain relationships available in literature. Using the known parabolic equation for stress-strain relationship of concrete, simpler formulas can be derived as follows:

$$\beta_1 = \frac{4\varepsilon'_c - \varepsilon_c}{6\varepsilon'_c - 2\varepsilon_c} \tag{6.10}$$

$$\alpha_1 = \frac{3\varepsilon'_c\varepsilon_c - \varepsilon_c^{\,2}}{3\beta_{1c}\varepsilon'^{\,2}_c} \tag{6.11}$$

In which,

$$\varepsilon'_c = \frac{1.71 \cdot f'_c}{E_c} \tag{6.12}$$

Therefore:

$$\varepsilon'_c = \frac{1.71(8147\text{psi})}{57000\sqrt{8147\text{psi}}} = 0.0027 \text{ in./in.} \tag{6.13}$$

$$\beta_1 = \frac{4(0.0027) - 0.002}{6(0.0027) - 2(0.002)} = 0.721 \tag{6.14}$$

$$\alpha_1 = \frac{3(0.0027)(0.002) - (0.002)^2}{3(0.721)(0.0027)^2} = 0.775 \tag{6.15}$$

The depth of the neutral axis, c, is then calculated as follows:

$$c = \frac{A_s f_s + A_f f_f}{\alpha_1 f'_c \beta_1 b} = \frac{1.88\,\text{in}^2(43{,}333\text{psi}) + (0.0416\text{in}^2)(550{,}000\text{psi})}{0.775(8140\text{psi})0.721(12\text{in})} = 1.91\,\text{ir} \tag{6.16}$$

Since 1.91 in. ≠ 1.95 in., further iteration is required. Assuming c= 1.92 in., the results of the iteration are summarized below:

c_{est} (in)	Failure Mode	ε_f	f_f (ksi)	ε_s	f_s (ksi)	ε_c	β_1	$\alpha 1$	c_{calc} (in)
1.92	FRP Rupture	0.0167	550	0.0150	43.33	0.00198	0.720	0.770	1.927

The nominal moment capacity is the calculated as follows:

$$M_n = 1.88(43.33)\left(16.5 - \frac{0.720(1.927)}{2}\right) + 1.0(0.0416)(550)\left(18.5 - \frac{0.720(1.927)}{2}\right)$$
$$M_n = 1695\,\text{kip}\cdot\text{in} = 141\text{ ft} - \text{k/ft} \qquad (6.17)$$

In which the full contribution of the FRP sheets is included without any reduction (R=1.0). The maximum concentrated live load was determined as follows:

$$P_L = \frac{4(M_n - M_D)}{L} = \frac{4(141 - 22.6)}{25.5} = 18.6\text{ kips/ft} \qquad (6.18)$$

The total capacity of the deck was obtained by multiplying the failure load P_L by the width of the deck (25 ft). The maximum theoretical live load that the deck can carry is therefore P_L = 464 kips (2065 kN).

6.3.2. Deck Strip with Near-Surface Mounted Carbon FRP Rods

Figure 6.6 illustrates a 12-in (305 mm) strip of the deck strengthened with near-surface mounted CFRP rods. For approximately 30% increase in capacity, the strengthening design called for $^7/_{16}$ in. (11 mm) diameter rods spaced at 15 in. (380 mm) or 0.12 in^2 (77 mm^2) per foot width of the deck. The effective depth is d_n =18.0 in. (457 mm) for the mounted rods. For the following calculations, the upper limit of the experimental strength of the CFRP rod of 183 ksi (1.26 GPa) was used in calculations (Yan, 1999). The upper limit of rod strength was used due to a better anchorage mechanism in the field.

The multiplier on the beam depth, k, and the cracked moment of inertia, I_{cr}, were calculated earlier as 0.279 and 1907 in^4, respectively. The tensile strain at the deck soffit at the time of FRP rods installation was 417 με. The strength analysis method was carried in the same manner presented earlier for beams with bonded FRP sheets. The only difference was the use of the effective depth d_n instead of "h" for bonded sheets. Hence, the nominal moment capacity equation for a reinforced concrete section strengthened with near surface mounted FRP rods becomes:

$$M_n = A_s f_s\left(d - \frac{\beta_1 c}{2}\right) + A_f f_f\left(d_n - \frac{\beta_1 c}{2}\right) \qquad (6.19)$$

No reduction factor is used for the contribution of the FRP rods since this technology is similar to conventional construction.

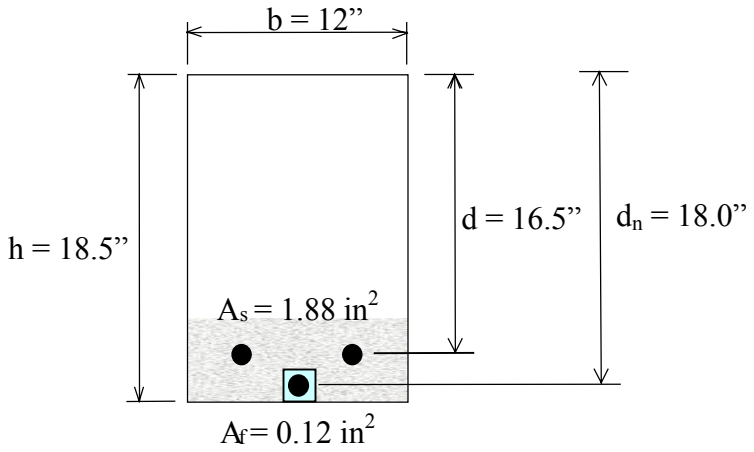

Figure 6.6. Cross-section of a deck strip showing bridge deck details.

Iteration Procedure. After two iterations, the value of c = 2.25 in. (57 mm) was assumed. The failure mode is predicted as follows:

If $\varepsilon_{fu} + \varepsilon_{bi} > \varepsilon_{cu}\left(\frac{d_n - c}{c}\right)$, then $\varepsilon_c = \varepsilon_{cu}$ → failure is controlled by concrete crushing.

If $\varepsilon_{fu} + \varepsilon_{bi} < \varepsilon_{cu}\left(\frac{d_n - c}{c}\right)$, then $\varepsilon_f = \varepsilon_{fu}$ → failure is controlled by FRP rupture.

$$0.0106 + 0.000417 = 0.011 < 0.003\left(\frac{18.0 - 2.25}{2.25}\right) = 0.021 \qquad (6.20)$$

Therefore, the failure mode was rupture of the FRP bars. Utilizing compatibility requirements, the strains of FRP, concrete and reinforcing steel can be determined as follows:

$$\varepsilon_f = \varepsilon_{fu} = 0.0106 \text{ in./in.} \qquad (6.21)$$

$$\varepsilon_c = (\varepsilon_{fu} + \varepsilon_{bi})\left(\frac{c}{d_n - c}\right) = (0.011)\left(\frac{2.25}{18.0 - 2.25}\right) = 0.0016 \text{ in./in.} \qquad (6.22)$$

$$\varepsilon_s = (\varepsilon_{fu} + \varepsilon_{bi})\left(\frac{d - c}{d_n - c}\right) = (0.011)\left(\frac{16.5 - 2.25}{18.0 - 2.25}\right) = 0.01 \text{ in./in.} \qquad (6.23)$$

Which produces stress levels in the FRP and reinforcing steel of:

$$f_f = f_{fu} = 183 \text{ ksi} \qquad (6.24)$$

$$\varepsilon_s \geq \varepsilon_{sy} \Rightarrow f_s = f_y = 43.33 \text{ ksi} \qquad (6.25)$$

The parameters that define the equivalent stress block are:

$$\varepsilon_c' = \frac{1.71(8147\text{psi})}{57000\sqrt{8147\text{psi}}} = 0.0027 \text{ in./in.} \quad (6.26)$$

$$\beta_1 = \frac{4(0.0027) - 0.0016}{6(0.0027) - 2(0.0016)} = 0.707 \quad (6.27)$$

$$\alpha_1 = \frac{3(0.0027)(0.0016) - (0.0016)^2}{3(0.707)(0.0027)^2} = 0.665 \quad (6.28)$$

Checking the value of c:

$$c = \frac{A_s f_s + A_f f_f}{\alpha_1 f_c' \beta_1 b} = \frac{1.88\,\text{in}^2(43{,}333\text{psi}) + (0.12\text{in}^2)(183{,}000\text{psi})}{0.665(8147\text{psi})0.707(12\text{in})} = 2.25\,\text{in} \quad (6.29)$$

Since the calculated value of "c" is the same as the assumed value, no further iteration is required. The nominal moment capacity is calculated as follows:

$$M_n = 1.88(43.33)\left(16.5 - \frac{0.707(2.25)}{2}\right) + 0.12(183)\left(18.0 - \frac{0.707(2.25)}{2}\right) \quad (6.30)$$

$$M_n = 1657 \text{ kip} \cdot \text{in} = 138 \text{ ft} - \text{k}$$

From which the equivalent concentrated load is determined as:

$$P_L = \frac{4(M_n - M_D)}{L} = \frac{4(138 - 22.6)}{25.5} = 18.1 \text{ kips/ft} \quad (6.31)$$

The total capacity of the deck was obtained by multiplying the failure load P_L by the width of the deck (25 ft). Thus, the maximum live load is P_L = 452 kips (2013 kN).

6.3.3. Deck Strip without FRP Strengthening

Figure 6.7 illustrates a 12-in (305 mm) strip of the original deck. The capacity of the deck was calculated using the traditional approach for under-reinforced flexural members. The depth of the equivalent stress block is calculated as follows:

$$a = \beta_1 c = \frac{A_s f_y}{0.85 f_c' b} = \frac{1.88\,\text{in}^2(43{,}333\text{psi})}{0.85(8{,}147\text{psi})(12\text{in})} = 0.98\,\text{in} \quad (6.32)$$

$$M_n = A_s f_y\left(d - \frac{a}{2}\right) = 1.88(43.33)\left(16.5 - \frac{0.98}{2}\right) = 1303 \text{ kip} \cdot \text{in} = 109\,\text{ft} - \text{k} \quad (6.33)$$

From which the equivalent concentrated load is calculated as 13.6 kips (60 kN) and the total theoretical live load is P_L = 339 kips (1507 kN).

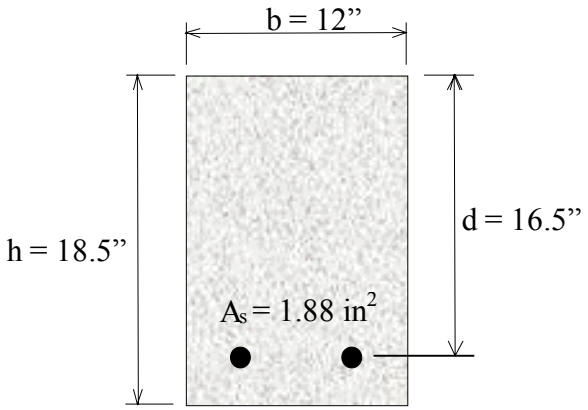

Figure 6.7. Cross section of an original deck strip.

6.4. COMPARISON OF ULTIMATE STRENGTHS WITH THE EXPERIMENTAL RESULTS

Table 6.1 shows a comparison of predicted the live load capacities using strength analysis method and those from field-testing of the bridge decks. The predicted Live load capacities were based on a concrete strength of 2500 psi (17.2 MPa), steel yield strength of 33,000 psi (227 MPa), CFRP rod strength of 144 ksi (990 MPa), and CFRP sheet strength of 550 ksi (3.8 GPa). For the CFRP sheets, due to the lower strength of concrete, the predicted failure mode was governed by concrete crushing at CFRP sheet stress of 409 ksi (2.8 GPa). Table 6.1 indicates that significant differences exist between theoretical and experimental results. The higher experimental values could be related to higher material strength of concrete, steel, and FRP, the effect of bridge deck skew, strain hardening of steel reinforcement, and the boundary conditions (end fixity) of the decks. It should be noted that other researchers have also investigated the experimental result of deck testing (Kemna, A. C., 1999 and Kemna D. J., 1999). Conclusions similar to what is presented next were provided.

Table 6.1. Comparison of Predicted and Experimental Capacities.

	Live Load Capacity, kip (kN)	
	Predicted[1]	Experimental
CFRP NSM	311 (1385)	596 (2651)
CFRP Sheets	311 (1385)	542 (2411)
No Strengthening	222 (987)	463 (2059)

1 Analytical based on assumed material strengths

Material Effects. The test results of three 4 in. x 8 in. (100 mm x 200 mm) concrete cylinders obtained from the bridge decks indicated that the average concrete compressive strength was 8,147 psi (56.2 MPa). Also, the test results of three coupons tested under uniaxial tension indicated that the average yield strength of the steel reinforcement was 43,333 psi (298

MPa). The tensile strength of the CFRP rods, as collected from literature, varied from 144 to 183 ksi (990 to 1300 MPa) (Yan, 1999). Since failure of most of tested rod specimens occurred at the anchorage, it is reasonable to assume that higher strength of the NSM CFRP rod could be achieved due to a better anchorage mechanism.

To account for the higher that expected live load capacity for Deck 1, a new capacity was calculated using the upper limit of rod strength (183 ksi or 1300 MPa). This value is still significantly lower that theoretical tensile strength of 349 ksi (2400 MPa), determined from the properties of the constituent materials (Yan, 1999).

Table 6.2 shows a comparison of moment and live load based on the assumed (initial) material strengths, true material strengths [concrete strength of 8,147 psi (56.2 MPa), steel yield strength of 43,333 psi (298 MPa), CFRP rod strength of 183 ksi (1300 MPa), and CFRP sheet strength of 550 ksi (3.8 GPa)], and the experimental capacities. Regarding Deck 2 (CFRP sheets), when considering the adjusted material strengths of concrete and steel, the resulting analytical failure mode is governed by rupture of the sheets.

Table 6.2 indicates that the CFRP strengthening was effective for increasing the member strength. The experimental capacities of the strengthened decks exceeded those theoretically predicted. Given that the design strength of the CFRP sheets provided by the manufacturer is conservative, the combined failure mode of rupture and peeling of the sheets as was observed in the field was still higher than the predicted values. The results of Table 6.2 indicate that the ratio of experimental to predicted capacity of the decks was higher for Deck 1 (NSM) than that for Deck 2 (sheets). Based on these observations, other researchers concluded that the CFRP sheets are less effective and that premature failure caused this lower ratio (Kemna, A. C., 1999 and Kemna, D. J., 1999).

Table 6.2. Comparison of SAM and Experimental Capacities.

	Moment Capacity, kip-ft/ft (kN-m/m)			Live Load Capacity, kip (kN)		
	Predicted*	Exp.**	Exp./Pred.	Predicted*	Exp.	Exp./Pred.
CFRP NSM	138 (614)	175 (777)	1.27	452 (2010)	596 (2651)	1.32
CFRP Sheets	149 (663)	161 (715)	1.08	496 (2205)	542 (2411)	1.09
No Strengthening	109 (485)	141 (626)	1.29	339 (1507)	463 (2059)	1.37

* Analytical based on the true material strengths

** Including dead loads

Table 6.2 shows that the ratio of experimental to predicted capacities are higher for the two end decks (NSM and unsrtrengthened). If a mixed mode of failure consisting of debonding and FRP rupture had not occurred in deck 2, a higher experimental capacity could have probably been achieved. Table 6.2 also indicates that using the true material strengths, although

considerably increased the predicted capacities of the decks, did not fully explain the higher experimental values. Additional differences between predicted and experimental capacities of the decks could be related to the effect of bridge deck skew, strain hardening of steel reinforcement, and the boundary conditions (end fixity) of the bridge decks.

Skew Effect. Based on an elastic finite element analysis of a typical bridge deck and considering the loading scheme used in testing, a 15-degree skew had minimal effects on the elastic behavior of the deck. The flexural behavior and capacity with 15-degree skew could therefore be predicted with good accuracy using the unit strip approach. This is due to the small skew angle and the distribution of the applied load on a line at mid-span parallel to the skewed supports. Plate effect is more dominant if the load was applied at a point rather than distributed across the width of the deck. For the current investigation, the skew effect on the capacity of the bridge decks was minimal and was therefore ruled out. A summary of these findings is given in Appendix C.

Strain-Hardening Effect. Strength analysis indicated that at failure, the strains of steel reinforcement for the deck strengthened with NSM rods, bonded sheets, and the unstrengthened deck are 0.0080, 0.0150, and 0.0391, respectively. Strain hardening of steel reinforcement was expected to begin at about 0.012 to 0.020 strain (Wang and Salamon, 1998). Accordingly, strain hardening had no contribution to the ultimate capacity of the deck strengthened with NSM rods, minimal contribution to the deck with bonded sheets, and could have contributed to the capacity of the unstrengthened deck. This will be examined further later in this chapter.

End Fixity Effect. The variation of deck boundary conditions is represented by different levels of end fixity. This may be related to different construction detailing (i.e., bottom reinforcement of the two end-span decks extended to the abutment walls) and aging influence (i.e., "freezing" of the supports). The exact level of fixity at the supports of each deck cannot be determined directly from the experimental results. Considering the symmetry of the bridge, the two supports of each deck were assumed to have the same fixity level.

The maximum moment in a flexural member due to a given loading condition depends on the level of its end fixity. The end fixity, referred to hereafter as F, could therefore be determined by comparing the theoretical and experimental flexural capacities. The relation between F and the maximum moment due to a given loading condition could be determined by a simple structural analysis procedure. Appendix D presents the derivation of the expressions that relate the end fixity to the maximum moments at mid-span, M_m, and at the supports, M_e. The moments resulting from the combined effect of concentrated load at mid-span, P, and uniformly distributed load, w, can be expressed as follows:

$$M_m = M_m^c + M_m^D = K_m^c PL + K_m^D wL^2 \tag{6.34}$$

$$M_e = M_e^c + M_e^D = K_e^c PL + K_e^D wL^2 \tag{6.35}$$

In which:

$$K_m^c = \frac{1}{4(F+1)} \tag{6.36}$$

$$K_e^c = \frac{F}{4(F+1)} \tag{6.37}$$

$$K_m^D = \frac{1}{8(2F+1)} \tag{6.38}$$

$$K_e^D = \frac{F}{4(2F+1)} \tag{6.39}$$

Where:
M_m = mid-span moment
M_e = end moment (at the support)
M^c_m = mid-span moment due to a concentrated load considering simple supports
M^c_e = end moment due to a concentrated load considering simple supports
M^D_m = mid-span moment due to distributed load considering simple supports
M^D_e = mid-span moment due to distributed load considering simple supports
K^c_m, K^c_e, K^D_m, and K^D_e = moment coefficient to determine the moments due to a given fixity level, F, from the corresponding moments defined above.

6.5. FLEXURAL BEHAVIOR ANALYSES

Three parts may be distinguished in the flexural behavior of any steel reinforced concrete section: prior to cracking, after cracking, and after yielding of steel reinforcement. The limit separating the first two parts is the cracking of the section. The limit separating parts two and three is the plastification of the steel reinforcement with no account for the non-linear behavior of concrete.

6.5.1. Un-cracked Section

The un-cracked section can be treated as a linear elastic member. Curvature at any section increases linearly with the applied load. The strain in steel, NSM rods, and surface bonded sheets are very small and were, therefore, ignored. The curvature, ϕ, at any loading level prior cracking can be determined as follows:

$$\phi = \frac{M}{I_g E_c} \tag{6.40}$$

The cracking moment of the section is governed by concrete tensile properties alone. Steel and FRP reinforcement have minimal effect on the cracking moment or the stiffness of the section. The member may experience cracking when the tensile stress in the extreme tension fiber exceeds the conservative tensile strength of concrete proposed by (ACI 318-95):

$$f_r = 7.5\sqrt{f'_c} \tag{6.41}$$

The cracking moment was calculated as follows:

$$M_{cr} = \frac{f_r b h^2}{6} \tag{6.42}$$

When the moment caused by live and dead loads exceeds the cracking moment, cracks will initiate and the properties of the cracked section will govern the behavior. The behavior from this point on is that of a cracked section.

6.5.2. Cracked Section (Before Yielding)

The initial concrete strain at the level of the NSM rods, ε_{ni}, due to the moment, M_i, at the time of FRP installation was calculated as follows:

$$\varepsilon_{ni} = \frac{M_i(d_n - kd)}{I_{cr}E_c} \tag{6.43}$$

Similarly, the concrete strain at the level of the surface bonded sheets, ε_{bi}, was calculated as follows:

$$\varepsilon_{bi} = \frac{M_i(h - kd)}{I_{cr}E_c} \tag{6.44}$$

The moment of inertia of the cracked section, I_{cr}, is calculated using the following general equation:

$$I_{cr} = \frac{b\,d^3}{3}k^3 + n\,A_s\,d^2\,(1-k)^2 + n_{f,n}\,A_{f,n}\,d_n^2\,(1-k)^2 + n_{f,sh}\,A_{f,sh}\,h^2\,(1-k)^2 \tag{6.45}$$

Strains of steel, ε_s, NSM rods, $\varepsilon_{f,n}$, and the bonded sheets, $\varepsilon_{f,sh}$, were calculated using the following:

$$\varepsilon_s = \varepsilon_c\left(\frac{d-c}{c}\right) \tag{6.46}$$

$$\varepsilon_{f,n} = \varepsilon_c\left(\frac{d_n - c}{c}\right) - \varepsilon_{ni} \tag{6.47}$$

$$\varepsilon_{f,sh} = \varepsilon_c\left(\frac{h-c}{c}\right) - \varepsilon_{bi} \tag{6.48}$$

However, if the flexural member did not have any cracks at the time of FRP application, the initial concrete strains, ε_{ni} and ε_{bi}, could be ignored. In addition, if the initial moment, M_i, of a cracked member was small compared to the total dead and live load moments, the initial concrete strains, ε_{ni} and ε_{bi}, are very small and were be ignored.

Based on the equilibrium condition of the cross section, the depth of the neutral axis, c, can be expressed as follows:

$$c = \frac{A_s f_s + A_{f,n} f_{f,n} + A_{f,sh} f_{f,sh}}{\alpha_1 f_c' b \beta_1} \tag{6.49}$$

The values of f_s and $f_{f,n}$ (or $f_{f,sh}$) can be determined using constitutive material laws. The full behavior of the strengthened member is established through iterative procedure. In this procedure, a concrete strain, ε_c, is assumed first. Next, a value for "c" was assumed. The strains in steel, NSM rods, and bonded sheets are then calculated and used to determine the stresses in reinforcement using the constitutive laws of materials. The corresponding depth of the neutral axis, c, was then calculated using the equilibrium equation. If the calculated depth, c, was the same as the assumed value, then equilibrium is satisfied and the behavior at the assumed concrete strain is obtained. A new value for ε_c is assumed and iterations are made again. If the calculated depth, c, is different than the assumed value, a new value for "c" is assumed and the iteration is continued until convergence is achieved. Once the depth of the neutral axis, reinforcement stresses, and stress block factors are determined, the bending moment is calculated as follows:

$$M = A_s f_s\left(d - \frac{\beta_1 c}{2}\right) + A_{f,n} f_{f,n}\left(d_n - \frac{\beta_1 c}{2}\right) + A_{f,sh} f_{f,sh}\left(h - \frac{\beta_1 c}{2}\right) \qquad (6.50)$$

The curvature of the flexural section can be determined as follows:

$$\phi = \frac{M}{EI} = \frac{\varepsilon_c}{c} \qquad (6.51)$$

Analysis was terminated when either the maximum compressive strain of concrete, ε_c, reaches 0.003 or the tensile strain in FRP, ε_f, reaches its ultimate strain, ε_{fu}.

The live load, P_L, corresponding to the given moment was determined using the following equation:

$$P_L = \frac{M - K_m^D w\ell^2}{K_m^C \ell} \qquad (6.52)$$

6.5.3. Cracked Section (After Yielding)

A cracked section after yielding of steel reinforcement is analyzed using the same approach outlined earlier (before cracking). From a computational stand-point, the only difference is that once the steel strain reaches the yielding strain ($\varepsilon_s = \varepsilon_y$), the yielding stress, f_y, is substituted for f_s in calculations.

6.5.4. Comparison of the Predicted Moment-Curvature Behavior

Figure 6.8 illustrates a comparison of the analytical moment-curvature relationships for unit strips of the three decks. This figure shows that a trade off exists between capacity and ductility.

Typically, a flexural member strengthened with surface bonded FRP will have higher capacity due to the addition of FRP. Prior to cracking, the member behavior is the same for all cases and is independent of reinforcement type. The contribution of FRP to the stiffness of the strengthened members, represented by $E_c I_{cr}$, will take place after the member has cracked and the contribution of the concrete is significantly reduced. As shown in the figure, the contribution of

FRP to the elastic stiffness of the member after cracking is insignificant. This is due to the relatively small amount of FRP added to the section compared with the area of existing steel. The stiffness of the cracked section will reduce further when the steel yields. At this stage, the section stiffness is only influenced by the compression concrete and FRP reinforcement. While the reinforced section had almost no stiffness after yielding, a proportional moment-curvature can be seen for sections with FRP reinforcement. It should be noted that the stiffness of the FRP strengthened strips is not constant after yielding. This is due to the non-linear behavior of concrete at higher strain levels. The stiffness after yielding is influenced by the amount and the stiffness of added FRP reinforcement (A_f and E_f) and is proportional to their product. The load level at which steel reinforcement yields increases with the addition of FRP.

The FRP will carry some of the tensile force thus, delaying the yielding of the steel reinforcement. The increase in the yielding load (or moment) will depend on the amount and stiffness of the added FRP. Increasing either parameter will increase the yielding load level. For unit strips with NSM rods, bonded sheets, and, no strengthening, the calculated yielding moments were 107.5, 106.0, and 102.5 ft-kip/ft (478, 472, and 456 kN-m/m), respectively. The flexural capacities and modes of failure of the strips are those determined earlier by SAM method.

Possible failure modes of FRP strengthened section are either FRP rupture or concrete crushing. In the case of failure controlled by concrete crushing, the neutral axis will migrate downward at ultimate load as a result of a larger compression block required to counter balance the additional tensile forces due to FRP addition. This results in smaller curvature at ultimate compared with the unstrengthened case. In the case of FRP rupture, the concrete strain ε_c is less than 0.003 in./in. (mm/mm) at failure. The combined effect of smaller maximum compressive strain and smaller depth of neutral axis will result in smaller curvature at ultimate.

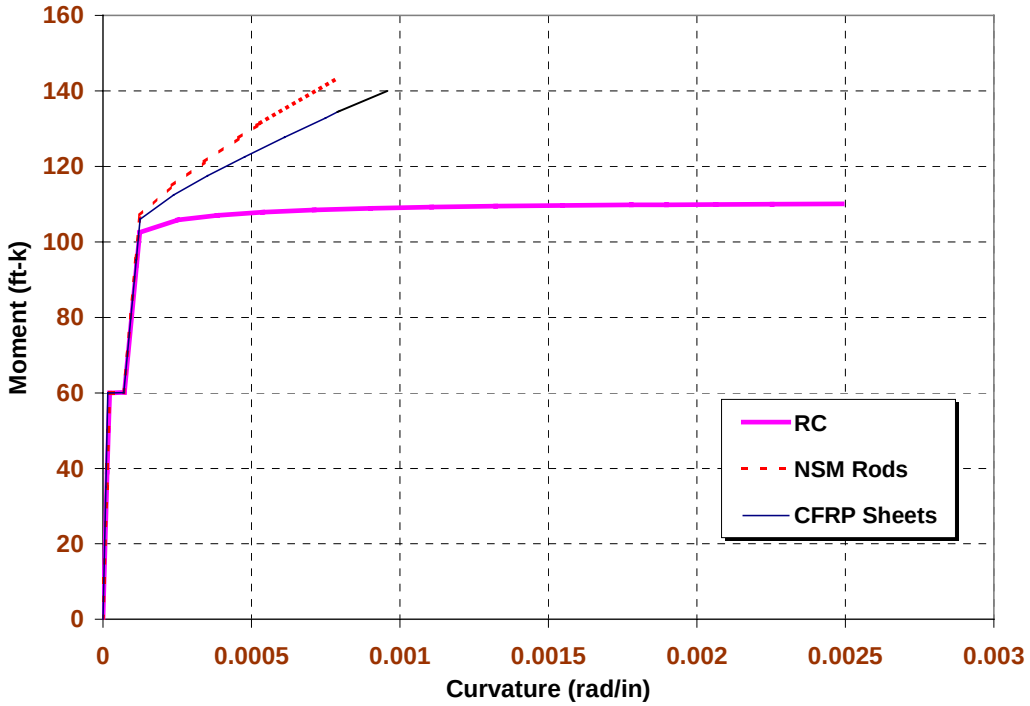

Note: 1 k-ft = 1.356 kN-m

Figure 6.8. Analytical moment-curvature relations for bridge deck strips.

6.5.5. Deflection Calculation

The bending deformations of a RC flexural member can be calculated by numerical integration of the curvature diagram. The moment-deflection diagram depends on the geometry of the flexural member, boundary conditions, and loading configuration. The differential bending rotation $d\theta$ can be expressed in terms of the curvature, Φ, as follows:

$$d\theta = \frac{M}{EI} dx = \Phi \, dx \tag{6.53}$$

Figure 6.9 shows the main steps in calculating the mid-span deflection of a simply supported beam having some fixity at the supports and loaded with uniformly distributed load over the entire span and a concentrated load at mid-span. Note that, in this figure, it is assumed that the end fixity is not large enough to cause cracking at the negative moment regions. This case simulates the actual behavior of the bridge decks observed in the field.

The curvature diagram was constructed by analyzing different sections along the length of the member at certain intervals (e.g., L/10). For each section, the moment acting on the section at the given load level is determined. The moment resulting from the concentrated load and acting at any section at a distance $0 \le X \le L/2$ from the support can be expressed as follows:

$$M^{c}(x) = 2M^{*c} \frac{x}{L} - M_{e}^{c} \tag{6.54}$$

The moment resulting from the distributed load at any section is expressed as follows:

$$M^{D}(x) = 2M_{M}^{D} - 4M^{*D}\left(\frac{x}{L} - \frac{1}{2}\right)^{2} \tag{6.55}$$

The curvature corresponding to the moment is determined at each section, thus obtaining the complete curvature diagram. The curvature is numerically integrated twice to obtain the rotation and the deflection of the member, successively. The constants of the integration are determined from the boundary conditions. Once the complete rotation diagram was constructed, the deflection at any section x can be determined by integrating the rotation diagram as follows:

$$\Delta(x) = \int_{0}^{x} \theta(x) dx \tag{6.56}$$

For the mid-span deflection, the integration limits are set from 0 to L/2. The approach utilized in this study is a replica of the conjugate beam method. Other methods for deflection calculations, such as the moment area method and the elastic load method can also be used.

The rotation at any section is determined using the following expression:

$$\theta(x) = \int_{0}^{L/2} \Phi(x) dx - \int_{0}^{x} \Phi(x) dx \tag{6.57}$$

For comparison purposes, the predicted moment/mid-span deflection diagrams were constructed for the three decks. Determination of the moment diagram at each load level was based on the procedure presented earlier taking into account the effect of the end fixity. Calculations were based on a unit strip of each deck loaded at mid-span with a point load and a distributed load due to the self-weight.

6.6. COMPARISON OF ANALYTICAL AND EXPERIMENTAL RESULTS

End fixity of each deck was initially calculated based on the theoretical flexural capacity of the deck. However, degree of fixity, material properties, etc. can all vary within reasonable ranges in order to achieve a better fit between theoretical and experimental results. This section illustrates the results of this empirical procedure that also accounted for maintaining consistency among the three decks and obtaining a reasonable match with experimental deflections and reinforcement strains.

6.6.1. Load-Deflection Relationships

Theoretical deflections were obtained by the double integration of the theoretical moment-curvature curves using the procedure outlined in Section 6.5.5.

6.6.1.1. Bridge Deck with NSM Carbon Rods

Figure 6.10 shows a comparison of the experimental deflections and deflections calculated using fixity level of 16 percent. Analytical deflection calculations were terminated when the moment capacity matched the experimental value. This was achieved at an FRP stress of 235 ksi (1620 MPa). From Figure 6.10, it could be concluded that this fixity level provided the best match in terms of the overall flexural behavior. This level of fixity was also similar to that obtained for the deck with no strengthening, as will be discussed later. The two decks were expected to have similar boundary conditions due to symmetry. However, this indicated that the tensile strength of the CFRP rods is higher than the initial assumption of 144 ksi (993 MPa).

Although a tensile strength of 235 ksi (1600 MPa) is about 28 percent higher than the maximum value of 183 ksi (1300 MPa) obtained from laboratory testing, this value is still significantly lower that theoretical strength of 349 ksi (2400 MPa), determined from the properties of the constituent materials (Yan, 1999). The exact strength of the CFRP rods cannot be determined but it could be concluded that the actual strength of the CFRP rods is larger than 183 ksi (1.26 GPa) and is approximately 235 ksi (1600 MPa).

6.6.1.2. Bridge Deck with Carbon FRP Sheets

Figure 6.11 shows a comparison of the predicted and the experimental load-deflection curves for two levels of ends fixity, 12 and 18 percent. The figure indicates that end fixity level of 12 percent provides a better match with experimental results. However, it does not explain the higher initial stiffness of deck demonstrated experimentally. This high initial stiffness can only be matched if the decks had a level of fixity significantly higher than 12 percent. Much higher fixity level would result is a much smaller maximum theoretical deflection, mid-span moment, and strains at ultimate that do not correlate with the measured experimental values. After the three decks were tested, this deck was jacked up and no shear key or any other possible rotational restraints were observed at the supports. There is no clear evidence as to what caused this higher initial stiffness.

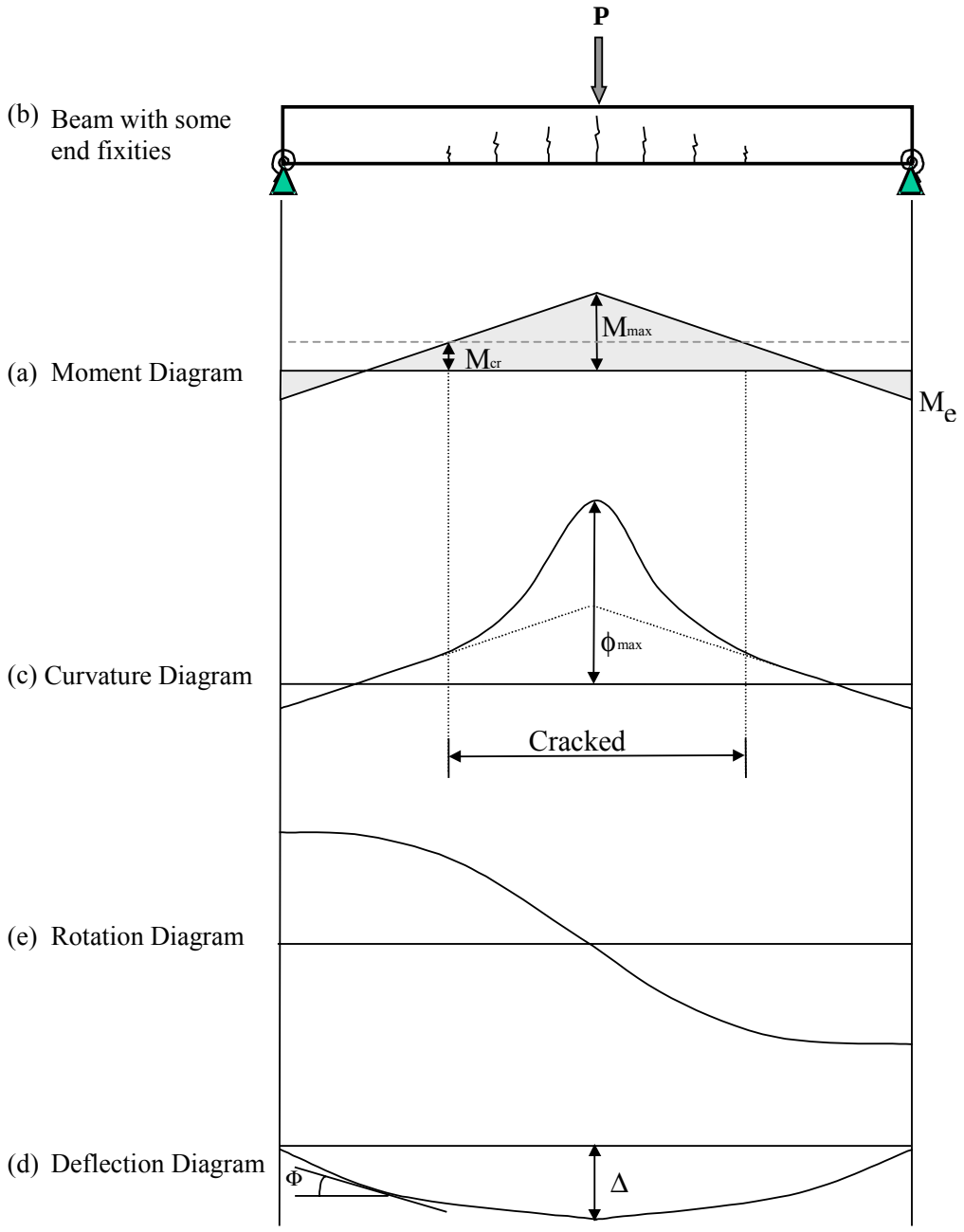

Figure 6.9. Behavior diagrams for a beam with end fixity under concentrated load.

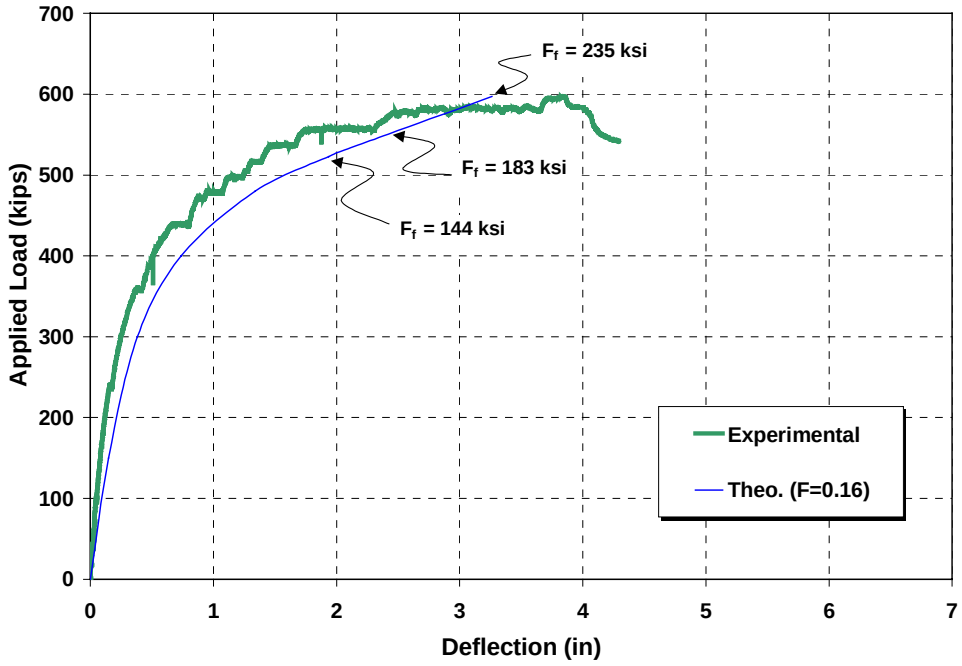

Note: 1 kip = 4.45 kN; 1 in = 25.4 mm

Figure 6.10. Comparison of mid-span deflections for the deck with NSM.

As shown in Figure 6.11, the deck exhibited some ductility prior to failure. This was related to the yielding of steel reinforcement as well as the gradual failure of bonded sheets, which was a combination of debonding and delamination at ultimate.

6.6.1.3. Bridge Deck with No Strengthening

Using the theoretical nominal moment capacity, the level of fixity of the unstrengthened deck was calculated as 26 percent. However, this fixity level was calculated without accounting for higher experimental capacity due to strain hardening of the steel reinforcement. In addition, the predicted load-reinforcement strain curves did not correlate well the experimental results for this fixity level. This is discussed further in the following section. A fixity level of 16 percent is correlated better with the experimental strain measurements. Figure 6.12 shows a comparison of the experimental and two theoretical load-deflection curves based on 16 and 26 percent fixity. Deflection calculations based on 16 percent fixity level provided better match with the measured deflections. It accounts for possible higher experimental capacity at failure due to the contribution of steel strain hardening.

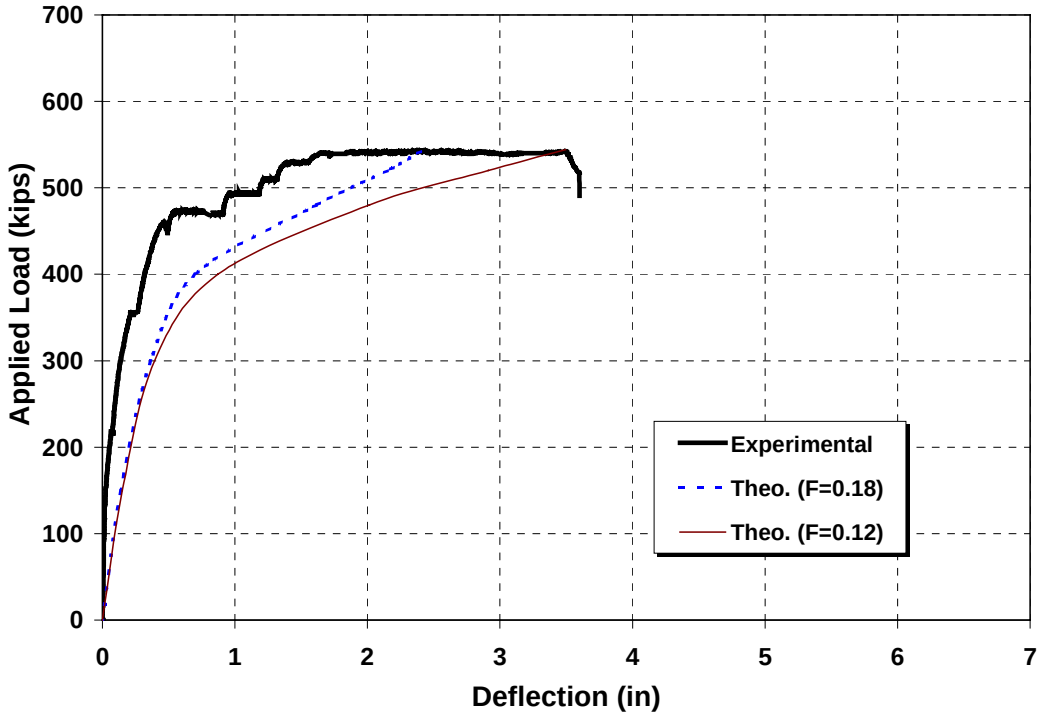

Note: 1 kip = 4.45 kN; 1 in = 25.4 mm

Figure 6.11. Comparison of mid-span deflections for the deck with CFRP sheets.

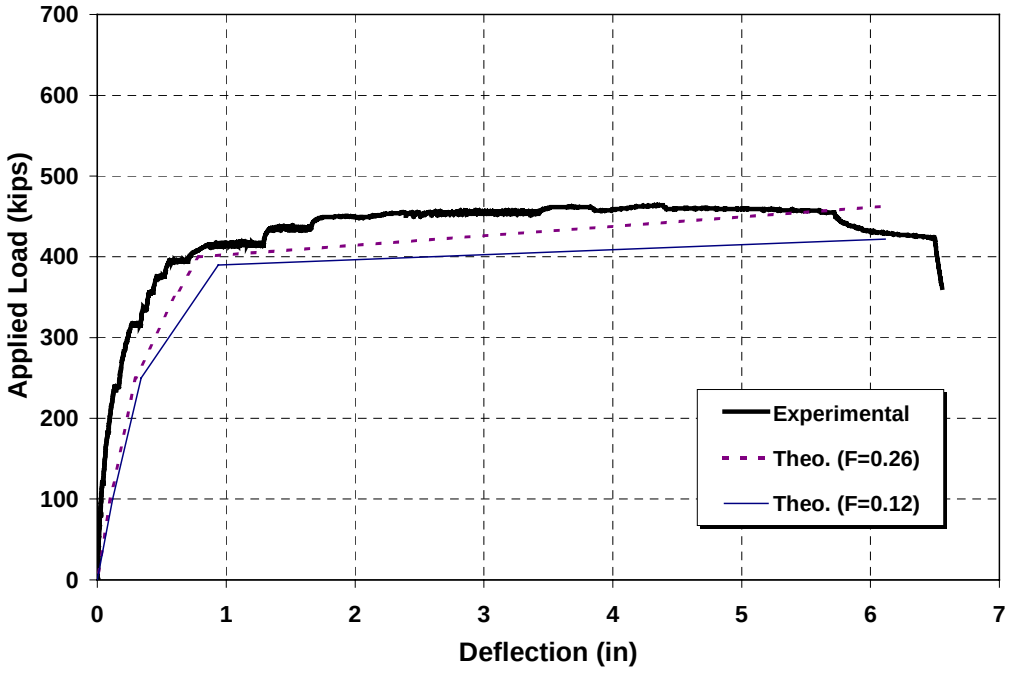

Note: 1 kip = 4.45 kN; 1 in = 25.4 mm

Figure 6.12. Comparison of mid-span deflections for the deck with no strengthening.

6.6.2. Cracking Moment

Based on field observations during testing and the comparison of experimental and theoretical results it was concluded that the cracking moments of the bridge deck exceeded that based on ACI 318-95 building code. Best correlation of cracking moments with experimental results was obtained for a tensile strength of concrete of $12\sqrt{f_c'}$ rather than the value of $7.5\sqrt{f_c'}$ of the ACI 318-95 building code. This could be related to higher tensile strength of concrete due to aging.

6.6.3. Load-Strain Relationships

Since the moment acting on a section is strictly related to the loading configuration and the boundary conditions, comparing the experimental and analytical strains can be used to verify the accuracy of the assumed boundary conditions. Many of the gages on FRP and steel reinforcement did not function due to over exposure to harsh environment (e.g., freezing/thaw and wet/dry cycles). However, data collected with the remaining strain gages were sufficient to draw conclusions. Strains measured at mid-span are more reliable as is more likely to have a cracked section at this location that correlates better with the theoretical analysis.

6.6.3.1. Bridge Deck with NSM Carbon Rods

Figure 6.13 shows a comparison of the analytical steel strain at mid-span and the measured strains of two strain gages S5 and S6. Prior to cracking, the measured strains were very small. Upon cracking, steel reinforcement started to measure strains. Good agreement was observed between theoretical and experimental curves. At higher load level, the cuts made on the bridge parapet closed, resulting in some contribution to the stiffness of the deck. Comparison of theoretical and experimental FRP strains is shown in Figure 6.14. Good agreement was also observed between theoretical and experimental FRP strains.

6.6.3.2. Bridge Deck with Carbon FRP Sheets

The steel reinforcement of the deck strengthened with carbon sheets were instrumented with three strain gages at mid-span. Two of these strain gages were found corrupted. Comparison of the theoretical and experimental steel strains is shown in Figure 6.15. The smaller measured strain is due to the strain gage location, which was at a few inches from a crack. The strain gage signal was lost prior to failure. Similarly a comparison of the theoretical and experimental strains measured on the FRP sheets are shown in Figure 6.16. Signals from both strain gages were lost prior to failure. Strain gage F15 started to pick up strain at a higher pace when a crack formed very close to its location.

6.6.3.3. Bridge Deck with No Strengthening

For the unstrengthened deck, the fixity level to satisfy theoretical nominal moment capacity was determined earlier as 26 percent. Figure 6.17 shows a comparison of the experimental and predicted steel strains. The analytical results indicated that the steel reinforcement would undergo yielding at a load level higher than that obtained from experimental results. While the experimental results indicated that steel yielding occurred at a load level of 380 kips (1689 kN), the theoretical analysis based on 26 percent fixity indicated that yielding would occur at about 430 kips (1911 kN). This indicated that the actual fixity level is lower that 26 percent.

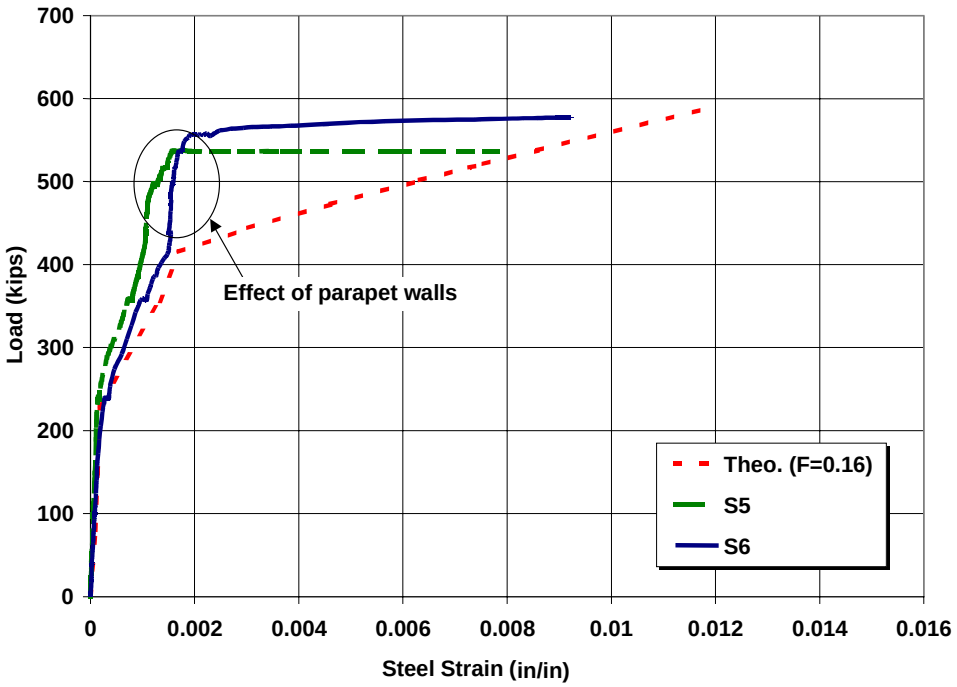

Note: 1 kip = 4.45 kN; 1 in/in = 1 mm/mm

Figure 6.13. Comparison of steel strains for the deck with NSM rods.

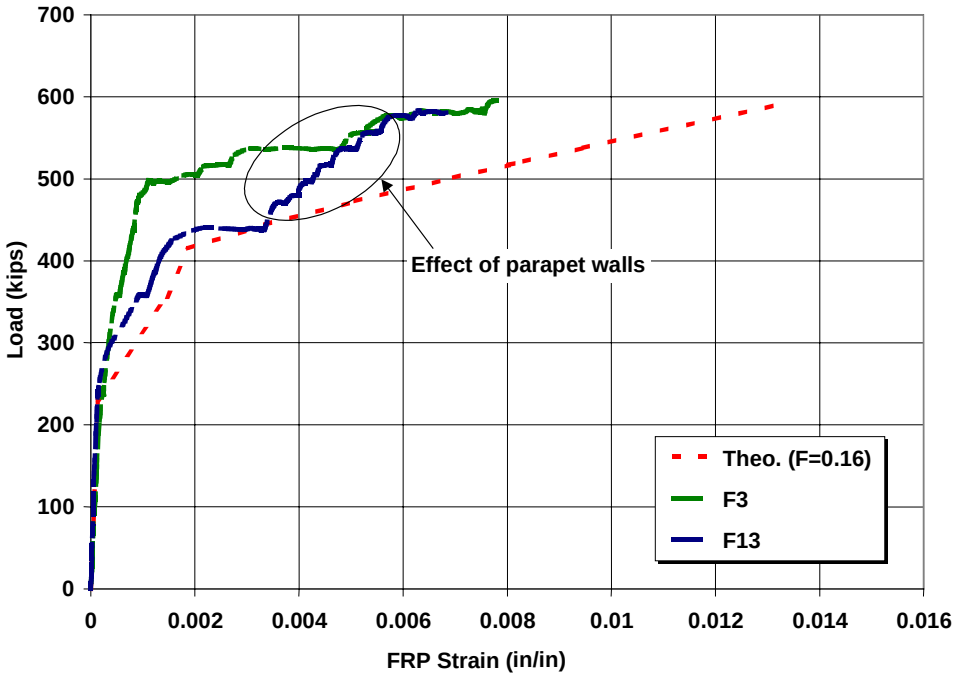

Note: 1 kip = 4.45 kN; 1 in/in = 1 mm/mm

Figure 6.14. Comparison of FRP strains for the deck with NSM rods.

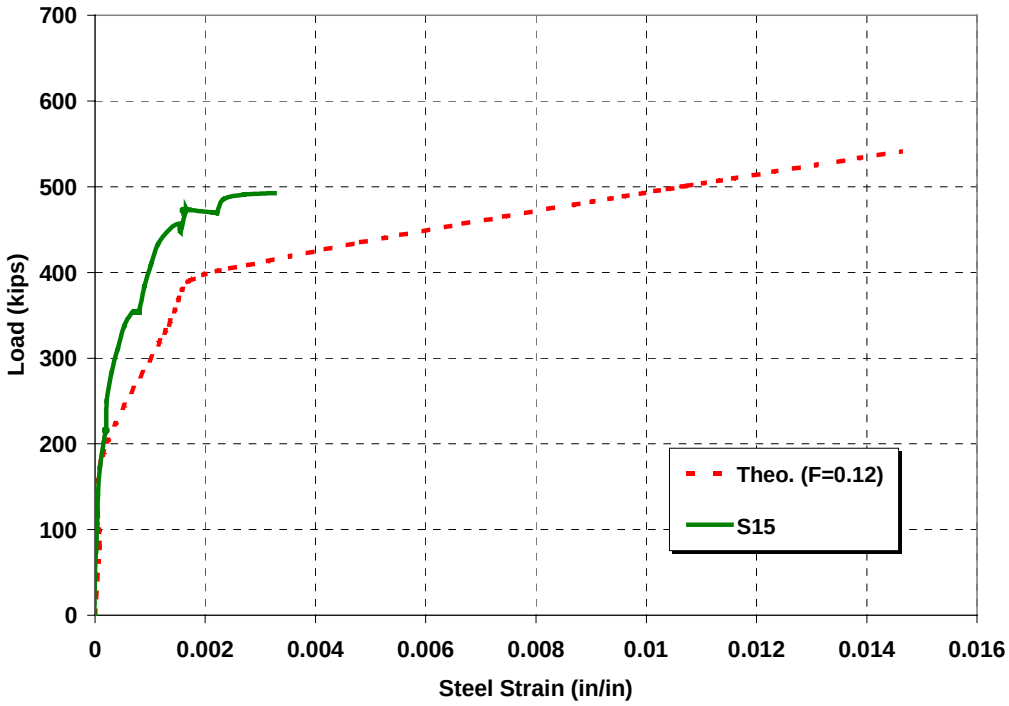

Note: 1 kip = 4.45 kN; 1 in/in = 1 mm/mm

Figure 6.15. Comparison of steel strains for the deck with FRP sheets.

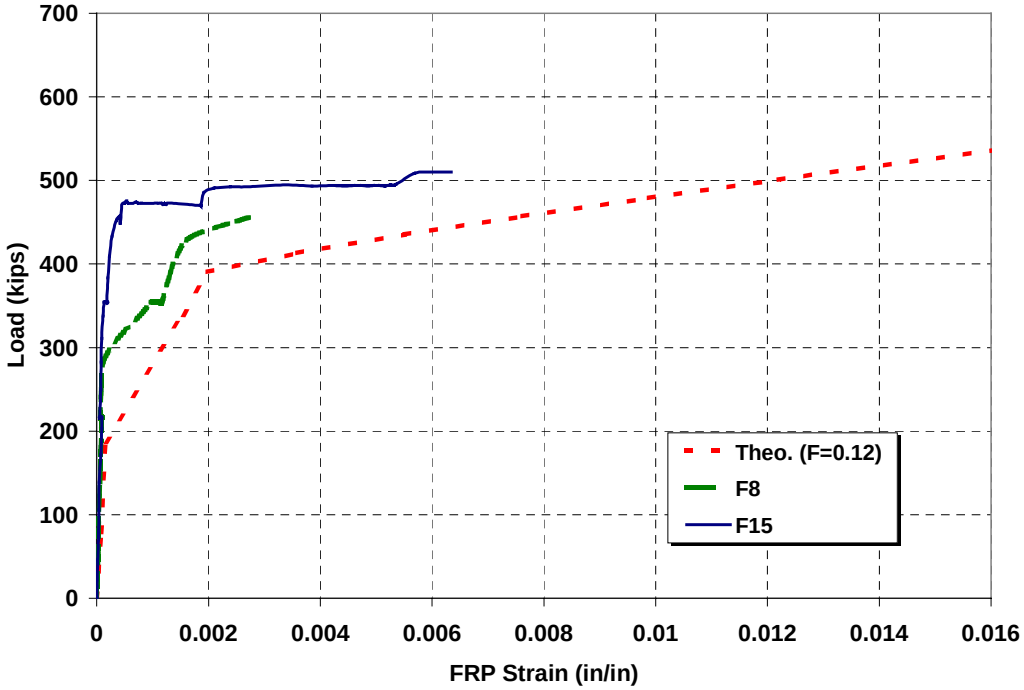

Note: 1 kip = 4.45 kN; 1 in/in = 1 mm/mm

Figure 6.16. Comparison of FRP strains for the deck with FRP sheets.

Analysis of the deck indicated that the strain of steel reinforcement at failure was 0.038 in./in. (mm/mm). Since strain hardening of steel reinforcement is expected to begin at about 0.012 to 0.020 in./in. (mm/mm) (Wang and Salmon, 1998), it is very likely that the strain hardening was achieved. This behavior was not observed for the decks with NSM rods and bonded sheets due to lower strain level at ultimate namely, 0.011 and 0.018 in./in. (mm/mm), respectively. As a result of this behavior, the actual capacity of the deck was higher that that predicted using the classical approach, which does not account for strain hardening. This approach will therefore overestimate the level of fixity. The actual level of fixity should be therefore determined such that steel yielding is achieved at a load level of 380 kips (1689 kN). Through back calculation, this level of end fixity was determined as 16 percent. Comparison of steel strain for this level of fixity and the experimental results are also shown in Figure 6.17.

6.7. SUMMARY

Based on comparison of theoretical and experimental flexural behavior, the fixity for the deck strengthened with NSM rods, bonded sheets, and the unstrengthened deck were determined to be approximately 16.0, 12.0, and 16.0 percent, respectively. For the deck strengthened with NSM CFRP rods, the experimental capacity exceeded the capacity based on CFRP strength of 144 ksi (993 MPa). More accurate capacity was calculated based on the upper limit of experimental test results of rods of 183 ksi (1.26 MPa). For the deck strengthened with CFRP sheets, the experimental capacity was slightly larger than the theoretical capacity. The actual capacity of the unstrengthened deck exceeded the analytical capacity due the strain hardening of steel reinforcement.

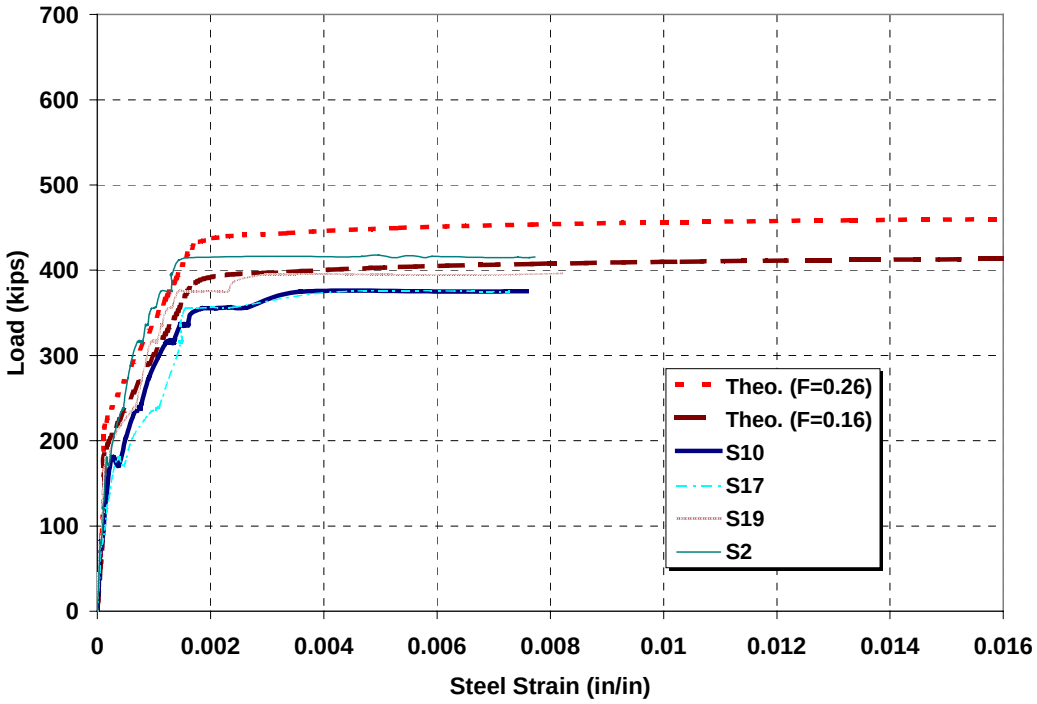

Note: 1 kip = 4.45 kN; 1 in/in = 1 mm/mm

Figure 6.17. Comparison of steel strains for the deck with no strengthening.

Table 6.3 shows a comparison of theoretical live load capacities determined using strength analysis method (SAM) and the experimental capacities based on these fixity levels. Table 6.4 shows a comparison of the corresponding mid-span deflection of the three decks.

The experimental failure modes of the bridge decks were as predicted theoretically based on the actual material properties. The rupture of FRP controlled failure of the strengthened decks while the classical mode of failure of yielding of steel reinforcement followed by the crushing of concrete was attained for the unstrengthened deck.

Table 6.3. Comparison of Live Load Capacities.

	(1) With End Fixity		(2) SAM	(3) Exp.	% Difference $\frac{(3)-(1)}{(1)}.100\%$
	Fixity	Live Load kip (kN)	Live Load kip (kN)	Live Load kip (kN)	
CFRP NSM*	16%	596 (2650)	496 (2200)	596 (2650)	0
CFRP Sheets	12%	544 (2420)	465 (1890)	542 (2410)	0
No Strengthening	16%	417 (1850)	337 (1500)	463 (2060)	11

* Based on CFRP rod strength of 235 ksi (1.62 GPa)

Table 6.4. Comparison of Mid- Span Deflections at Ultimate Load Capacity.

	Mid- Span Deflection, in (mm)			% Difference $\frac{(Exp.)-(Theo.)}{(Theo.)}.100\%$
	Theoretical		Experimental	
CFRP NSM	F = 16.0 %	3.26 (83)	3.87 (98)	19
CFRP Sheets	F = 12.0 %	3.49 (89)	3.52 (89)	0
No Strengthening	F = 16.0 %	6.11 (155)	6.51 (165)	7

7. SUMMARY, CONCLUSIONS, AND RECOMMENDATIONS

7.1. SUMMARY

The primary purpose for conducting this research program was to verify through full scale testing the feasibility and effectiveness CFRP composites for the upgrade/strengthening of solid RC bridge deck. This is a vital aspect of the research program since full-scale testing allows for a better understanding of the behavior of strengthened/unstrengthened bridge decks. Full-scale verification of the capacity improvement would allow for more applications of FRP technology for the strengthening/upgrade of deficient bridges and structures. The full-scale field tests demonstrated the actual behavior of a structure and lead to a better understanding of the performance of the system as a whole, the influence of materials and boundary conditions, and therefore the strengthening design requirements. However, in order to obtain reliable information from destructive load testing, great care must be taken in the design of the test and the instrumentation. Measurements of load and deflection are very useful in calibrating analytical models or determine the stiffness behavior. The boundary rotations and material strains should also be measured.

Volume I of the research program aimed at demonstrating the feasibility and effectiveness of strengthening RC bridge decks with two systems of externally bonded FRP reinforcement to increase their flexural strengths as well as verifying design methodology and capacity improvement. Load rating using MoDOT guidelines indicated that Bridge J857 did not require any load posting. Inventory rating based on HS20 truck indicated that the bridge decks had a deficiency in ultimate strength capacity. The level of deficiency would increase if an HS20 Modified truck were considered. Two of the three simply supported decks were strengthened and tested to failure. One span was strengthened using near-surface mounted (NSM) CFRP rods while the second span was strengthened using externally bonded CFRP sheets. The objective of the strengthening scheme was to increase the flexural capacity by approximately 30%. Each of the three spans was tested to failure by applying quasi-static load cycles.

7.2. CONCLUSIONS

Based on the outcome of the strengthening of the bridge decks, their observed behavior during testing to failure, and the comparison of theoretical and experimental results, the following conclusions can be drawn:

1) The bridge slab had far more capacity than had been anticipated. The higher experimental capacity of the unstrengthened deck was related to higher than anticipated material strengths and the influence of strain hardening of the steel reinforcement.

2) Application of the FRP strengthening system was characterized by speed and ease of installation. However, the installation of FRP strengthening systems is deceptively simple. Caution should be paid to ensure proper application in terms of material handling, fiber alignment (for FRP sheets), and mixing and application of epoxies. The surface to which CFRP sheets should be smooth and cavities should be appropriately patched. Improper surface preparation may cause premature failure due to rupture/debonding of bonded sheets.

3) Elastic finite element analysis (FEA) of the deck indicated that for the loading configuration considered in this study the moment distribution was similar to that obtained using a closed-form beam analysis. This was the result of the small skew angle of the deck (15 degree) and the load configuration in which load was applied on four points that was distributed across the width of the deck parallel to the supports.

4) The addition of FRP reinforcement had insignificant contribution to the stiffness of strengthened decks prior to steel yielding. This behavior was related to the relatively small amount of added FRP reinforcement. The stiffness of strengthened decks after the yielding of the steel reinforcement was related to the axial stiffness of FRP reinforcement. Similar results were obtained from the analytical investigation. For simplicity, when checking serviceability requirements of FRP strengthened decks, the contribution of the FRP reinforcement should be ignored.

5) The measured response of the decks from testing to failure indicated that some level of restraint existed even though the joints between the decks were cut clean. A strengthening design based on the assumption of simple supports was therefore conservative.

6) The experimental failure modes of the bridge deck strengthened with NSM rods was as theoretically predicted (rupture of the CFRP rods). Failure of the deck strengthened with CFRP sheets was a mixture of debonding and rupture of the CFRP sheets. The classical mode of failure of yielding of steel reinforcement followed by the crushing of concrete was attained for the unstrengthened deck.

7) The strengthened decks exhibited ductile behavior prior to failure. This behavior was due to the fact that steel reinforcement yielded prior to FRP failure. There is trade off between strength increase and ductility.

8) In deck 2, it is likely that the externally bonded reinforcement did not attain its full potential due to a mixed mode type of failure consisting of debonding and rupture.

9) The approach utilized in this study (based on equilibrium of forces and compatibility of strains) for design/analysis of an RC deck strengthened with NSM FRP rods is satisfactory. The approach is also appropriate for an RC deck strengthened with CFRP sheets when the governing mode of failure is that of fiber rupture.

7.3. RECOMMENDATIONS FOR FUTURE RESEARCH

The following are recommendations for future research that are based on experimental observations and interpretation of test results.

1) There is need for a research program to develop model construction specifications for agencies engaged in the FRP repair and inspection of highway bridges. The study should develop recommended specifications, supporting tests, and field procedures to be integrated into existing state highway agency oversight activities in product acceptance, construction contracting, inspection, and repair with FRP composites.

2) With the development of externally applied FRP sheets and near surface mounted rods, durability performance may be considered a significant concern since these systems incorporate FRP at or near the surface of the concrete where the concrete has its greatest susceptibility to degradation from external influences. A research program that identifies both the strengths and limitations for various FRP materials under several exposure conditions could address the durability issues. The research program should also identify the construction procedure that ensures the long-term performance for FRP repair and retrofit systems bonded to concrete structural elements. The aim of this program would be the ability to predict the long-term performance of FRP systems using test methods developed for conductance over a short period of time.

3) Application of NSM FRP rods do not require any surface preparation work and requires minimal installation time compared to FRP sheets. Since the effectiveness of this type of reinforcement is strictly related to the quality of bond between the reinforcement and the surrounding material, the good performance of bond between NSM FRP rods and concrete is crucial for this technique to be effective. Groove sides roughness, application of primer coating, and concrete strength are all factors that can affect bond characteristics of epoxy with concrete and should be investigated.

4) Research is also needed to investigate the variables pertaining to the type of rod to be used, that is, diameter, type of FRP material (Glass, Aramid, or Carbon FRP) and surface condition of the rod (smooth or deformed) in order to assess their influence on the effectiveness of the NSM system. In addition, the issue of groove dimensioning of NSM FRP rods should be addressed. No literature addressing the effect of groove dimensions on the bond for near surface mounted bars was available.

8. REFERENCES

AASHTO (1983), Manual for Maintenance Inspection of Bridges, American Association of State Highway and Transportation Officials, Washington D.C.

AASHTO (1996), Standard Specifications for Highway Bridges, Sixteenth Edition, American Association of State Highway and Transportation Officials, Washington D.C.

ACI Committee 440 (1996), "State-of-the-Art Report on FRP for Concrete Structures," (ACI 440R-96), Manual of Concrete Practice, American Concrete Institute, Farmington Hills, Michigan, 68 pp.

ACI Committee 440 (2000), "Guide for the Design and Construction of Externally Bonded FRP Systems for Strengthening Concrete Structures," Draft Document. Revised May, 2000.

ACI Committee 440H (2000), "Provisional Design Recommendations for Concrete Reinforced with FRP Bars," Draft Document. Revised November, 2000. In print.

Benmokrane, B. and Rahman, H., Editors (1998), "Durability of Fiber Reinforced Polymer (FRP) Composites for Construction," Proceedings of the First International Conference (CDCC '98), Quebec, Canada, 692 pp.

Benmokrane, B., Gao, D., Ton-That, T. M., and Zhang, B. (1999), "Standard Test Methods for FRP Rod and Sheet," Published by Intelligent Sensing for Innovative Structures (ISIS)-Canada, University of Manitoba, Winnipeg, Canada, 65 pp.

Butalia, T. S., Kant, T., and Dixit, V. D. (1990), "Performance of Heterosis Element For Bending of Skew Rhombic Plates," *Computer & Structures*, Vol. 34, No. 1, pp. 23-49.

Castro, A., Kim, R.Y., Fowler, C., and Mistretta, J.P. (1996), "Rehabilitation of Concrete Bridges Beams with Externally-Bonded Composite Plates," Part1," Proceeding of the First International Conference on Composites in Infrastructure (ICCI-96), Tucson, Arizona, pp. 857-869.

El-Badry, M., Editor (1996), "Advanced Composite Materials in Bridges and Structures (ACMBS-II)," Proceedings of the Second International Conference, Montreal, Canada, 1027 pp.

GangaRao, H.V.S., Thippeswamy, H.K., Kumar, S.V., and Franco, J.M. (1997), "Design, Construction, and Monitoring of the First FRP Reinforced Concrete Bridge Deck in the United States," Non-Metallic (FRP) Reinforcement for Concrete Structures, Proceedings of the 3rd Int. Symposium, Sapporo, Japan, Vol. 1, 647-656.

Goldstein, H. (1996), "Catching Up on Composites," Civil Engineering, May, pp.47-49.

Huria, V., Lee, K. L, and Aktan, A. E. (1993), "Integrated Inspection and Rating of RC Slab Bridges," submitted as technical notes, Journal of Structural Engineering, ASCE, March.

Iyer, S.L. and Sen, R., Editors (1991), "Advanced Composite Materials in Civil Engineering Structures," Proceedings of the Specialty Conference, American Society of Civil Engineers, New York, New York, 443 pp.

Japan Society of Civil Engineers (JSCE) (1997a), "Recommendation for Design and Construction of Concrete Structures Using Continuous Fiber Reinforcing Materials," Concrete Engineering Series, No. 23, 325 pp.

Japan Society of Civil Engineers (JSCE) (1997b), Proceeding of the Third International Symposium on Non-Metallic (FRP) Reinforcement for Concrete Structures (FRPRCS-3), Japan Concrete Institute, Sapporo, Japan, Vol. 1&2.

Kemna, A. C. (1999), "The Theoretical Analysis Regarding Flexure of a Reinforced Concrete Slab Bridge Strengthened with Carbon Fiber Reinforced Plastics," Master thesis, University of Missouri-Columbia, Columbia, Missouri.

Kemna, D. J. (1999), "Field Testing of a Concrete Slab Bridge Externally Strengthened with Carbon Fiber Reinforced Polymers," Master thesis, University of Missouri-Columbia, Columbia, Missouri.

L'Hermite, R.L, and Bresson, J. (1967), "Beton Arme' par Collage des Armatures," RILEM International Symposium, Resin in Building Construction, Part 2, Paris, pp. 175-203.

MacGregor, J. C. (1997), Reinforced Concrete Mechanics and Design, 3rd ed, Prentice-Hall, Inc., pp 82-133.

Master Builders Technologies (MBT) (1998), MBrace Composite Strengthening System: Engineering Design Guidelines, Second Edition, Cleveland, Ohio.

Meier, U., and Kaiser, H. P. (1991), "Strengthening of Structures with CFRP Laminates," Advanced Composite Materials in Civil Engineering Structures, ASCE Specialty Conference, pp. 224-232.

Meier, U. (1987), " Bridge Repair with High Performance Composite Materials," Material und Technik, V. 4, pp. 125-128 (in German).

MoDOT Bridge Load Rating Manual (1996), Missouri Department of Transportation, Jefferson City, Missouri, pp 4.1-4.28

Nanni, A. (1997), "Carbon FRP Strengthening: New Technology Becomes Mainstream," Concrete International, American Concrete Institute, Vol. 19, No. 6, June, pp. 19-23.

Nanni, A., Editor (1993), "Fiber-Reinforced-Plastic (FRP) Reinforcement for Concrete Structures: Properties and Applications," Developments in Civil Engineering, Elsevier Science Publishers, Amsterdam, The Netherlands, Vol. 42, 450 pp.

Nanni, A. and Dolan, C.W., Editors (1993), "Fiber-Reinforced-Plastic Reinforcement for Concrete Structures, SP-138," American Concrete Institute, Detroit, Michigan, 977 pp.

Nanni, A., Focacci, F., and Cobb, C. A. (1998), "Proposed Procedure for the Design of RC Flexural Members Strengthened with FRP Sheets," Proceeding of the Second International Conference on Composites in Infrastructure (ICCI-98), Tucson, Arizona, Vol. 1, pp. 187-201.

Neale, K.W. and Labossiere, P., Editors (1992), "Advanced Composite Materials in Bridges and Structures," Proceedings of the First International Conference (ACMBS-I), Sherbrooke, Canada, 705 pp.

Rubinsky, I. A., and Rubinsky, A. (1954), "An Investigation into the Use of Fiber-Glass for Prestressed Concrete," Magazine of Concrete Research, V. 6.

Saadatmanesh, H. and Ehsani, M. R., Editors (1998), "Fiber Composites in Infrastructure," Proceeding of the Second International Conference on Composites in Infrastructure (ICCI-98), Tucson, Arizona.

Sharif, A., and Baluch, M.H., (1996), "External FRP Plates to Strengthen Reinforced Concrete Beams," Proceeding of the First International Conference on Composites in Infrastructure (ICCI-96), Tucson, Arizona, pp. 814-828.

Small, E. P. (1998), "Condition of the Nation's Highway Bridges," TR News, Transportation Research Board, No. 194, Jan-Feb, pp. 3-8.

Swamy, R.N., Jones, R. and Bloxham, J.W. (1987), "Structural Behavior of Reinforced Concrete beams Strengthened by Epoxy-Bonded steel Plates", The Structural Engineer, Vol. 65A, No. 2, pp. 59-68.

Taerwe, L., Editor (1995), "Non-Metallic (FRP) Reinforcement for Concrete Structures," Proceeding of the Second International RILEM Symposium (FRPRCS-2), Ghent, Belgium, 714 pp.

Todeschini, C., Bianchini, A. C., and Kesler, C. E. (1964), "Behavior of Concrete Columns Reinforced with High Strength Steels," ACI Journal, Proceeding, Vol. 61 No. 6, pp. 701-716.

Vecchio, F. J., and Collins, M. (1986), "The Modified Compression Field Theory For reinforced Concrete Element Subjected to Shear," ACI Journal, Proceedings, Vol. 83, No. 2, March-April, pp. 219-231.

Wang, C. K., and Salmon, C. G. (1998), Reinforced Concrete Design, John Wiley and Sons, 1042 PP.

White, T.D., Editor (1992), "Composite Materials and Structural Plastics in Civil Engineering Construction," Proceeding of the Materials Engineering Congress, American Society of Civil Engineers, New York, New York, pp. 532-718.

Whitney, C. S. (1942), "Plastic Theory of reinforced Concrete Design," Transactions, ASCE, 107, pp. 251-326.

Wines, J. C., et al. (1966), "Laboratory Investigation of Plastic-Glass Fiber Reinforcement for Reinforced and Prestressed Concrete," U.S. Army Corps of Engineers, WES, V. 1 & 2, Vicksburg, MS, 228 pp.

Xiao, Y. and Ma, R. (1997), "Seismic Retrofit of RC Circular Columns Using Prefabricated Composite Jacketing," Journal of Structural Engineering - ASCE, Vol. 123, No. 10, pp. 1357-1364.

Yan, X. (1999), " Thesis," Constructability and Performance of Concrete Members Prestressed with CFRP Tendons, University of Missouri-Rolla, Rolla, Missouri.

Yan, X., Miller, B., Nanni, A., and Bakis, C.E. (1999), "Characterization of CFRP Bars Used as Near-Surface Mounted Reinforcement", Proceedings 8th International Structural Faults and Repair Conference, M.C. Forde, Ed., Engineering Technics Press, Edinburgh, Scotland, 10 pp., CD-ROM version.

APPENDIX A:

ORIGINAL BRIDGE PLANS

MISSOURI STATE HIGHWAY DEPARTMENT

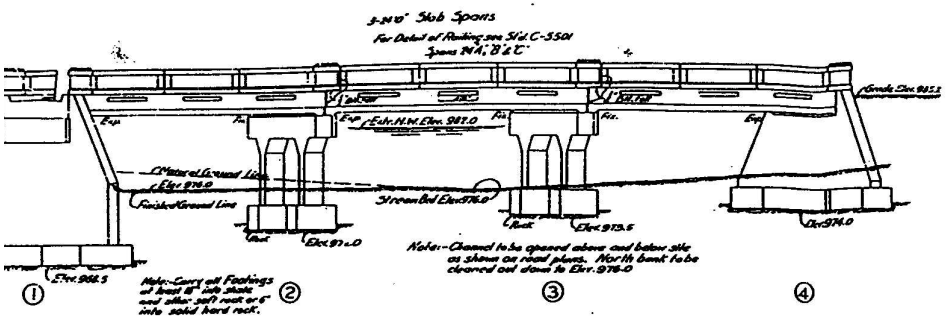

ELEVATION

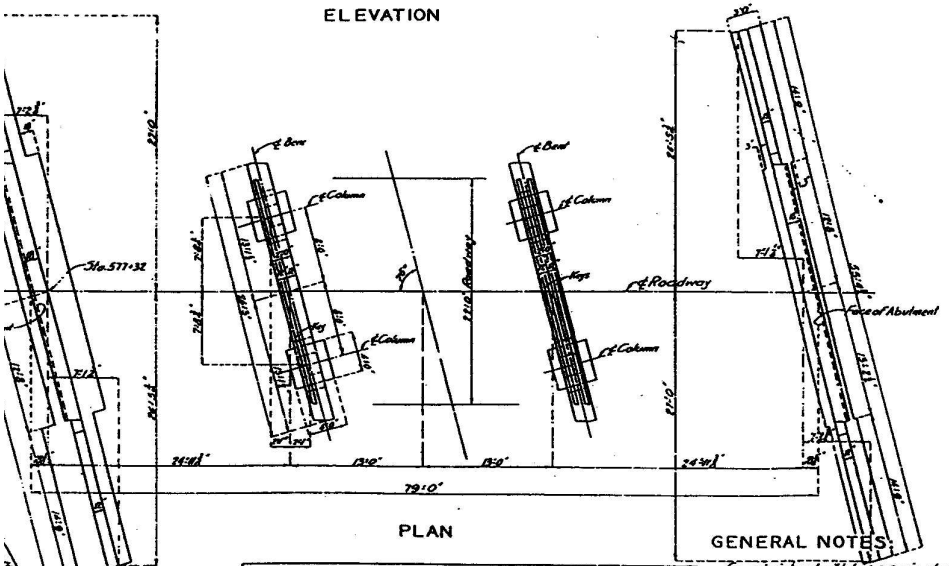

PLAN

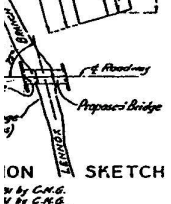

SKETCH

COMPLETE BILL OF REINFORCING STEEL

No	Size	Length	Mark	Location
				Superstructure
24	1"	9'6"	Bm1	Rod
54	1"	8'	Bt	"
60	1"	9'0"	Bm3	Sub-post
31	1"	4'6"	Rm1	Rod
648	3/4"	18'	Rt	Bolster
24	1"	7'5"	Rm1	Rod
6	1"	7'5"	Rt	Rod
16	1"	7'6"	Rm1	Rod
6	1"	18'8"	Rm1	"
12	3/4"	20'3"	Cm1	Curb
6	3/4"	25'8"	Cm1	"
72	3/4"	15'	Ct	"
177	1"	25'8"	St	Slab
33	1"	22'5"	St	"
12	1"	26'8"	St	"
6	1"	25'0"	St	"
				Substructure
				Abutment No1.
26	1"	12'9"	A1	Abutment
20	1"	8'0"	A2	"
19	1"	7'6"	A3	"
56	1"	6'8"	B1	Footing
21	1"	25'6"	H1	Abutment
24	1"	16'9"	H2	Wings
7	1"	21'0"	H3	"
2	1"	15'0"	H4	"
1	1"	19'6"	H5	"
14	1"	21'0"	W1	"
10	1"	15'0"	W2	"
22	3/4"	8'0"	W3	"
4	1"	10'9"	W1	"
2	3/4"	9'9"	W3	"

Bending Sketches & Cutting Programs

Superstructure:

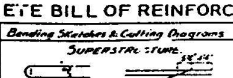

Substructure:

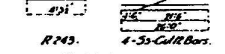

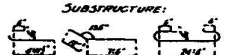

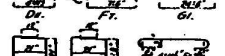

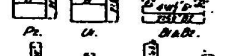

No	Size	Length	Mark	Location
				Beat No 2
5	1"	41'1"	Dr	Footing
14	1"	8'6"	Fr	Haunch
12	1"	71'3"	Gr	Beam
1	1"	71'3"	Gr	"
8	1"	8'8"	Pr	Column
8	1"	8'0"	Pr	"
32	1"	9'0"	Ur	Beam
				Beat No 3.
8	1"	6'3"	Dr	Footing
10	1"	8'6"	Fr	Haunch
12	1"	37'3"	Gr	Beam
1	1"	18'3"	Gr	"
6	1"	8'8"	Pr	Column
8	1"	7'5"	Pr	"
30	1"	9'0"	Ur	Beam
				Abutment No 4.
28	1"	7'5"	A2	Abutment
14	1"	10'9"	A5	"
13	1"	8'0"	A6	"
55	1"	4'5"	B2	Footing
13	1"	25'6"	H7	Abutment
7	1"	23'0"	H3	Wing
2	1"	19'6"	H2	"
1	1"	21'0"	H6	"
14	1"	20'0"	W6	"
7	1"	18'3"	W5	"
14	1"	7'6"	W6	"
4	1"	16'9"	W7	"
2	1"	4'0"	W8	"
8	1"	16'9"	W2	Footing

Note:- Dimensions given are along center line and are for computed lengths.
Reinforcing bars ¾" or over in diameter which are bent to an angle greater than 30° shall be of structural grade.

ESTIMATED QUANTITIES

Item		Superstr.	Substr.	Total
Excavation Class 1	Cu.Yds.		70	70
Excavation Class 2	Cu.Yds.		190	190
Concrete 1:2:3 mix "A"	Cu.Yds.	8.4		8.4
Concrete 1:2:4 mix "B"	Cu.Yds.		99.5	99.5
Concrete 1:2:3½ mix "X"	Cu.Yds.	114.8		114.8
Reinforcing Steel	Lbs.	14850	7840	22690

Note: Bridge excavation above Elev. 976.0 will be paid for as class 1 bridge excavation.
Bridge excavation below Elev. 976.0 will be paid for as class 2 bridge excavation.

GENERAL NOTES:

Concrete in handrail to be 1:2:3 mix, class "A". Concrete in slabs and curbs to be 1:2:3½ mix, class "X". All other concrete to be 1:2:4 mix, class "B" concrete.

Exposed edges to be beveled ¾" where no other bevel is noted.

Iron name plates type "A" as shown on Standard 3-48 to be furnished and placed by contractor. Cost of name plates to be included in price bid for other items.

Fibre bituminous felt is used in expansion or partition joints in concrete, stitched 6" in vertical joint securely to one face of concrete with copper wire.

Only sufficient camber to be used in construction to insure against settlement below lines given as finished grade. No permanent camber required in individual spans.

Excavation to be in accordance with Section 1 of Standard Specifications issued April 1, 1930.

Note:- This drawing is not to scale. Follow dimensions.

FINISHED

(Sheet 1 of 3)

B.M. Elev. 976.19 - Notch in 12" black walnut tree #721. Sta. 576+30.6

BRIDGE OVER LENNOX BRANCH

STATE ROAD FROM ROLLA TO SALEM

ABOUT 12 MILES SOUTH OF ROLLA

PROJECT NO. R 72 AP-53 STA. 577+32

FINISHED

PHELPS COUNTY

Submitted by M. K. Boyle, Bridge Engineer, date 9/27/31

Approved by T. H. Cutler, Chief Engineer, date 9/27/31

STD.S-810
STD.C-550I
J-857

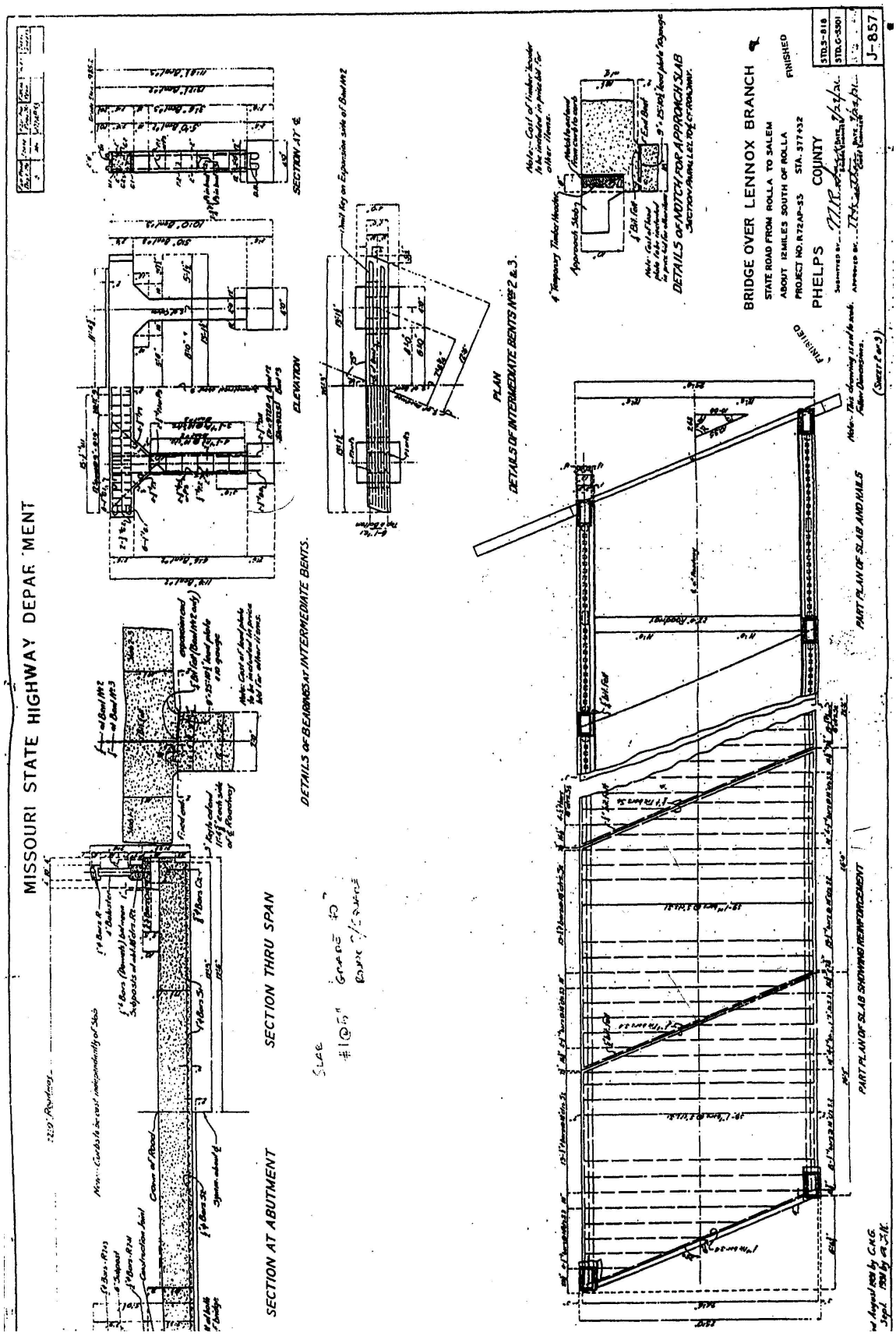
MISSOURI STATE HIGHWAY DEPARTMENT
BRIDGE OVER LENNOX BRANCH
STATE ROAD FROM ROLLA TO SALEM
ABOUT 12 MILES SOUTH OF ROLLA
PROJECT NO. R72AP-33
STA. 377+32
FINISHED
PHELPS COUNTY
J-857
SECTION AT ABUTMENT
SECTION THRU SPAN
DETAILS OF BENTS AT INTERMEDIATE BENTS.
ELEVATION
SECTION AT "E"
PLAN
DETAILS OF INTERMEDIATE BENTS Nos 2 & 3.
DETAILS OF NOTCH FOR APPROACH SLAB
PART PLAN OF SLAB AND WALLS
PART PLAN OF SLAB SHOWING REINFORCEMENT

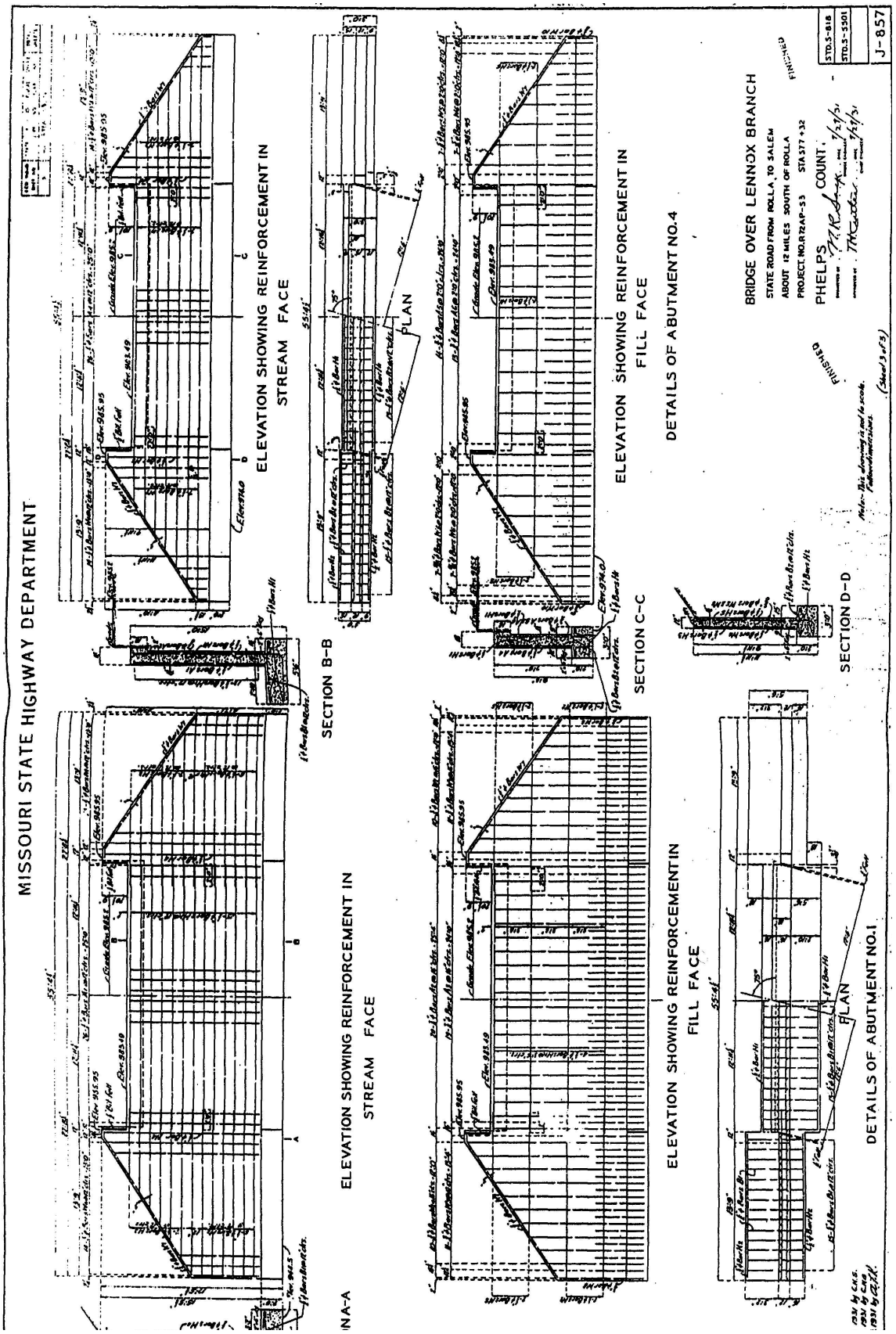
MISSOURI STATE HIGHWAY DEPARTMENT
ELEVATION SHOWING REINFORCEMENT IN STREAM FACE
PLAN
SECTION B-B
ELEVATION SHOWING REINFORCEMENT IN FILL FACE
SECTION C-C
DETAILS OF ABUTMENT NO.4
SECTION D-D
ELEVATION SHOWING REINFORCEMENT IN STREAM FACE
ELEVATION SHOWING REINFORCEMENT IN FILL FACE
DETAILS OF ABUTMENT NO.1
BRIDGE OVER LENNOX BRANCH
STATE ROAD FROM ROLLA TO SALEM
ABOUT 12 MILES SOUTH OF ROLLA
PROJECT NO.R72AF-53 STA 377+32
PHELPS COUNT
STD.5-818
STD.5-1501
J-857

APPENDIX B:

BRIDGE STRENGTHENING DESIGN

The approach discussed hereafter is used to determine the bending moment capacity of RC members strengthened with NSM FRP rods to meet the desired strength of 102 ft-k/ft (453 kN-m/m). The strengthening design approach is based on iteration procedure in which a concrete strain at failure is first assumed and the depth of neutral axis is determined by trial and error.

Conversion factors

1 in. =25.4 mm
1 in./in. =1 mm/mm
1 in^2 = 645 mm^2
1 kip = 4.45 kN
1 psi = 6.895E-3 MPa
1 ksi = 6.895 MPa
1 ft-k/k = 4.45 kN-m/m

Design of NSM Strengthening

The sectional and material properties are listed below.

h	=	18.5	in.
b	=	12	in.
d	=	16.5	in.
d_n	=	18.0	in.
f'_c	=	2500	psi
A_s	=	1.88	in^2
f_y	=	33000	psi
E_s	=	29000	ksi
A_f	=	0.12	in^2
f_{fu}	=	144000	psi
E_f	=	17200	ksi

After few iterations, assume ε_c **= 0.00214**

$$\varepsilon'_c = \frac{1.71(2500)}{57000\sqrt{2500}} \qquad = 0.0015 \text{ in./in.}$$

$$\beta_1 = \frac{4*0.0015 - 0.00214}{6*0.0015 - 2*0.00214} \qquad = 0.818$$

$$\alpha_1 = \frac{3*0.0015*0.00214 - 0.00214^2}{3*0.818*0.0015^2} \qquad = 0.915$$

The multiplier on the beam depth to find the depth of the neutral axis of the cracked section is calculated as k = 0.279. This produces a cracked moment of inertia of I_{cr} = 1907 in^4. The tensile strain at the deck soffit at the time of FRP installation is calculated to be 417 με.

Assuming c = ***3.53*** in., the strain and stress of steel and FRP reinforcement are determined as follows:

$$\varepsilon_f = 0.00214 * \frac{18 - 3.53}{3.53} - 0.000417 \qquad = 0.00836 \text{ in./in.}$$

$$f_f = 17200 * 0.00836 \le 144 \qquad = 143.8 \text{ ksi}$$

$$\varepsilon_s = 0.00214 * \frac{16.5 - 3.53}{3.53} \qquad = 0.00787 \text{ in./in.}$$

$$f_s = 29000 * 0.00787 \le 33 \qquad = 33 \text{ ksi}$$

These results indicate that the stress in FRP reaches its ultimate strength before the concrete. Therefore, the rupture of FRP reinforcement governs failure.

The depth of neutral axis is determined as follows:

$$c = \frac{1.88(33{,}000) + 0.12(143{,}800)}{0.915 * 0.818 * 2500 * 12} \qquad = 3.53 \text{ in.}$$

The moment capacity is determined as follows:

$$M_n = \left(1.88 * 33\left(16.5 - \frac{0.818 * 3.53}{2}\right) + 0.12 * 143.8\left(18.0 - \frac{0.818 * 3.53}{2}\right)\right) * 1/12$$

M_n = 102 ft-k/ft

Design of Surface Bonded Sheets Strengthening

The sectional and material properties are listed below.

h	=	18.5	in.
b	=	12	in.
d	=	16.5	in.
f'_c	=	2500	psi
A_s	=	1.88	in^2
f_y	=	33000	psi
E_s	=	29000	ksi
A_f	=	0.0416	in^2
f_{fu}	=	550000	psi
E_f	=	33000	ksi

After few iterations, assume ε_c = **0.003**

$$\varepsilon'_c = \frac{1.71(2500)}{57000\sqrt{2500}} \qquad = 0.0015 \text{ in./in.}$$

$$\beta_1 = \frac{4*0.0015 - 0.003}{6*0.0015 - 2*0.003} \qquad = 0.833$$

$$\alpha_1 = \frac{3*0.0015*0.003 - 0.003^2}{3*0.833*0.0015^2} \qquad = 0.900$$

The multiplier on the beam depth to find the depth of the neutral axis of the cracked section is calculated as k = 0.279. This produces a cracked moment of inertia of I_{cr} = 1907 in^4. The tensile strain at the deck soffit at the time of FRP installation is calculated to be 417 με.

Assuming c = ***3.51*** in., the strain and stress of steel and FRP reinforcement are determined as follows:

$$\varepsilon_f = 0.003*\frac{18.5 - 3.51}{3.51} - 0.000417 \qquad = 0.0124 \text{ in./in.}$$

$$f_f = 33{,}000*0.0123 \le 550 \qquad = 409.3 \text{ ksi}$$

$$\varepsilon_s = 0.003*\frac{18.5 - 3.51}{3.51} \qquad = 0.01162 \text{ in./in.}$$

$$f_s = 29000*0.01098 \le 33 \qquad = 33 \text{ ksi}$$

These results indicate that failure is governed by concrete crushing. The depth of neutral axis is determined as follows:

$$c = \frac{1.88(33{,}000) + 0.0416(409{,}300)}{0.900 * 0.833 * 2500 * 12} = 3.51 \text{ in.}$$

The moment capacity is determined as follows:

$$M_n = (1.88 * 33(16.5 - \frac{0.833 * 3.51}{2}) + 0.0416 * 409.3(18.0 - \frac{0.833 * 3.51}{2})) * 1/12$$

$M_n = 102$ ft-k/ft

APPENDIX C:

LINEAR FINITE ELEMENT MODELING OF BRIDGE DECKS

Skewed plates are often used in modern structures in spite of the mathematical complexity involved in their study. For bridge construction, complex alignment problems in bridges are often solved by the use of skew plates. Analytical methods, with the exemptions of the simplest cases, are inadequate for solution of skew plates. The finite element (FE) method, on the other hand, appears to be the most recommended numerical technique.

The reported research provided an opportunity to evaluate the reliability of linear finite element modeling of the bridge deck to assess deflections under loads in the elastic range. With a reliable FE model, it will be possible to address some of the structural engineering aspects of modeling a bridge deck. The experimental results can be used to gage the boundary conditions of the deck as well as determining deflections and the magnitude and location of the maximum bending moments resulting from different loading configurations. The following reports on the analyses that were conducted as a part of this research program. It begins with a simple modeling of a plate element with a given skew angle and boundary conditions similar to the actual bridge deck. The mesh layout was refined until the model yielded results with acceptable error. The model was benchmarked using two loading conditions, uniform and concentrated loading. Limited amount of literature that addresses plates with a skew angle less than 30-degree were sited. Only one sited reference provided the analytical solution for plates with a 15-degree skew (Butalia, 1990).

A two-dimensional plate with given thickness was used to model the bridge deck. The deck slab was assumed to be simply supported. Initially, no rotational springs were assumed at the supports for the FE model. FE analysis was achieved using ABAQUS. However, the modeling of a plate structure could be achieved using any FE software package. The ABAQUS software was mainly used due to its availability.

The element type used for this study is S4R, general-purpose shell element. This element type allows transverse shear deformation. They use thick shell theory as the shell thickness increases and become discrete Kirchhoff thin shell element as the thickness decreases; the transverse shear deformation becomes very small as the shell thickness decreases. This element type accounts for finite membrane strains and will allow for change in thickness. They are therefore suitable for large strain analysis involving materials with a nonzero effective Poisson's ratio.

An initial model was built for a 25 ft by 25 ft (7.6 m by 7.6 m) plate with a thickness of 1.5 ft (0.46 m) and a 15-degree skew. To replicate the actual boundary conditions of the deck, two opposite edges were simply supported and the other two were free. Two loading conditions were used to benchmark the model: a uniform loading that covered the entire plate and a concentrated load at the center of the plate. The mesh was refined until the FE solution and the analytical solution converged and the error was minimized. Errors within 5% were obtained for a mesh of 40 by 40 elements. This model was therefore considered satisfactory. The elements mesh for this configuration is shown in Figure C.1. For the skew plate shown in Figure C.2, the analytical solution for the bending moment and deflection at the center of the plate under uniform loading are given by the following formulas (Butalia, 1990):

$$M_c = 46.664 \cdot Qa^2 \cdot 10^{-2} \tag{C-1}$$

$$\Delta_c = 18.556 \cdot \frac{Qa^4}{D} \cdot 10^{-2} \tag{C-2}$$

For a concentrated load at the center of the plate, the bending moment and deflection at the center of the plate are given by the following formulas:

$$M_c = 45.126 \cdot Ca^2 \cdot 10^{-2} \qquad \text{(C-3)}$$

$$\Delta_c = 85.811 \cdot \frac{Ca^2}{D} \cdot 10^{-3} \qquad \text{(C-4)}$$

The case given in Figure C.2 is identical to the model shown in Figure C.1. Therefore, the analytical solutions given by Equations C-1 through C-4 are valid for comparison. Table C.1 presents the moment and deflection at the center of the plate under both loading conditions. The FE solution could be improved further by refining the mesh. However, such an approach will significantly increase the running time for the FE analysis and result in a very minor improvement in the error.

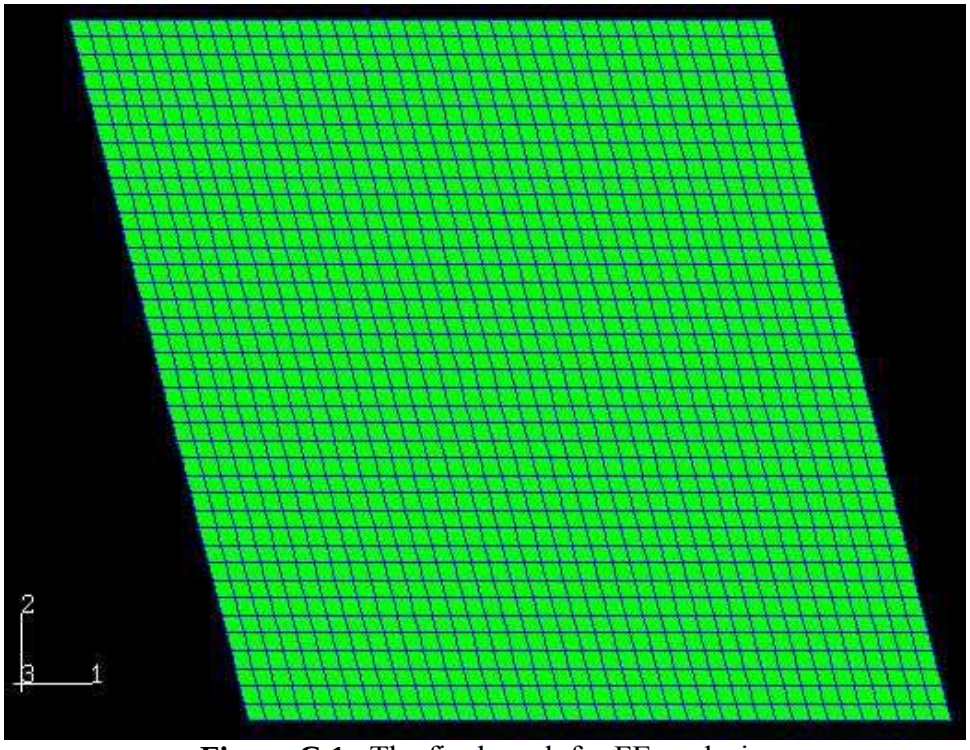

Figure C.1. The final mesh for FE analysis.

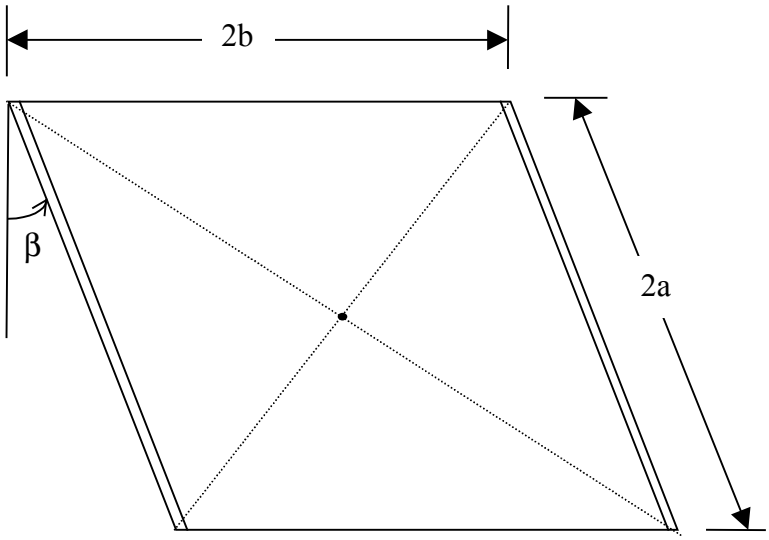

Figure C.2. Skew plate with a=b.

Table C.1. Comparison of ABAQUS solution and the analytical solution.

		Uniform Loading		Concentrated Loading	
		Q = 1 kips/ft^2 (48 kN/m^2)		C = 300 kips (1334 kN)	
Mesh Size	Analysis	Moment k-ft (kN-m)	Deflection in. (mm)	Moment k-ft (kN-m)	Deflection in. (mm)
	Analytical	72.91 (98.87)	0.01882 (0.48)	135.4 (183.60)	0.0167 (0.42)
32 × 32	ABAQUS	69.91 (94.80)	0.01905 (0.48)	127.3 (172.62)	0.0174 (0.44)
	Error	-4.9%	+1.2%	-6.0%	+4.2%
40 × 40	ABAQUS	69.65 (94.45)	0.0192 (0.49)	134.3 (182.11)	.0172 (0.44)
	Error	-4.5%	+2.0%	-1.1%	+3.0%

The contour sketches for both loading conditions are shown in Figure C.3. This Figure indicates that for a uniform loading condition with a small skew angle of 15 degrees, the beam strip approach can reasonably estimate the moment at the center of the span.

To investigate the influence of bridge skew on its behavior, four concentrated loads were applied to the model at locations corresponding to the locations of the hydraulic jacks on the bridge deck. FEM analysis was then carried out for different load magnitudes to determine mid-span deflection. In addition, the elastic deflections of the deck were determined for the same

loads assuming simply-supported solid concrete slab. The results of these analyses are shown in Figure C.4. This Figure shows that accounting for the skew of the bridge improved the theoretical deflections. However, this did not fully explain the higher initial stiffness of the bridge deck observed in the experimental results. This indicated that other parameters (e.g., end fixity) might have contributed to the initial stiffness of the bridge.

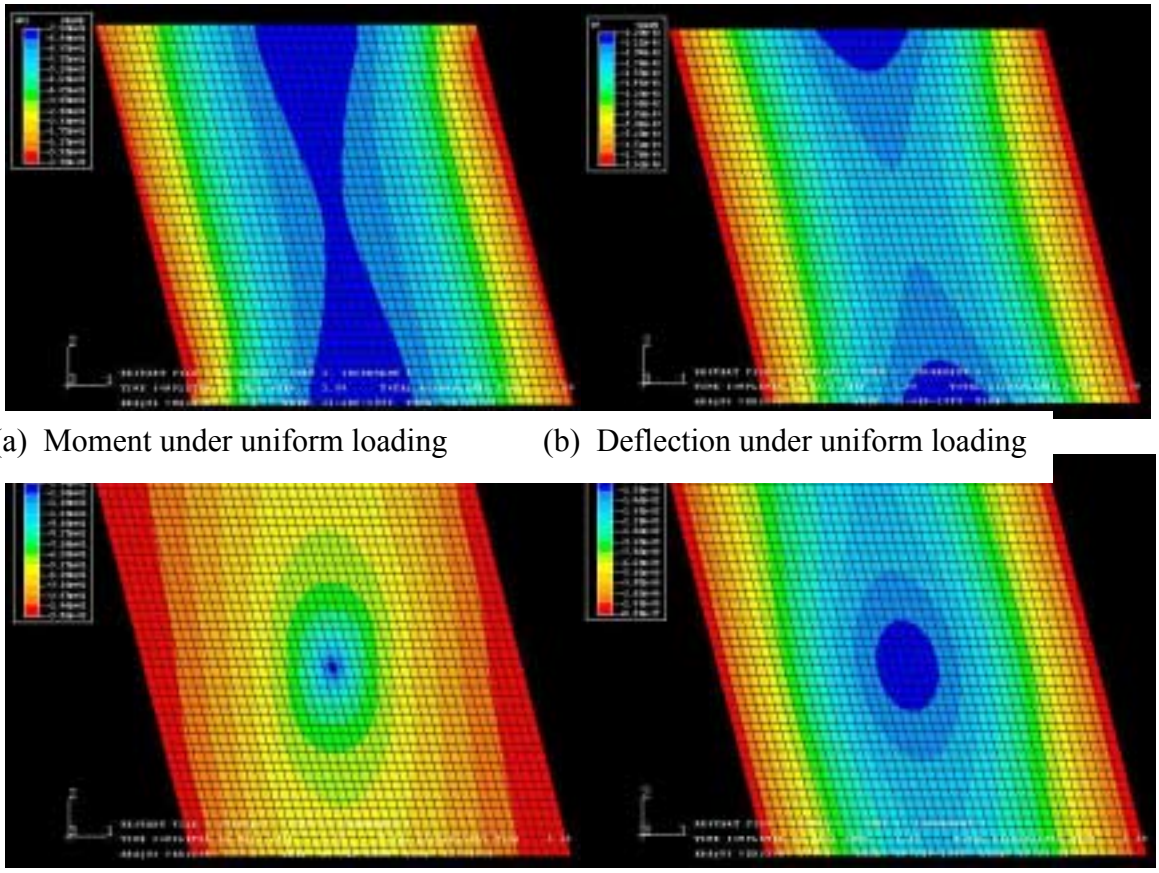

(a) Moment under uniform loading (b) Deflection under uniform loading

(c) Moment under concentrated load (d) deflection under concentrated load

Figure C.3. ABAQUS output - moment and deflection contours.

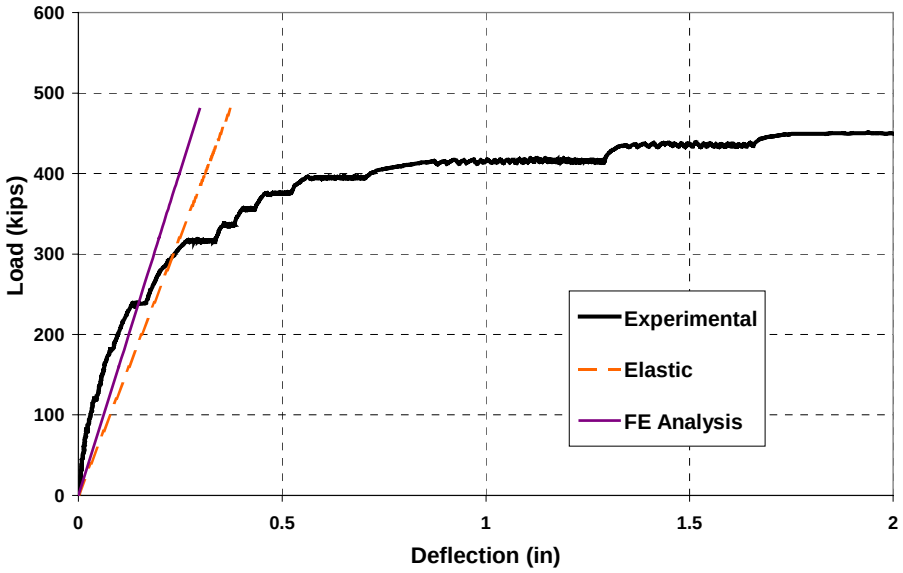

1 kip =4.45 kN, 1 in = 25.4 mm

Figure C.4. Comparison of theoretical and experimental elastic deflections

APPENDIX D:

DERIVATION OF MOMENT-END FIXITY RELATIONSHIP

The moment diagram of a beam is a function of the loading configuration and the boundary conditions. Consider the beam shown in Figure D.1. The beam is subjected to a uniformly distributed load, w, and a concentrated live load, P, at its mid-span. The beam has end fixities, F, represented by two rotational springs at the supports. To determine the effect of end fixity on the moment distribution, the concentrated load and the distributed load will be examined separately.

Concentrated Load. For a simply supported beam subjected to a concentrated load at mid-span, the maximum moment at mid-span, M^{*c}, is given by the following:

$$M^{*c} = \frac{PL}{4} \tag{D-1}$$

As the end fixity changes from zero (no end restraints) to 100% (fully fixed ends), the value of the maximum moment varies from PL/4 to PL/8, as shown in Figure D.2. In addition, at any level of fixity, the sum of the absolutes of the positive moment at mid-span and the negative moment at the support is equal to the moment M^{*c}, or:

$$M^{*c} = \left|M_e^c\right| + \left|M_m^c\right| = \frac{PL}{4} \tag{D-2}$$

The level of fixity, F, can be related to these moments as follows:

$$F = \left|\frac{M_e^c}{M_m^c}\right| * 100\% \tag{D-3}$$

Which can also be expressed as:

$$F = \frac{M_e^c}{M^{*c} - M_e^c} * 100\% = \frac{M^{*c} - M_m^c}{M_m^c} * 100\% \tag{D-4}$$

From which, the moment at mid-span can be related to the level of fixity by the following expression:

$$M_m^c = \frac{M^{*c}}{F+1} = \frac{PL}{4(F+1)} = K_m^c PL \tag{D-5}$$

In which K^c_m is a moment coefficient expressed as follows:

$$K_m^c = \frac{1}{4(F+1)} \tag{D-6}$$

Similarly the end moments can be related to the level of fixity by the following expression:

$$M_e^c = \frac{M^{*c}F}{F+1} = \frac{PLF}{4(F+1)} = K_e^c PL \qquad \text{(D-7)}$$

In which K^c_e is a moment coefficient expressed as follows:

$$K_e^c = \frac{F}{4(F+1)} \qquad \text{(D-8)}$$

Distributed Load. For a simply supported beam subjected to distributed load over the entire span (see Figure D.3a), the maximum moment at mid-span, M^{*c}, is given by the following:

$$M^{*D} = \frac{wL^2}{8} \qquad \text{(D-9)}$$

As the fixity level changes from zero (no end restraints) to 100% (fully fixed restrained), the value of the maximum moment will vary from $wL^2/8$ to $wL^2/24$, as shown in Figure D.3b. In addition, at any level of fixity, the sum of the absolutes of the positive moment at mid-span and the negative moment at the support is equal to the moment M^{*D}, or:

$$M^{*D} = M_e^D + M_m^D = \frac{wL^2}{8} \qquad \text{(D-10)}$$

Considering this variation of mid-span and end moments, the level of fixity can be related to these moments by the following:

$$F = \frac{M_e^D}{2M_m^D} * 100\% \qquad \text{(D-11)}$$

From which the following is derived:

$$F = \frac{M_e^D}{2(M^{*D} - M_e^D)} * 100\% = \frac{2(M^{*D} - M_m^D)}{M_m^D} * 100\% \qquad \text{(D-12)}$$

The moment at mid-span is related to the level of fixity as follows:

$$M_m^c = \frac{M^{*D}}{2F+1} = \frac{wL^2}{8(2F+1)} = K_m^D wL^2 \qquad \text{(D-13)}$$

In which K^D_m is a parameter expressed as follows:

$$K_m^D = \frac{1}{8(2F+1)} \qquad \text{(D-14)}$$

Similarly, the end moments can be expressed in terms of the fixity as follows:

$$M_e^D = \frac{2M^{*D}F}{2F+1} = \frac{wL^2F}{4(F+1)} = K_e^c wL^2 \quad \text{(D-15)}$$

In which the parameter K^D_e is expressed as follows:

$$K_e^D = \frac{F}{4(2F+1)} \quad \text{(D-16)}$$

The moments at mid-span and at the supports due to the combined effect of concentrated and distributed loads can be determined using superposition as follows:

$$M_m = M_m^c + M_m^D = K_m^c PL + K_m^D wL^2 \quad \text{(D-17)}$$

$$M_e = M_e^c + M_e^D = K_e^c PL + K_e^D wL^2 \quad \text{(D-18)}$$

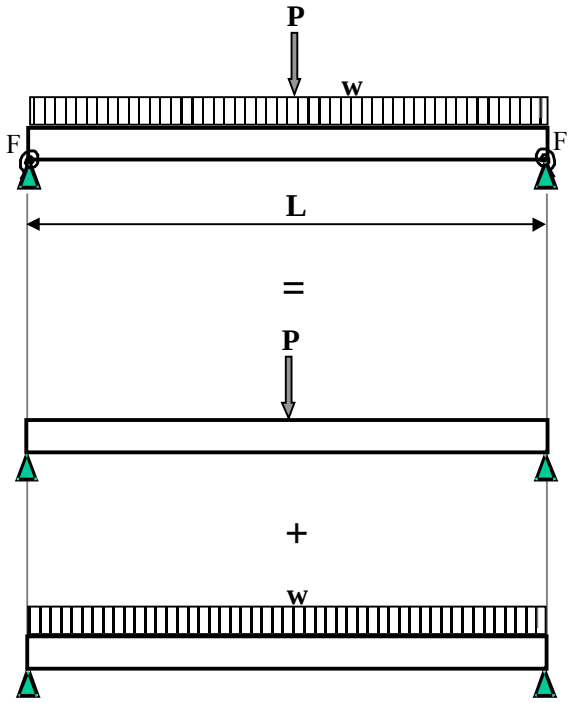

Figure D.1. Superposition of the deck loading.

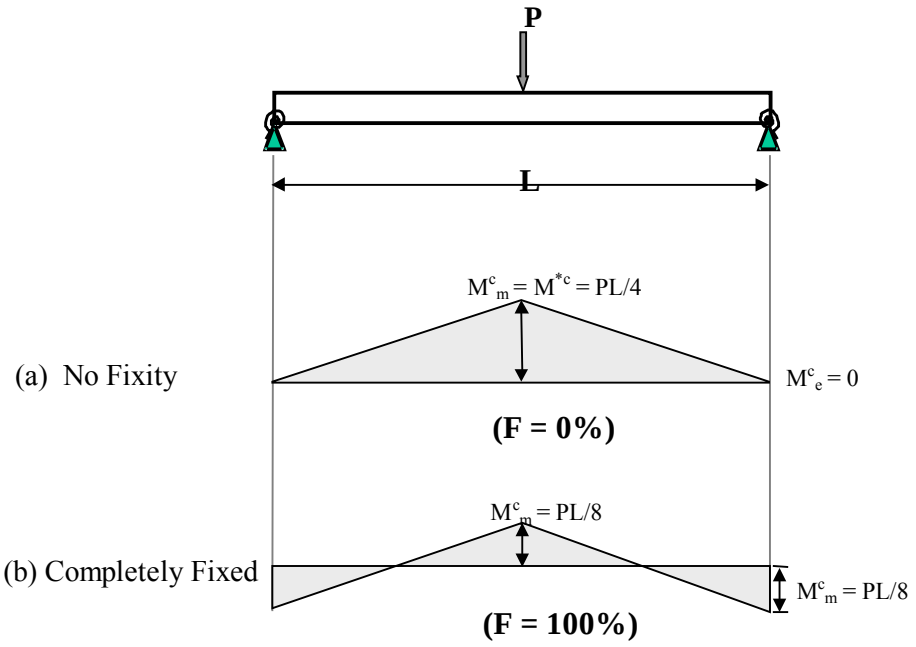

Figure D.2. Moment diagrams for a flexural beam under concentrated load with various end conditions.

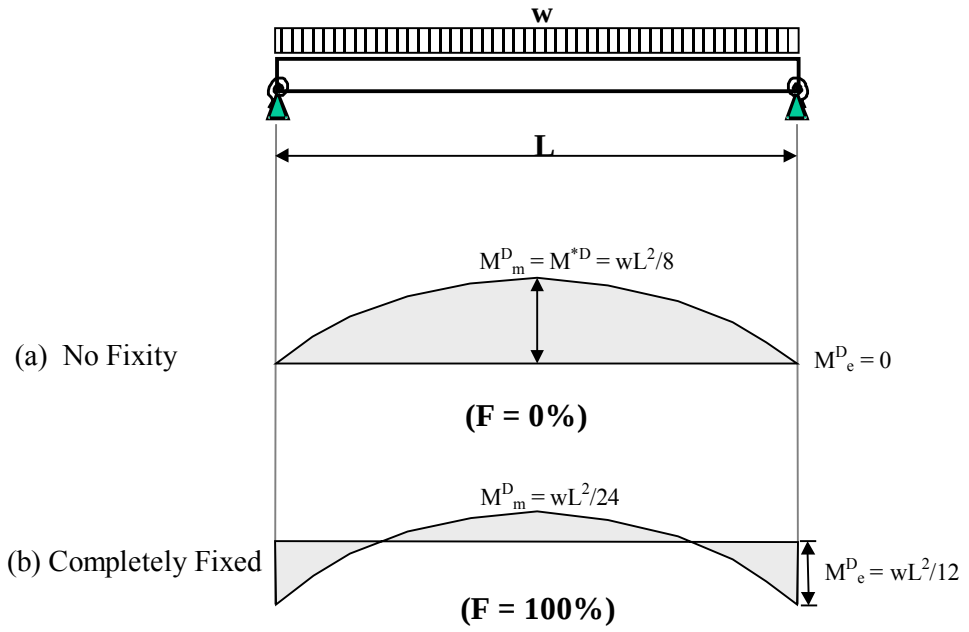

Figure D.3. Moment diagrams for a flexural beam under distributed load with various end conditions.